Punching Shear Behaviour of GFRP-RC Slab-Column Interior Connections with High Strength Concrete and Shear Reinforcement

by

Ahmed Mohamed Hamed Hussein

A Thesis submitted to the Faculty of Graduate Studies of

University of Manitoba

in partial fulfillment of the requirements of the degree of

Master of Science

Department of Civil Engineering

University of Manitoba

Winnipeg, MB, Canada

ABSTRACT

In North America, parking structures are often subjected to harsh environments such as freezing/thawing and wetting/drying cycles as well as de-icing salts which make it vulnerable to corrosion of steel reinforcement. Over the past few decades, the use of fibre-reinforced polymers (FRPs) instead of steel reinforcement proved to be a promising solution to the corrosion problem.

Reinforced concrete (RC) flat plate systems are commonly used and preferred in structures such as parking garages since the absence of beams allows for more clearance for the vehicles. However, flat plates are susceptible to punching shear failure, which occurs without an ample warning due to its brittle nature. This type of sudden failure might result in human casualties and large damages. On the other hand, FRP bars have a relatively low modulus of elasticity and transverse stiffness compared to steel bars which result in a lower shear capacity of FRP-RC structures compared to their counterparts reinforced with steel. To date, the available research has been focused on punching shear behaviour of FRP-RC slabs under concentric punching (without considering the unbalanced moment), which hardly occurs in a real structure. Therefore, the objective of this research is to investigate the punching shear behaviour of FRP-RC slab-column connections subjected to shear and unbalanced moment.

In this study, six full-scale RC flat plate slab-column interior connections reinforced with glass (G) FRP bars were constructed and tested to failure. The dimensions and flexural reinforcement ratios of the connections were obtained by performing an elastic analysis of a multistory parking structure. The resulting dimensions were 2,800×2,800×200 mm with 300-mm square central columns extending 1,000 mm above and below the slabs. The test connections were divided into two series addressing different parameters; each series consisted of three connections. Series 1

investigated the flexural reinforcement ratio when high strength concrete (HSC) is used, while Series 2 investigated the type of GFRP shear reinforcement (headed studs and corrugated bars) when normal strength concrete (NSC) is used. Test results showed that increasing the reinforcement ratio increased punching capacity and post-cracking stiffness for HSC connections. Also, both types of shear reinforcement increased the punching capacity and deflection of NSC connections.

To whom I owe everything and without whom I would have nothing

To Mom and Dad

ACKNOWLEDGMENTS

I write from the depths of my appreciation to my advisor Dr. Ehab El-Salakawy, P.Eng, FCSCE, Professor and Canada Research Chair in Durability and Modernization of Civil Structures, Department of Civil Engineering, University of Manitoba for his continuous guidance, untiring support, encouragement and extreme patience throughout this work.

I would like to thank all my colleagues for their support and help during construction and testing of the specimens. Also, many thanks to the W. R. McQuade Structures Laboratory technical staff, without whom the experimental part of this work would not have been possible.

The financial support received from the Natural Science and Engineering Research Council of Canada (NSERC), through the Canada Research Chairs and Discovery programs is greatly appreciated. Sincere thanks to Pultrall Inc. for generously providing the GFRP shear reinforcement.

I would like to thank my dear colleagues for their continuous support specially Mohammed El-Gendy, Ahmed Gaber, Karam Mahmoud and Ahmed Ghazy whose comments and suggestions were remarkable.

Finally, I would like to express my love and gratitude to my family whose unconditional love, patience and support always kept me going through my life.

Ahmed Mohamed H. Hussein, July 2017

TABLE OF CONTENTS

ABSTRACT i

ACKNOWLEDGMENTS iv

TABLE OF CONTENTS v

LIST OF TABLES ix

LIST OF FIGURES x

CHAPTER 1: INTRODUCTION 1

1.1. BACKGROUND 1

1.2. PROBLEM DEFINITION 2

1.3. SCOPE OF WORK 5

1.4. OBJECTIVES 6

1.5. WORK METHODOLOGY 6

1.6. THESIS ORGANIZATION 7

CHAPTER 2: LITERATURE REVIEW 8

2.1. INTRODUCTION 8

2.2. FRP REINFORCING MATERIAL FOR CONCRETE STRUCTURES 8

2.2.1 Constituents 8

2.2.2. Properties of FRP Composite Bars 9

2.3. BEHAVIOUR OF RC FLAT PLATES 12

2.3.1. Flexural Behaviour 13

2.3.2. Shear Behaviour 14

2.4. BUILDING CODE PROVISIONS FOR PUNCHING SHEAR 18

2.4.1. Steel-RC Slab-Column Connections 18

2.4.2. FRP-RC Slab-Column Connections 27

2.5. RESEARCH ON STEEL-RC SLAB-COLUMN CONNECTIONS 29

2.5.1. Effect of Flexural Reinforcement Ratio 29

2.5.2. Effect of Shear Reinforcement 30

2.5.3. Effect of Concrete Compressive Strength 30

2.5.4. Effect of Moment-to-Shear Ratio 31

2.6. YIELD LINE THEORY 32

2.7. RESEARCH ON PUNCHING SHEAR OF FRP-RC SLABS 35

2.7.1. Previously Proposed Design Models 35

2.7.2. Effect of Different Parameters 38

CHAPTER 3: EXPERIMENTAL PROGRAM 45

3.1. GENERAL 45

3.2. TEST CONNECTIONS 45

3.3. MATERIALS 54

3.3.1. Concrete 54

3.3.2. Reinforcement 54

3.4. TEST SET-UP AND PROCEDURE 56

3.5. INSTRUMENTATION 59

3.5.1. Reinforcement Strain Gauges 59

3.5.2. PI-Gauges and Concrete Strain Gauges 60

3.5.3. Load Cells 61

3.5.4. Linear Variable Displacement Transducers (LVDTs) 61

CHAPTER 4: EXPERIMENTAL RESULTS AND DISCUSSION 63

4.1. GENERAL 63

4.2. SERIES 1: EFFECT OF FLEXURAL REINFORCEMENT RATIO 63

4.2.1. Mode of Failure and Cracking Pattern 63

4.2.2. Deflections 69

4.2.3. Flexural Reinforcement and Concrete Strains 71

4.2.4. Ultimate Strength 76

4.2.5. Code Comparisons 77

4.3. SERIES 2: EFFECT OF SHEAR REINFORCMEENT 79

4.3.1. Mode of Failure and Cracking Pattern 79

4.3.2. Deflections 84

4.3.3. Flexural Reinforcement and Concrete Strains 85

4.3.4. Shear Reinforcement Strains 89

4.3.5. Ultimate Strength 95

4.3.6. Proposed Design Equations for Shear-Reinforced Slab-Column Connections 96

4.3.7. Predicted Punching Capacity for Connections with Shear Reinforcement 97

CHAPTER 5: CONCLUSIONS AND FUTURE WORK 99

5.1. SUMMARY AND CONCLUSIONS 99

5.1.1. Conclusions from Series 1 Connections (Flexural reinforcement ratio) 99

5.1.2. Conclusions from Series 2 Connections (Shear reinforcement) 101

5.2. FUTURE WORK 102

REFERENCES 103

APPENDIX A A-1

APPENDIX B B-1

APPENDIX C C-1

LIST OF TABLES

Table 2.1: Typical densities of reinforcing bars (ACI Committee 440 2015) 9

Table 2.2: Typical coefficient of thermal expansion (ACI Committee 440 2015) 10

Table 2.3: Typical tensile properties for reinforcing bars (ACI Committee 440 2015) 11

Table 2.4: Values of k for rectangular loaded areas (EN 1992-1-1:2004) 25

Table 3.1: Details of test connections 48

Table 3.2: Concrete properties 54

Table 3.3: Mechanical properties of the used GFRP reinforcement 55

Table 4.1: Test results for Series 1 connections 69

Table 4.2: Failure and normalized load and flexural capacities for Series 1 connections 77

Table 4.3: Code comparisons for Series 1 connections 78

Table 4.4: Test results for Series 2 connections 83

Table 4.5: Failure and normalized load and flexural capacities for Series 2 connections 96

Table 4.6: Predictions for Series 2 connections 98

LIST OF FIGURES

Figure 1.1: Typical flat plate system 3

Figure 2.1: Typical stress-strain relationship 11

Figure 2.2: Different punching failures (reproduced from Alexander and Simmonds 1986) 16

Figure 2.3: Assumed linear shear stress distribution for interior connections 20

Figure 2.4: Shear distribution due to an unbalanced moment at a slab-column interior connection (EN 1992-1-1:2004) 25

Figure 2.5: Moment curvature response of FRP-RC sections (reproduced from Gar et al. 2014) 33

Figure 2.6: Different yield line patterns for FRP-RC slab-column connections 34

Figure 3.1: Dimensions and flexural reinforcement layouts (all dimensions are in mm) 48

Figure 3.2: Typical column reinforcement (all dimensions are in mm) 50

Figure 3.3: Shear reinforcement layout (all dimensions are in mm) 50

Figure 3.4: Reinforcement configuration 52

Figure 3.5: Details of shear reinforcement (all dimensions are in mm) 55

Figure 3.6: Test setup (all dimensions are in mm) 57

Figure 3.7: Typical strain gauges layout on the flexural reinforcement 59

Figure 3.8: Strain gauges layout on the shear reinforcement 60

Figure 3.9: Typical PI-gauges/ concrete strain gauges arrangement 61

Figure 3.10: Typical arrangement of LVDTs (all dimensions are in mm) 62

Figure 4.1: Cracking pattern on the tension face of the slab at failure (Series 1) 65

Figure 4.2: Cross-section and schematic drawing of internal cracks (Series 1) 67

Figure 4.3: Vertical load-deflection relationship (Series 1) 70

Figure 4.4: Post-cracking stiffness vs. flexural reinforcement ratio (Series 1) 70

Figure 4.5: Vertical load-flexural strains relationship (Series 1)..... 72

Figure 4.6: Flexural reinforcement strain profile in direction parallel to the direction of the unbalanced moment for Series 1 connections 73

Figure 4.7: Flexural reinforcement strain profile in direction perpendicular to the direction of the unbalanced moment for Series 1 connections 74

Figure 4.8: Normalized failure load vs. flexural reinforcement ratio (Series 1)..... 77

Figure 4.9: Cracking pattern on the tension face of the slab at failure (Series 2)..... 80

Figure 4.10: Cross-section and schematic drawing of internal cracks (Series 2) 82

Figure 4.11: Vertical load-deflection relationship (Series 2)..... 84

Figure 4.12: Vertical load-flexural strains relationship (Series 2)..... 85

Figure 4.13: Flexural reinforcement strain profile in direction parallel to the direction of the unbalanced moment for Series 2 connections 86

Figure 4.14: Flexural reinforcement strain profile in direction perpendicular to the direction of the unbalanced moment for Series 2 connections 87

Figure 4.15: Shear reinforcement strains versus distance from column face for N-1.0-S5..... 90

Figure 4.16: Shear reinforcement strains versus distance from column face for N-1.0-S6..... 92

Figure 4.17: Shear reinforcement strains versus distance from column face for N-1.0-C5 93

CHAPTER 1: INTRODUCTION

1.1. BACKGROUND

The tendency of bare steel to corrode is well known, and it has always been stated that concrete is much more durable than steel. Thus, the combination of concrete and steel is favorable, not only because of the mechanical performance but also, the concrete cover and the high alkalinity of cement paste, both provide the steel with a protective environment, physically and chemically which can eliminate steel corrosion problems (Bentur et al. 1997). However, in practice, with the existence of concrete cracks, oxygen and water, corrosion occurred, sometimes seriously, due to harsh environment, which makes corrosion-related deterioration in concrete structures a major durability issue. Generally, corrosion of embedded steel leads to structural degradation, loss of capacity and as a result, it decreases the service life of the structure, consequently, increasing the cost of repairs and maintenances of the structure.

Many solutions have been proposed to overcome the corrosion problem, such as increasing the concrete cover, decreasing the penetrability of concrete by using appropriate dosages of supplementary cementitious materials, corrosion inhibitors and/or the use of different kinds of steel reinforcement (e.g., stainless steel, epoxy-coated steel and galvanised steel). However, even with the aforementioned protective measures, repair and maintenance procedures still cannot be avoided and their cost can be quite high. Recently, there have been increasing interests in the use of non-corrodible fibre-reinforced polymer (FRP) composites as an alternate promising solution for the steel corrosion problem.

In addition to corrosion immunity, FRP offers more advantages compared to the conventional steel, such as electrical and magnetic non-conductivity, higher longitudinal tensile strength, higher

fatigue endurance, light weight and the possibility to reduce the concrete cover. However, the behaviour of the FRP material is quite different from steel, it exhibits a linear-elastic behaviour up to failure whereas steel yields. Also, FRP has a relatively lower modulus of elasticity compared to steel reinforcement which results in wider cracks and consequently reducing the aggregate interlock and the uncracked concrete contribution to the shear strength. Moreover, FRP material is unidirectional, which adversely affects the shear strength and dowel action ACI 440.1R-15 (ACI Committee 440 2015). Accordingly, a change in the design philosophy and guidelines dealing with steel-RC structures is needed for FRP reinforcement, which requires experimental investigations to account for these mechanical and physical differences.

During the past decades, many experimental investigations have been conducted to develop a further understanding of the behaviour of FRP-reinforced concrete (RC) elements, including flat plates. In this aspect, few studies were carried out to investigate the punching shear behaviour of FRP-RC flat plate systems, accordingly, codes and guidelines have been developed for the design of such members (JSCE 1997; CSA 2012; ACI Committee 440 2015). However, still, researches in this area are in the early stages.

1.2. PROBLEM DEFINITION

Flat plate structures are a common economical form utilizing a slab of uniform thickness, supported directly on columns or load bearing walls (Figure 1.1). Beams, drop panels and column capitals are not used which make its soffit continuously flat. Flat plate structures are used widely and preferred in constructions for its simplicity associated with both construction formwork and installation of electrical and mechanical services. Furthermore, the absence of beams provides flexibility for placing partition walls and reducing the story height. Consequently, reducing construction time and labor costs.

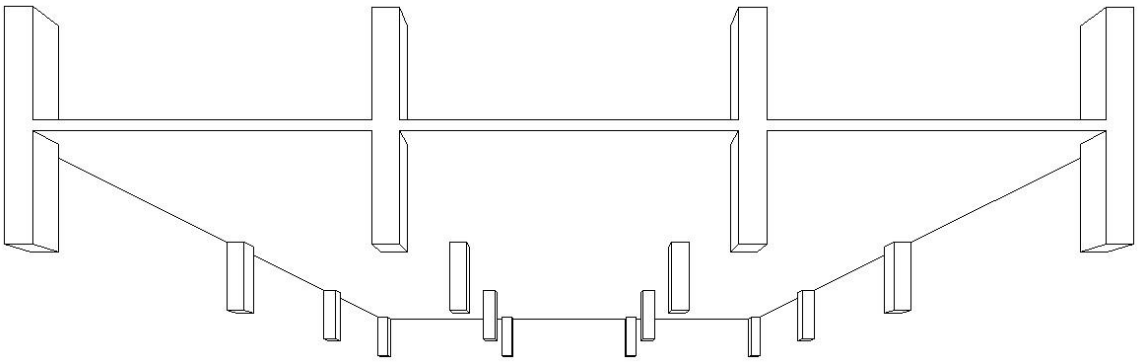

Figure 1.1: Typical flat plate system

Parking structures have become important elements in today's urban and suburban environments. Many of parking structures in North America are constructed using flat plate systems, taking the advantage of absence of beams. However, parking structures are often subjected to harsh environments such as freezing/thawing, wetting/drying cycles and de-icing salts which make them vulnerable to corrosion. One of the important elements that suffer most is the slab system, as it represents the largest portion of any structure exposed to such conditions. Fortunately, replacing corrodible steel reinforcement with FRP would overcome the steel corrosion problem.

The slab-column connection in a flat plate system is the critical component in design, as it is often subjected to large shear forces and bending moments. However, based on the type of loading and the geometry of the slab-column connection, there are two different types of shear failures that have been observed in flat plate systems. The first is one-way shear or beam action which involves an inclined crack extending across the entire width of the slab. The second type is two-way shear or punching shear, where the column punches through the slab. The later failure mechanism is very dangerous because of its brittle nature, also, it may trigger the initiation of a progressive collapse for the whole structure.

The combination of shear forces and unbalanced moments transferred between the slab and the column reduces the punching shear capacity of the connection, consequently, punching shear failure occurred. The unbalanced moments for slab-column connections occur due to lateral loads such as wind or seismic loads, even when resisted by shear walls, still, some moment transfer occurred at corner, edge and first interior columns (Hawkins 1974). Furthermore, uneven gravity loading, different lengths of adjacent spans, discontinuity of slabs at exterior connections and/or eccentric loading will cause unbalanced moments as well. Therefore, rigorous calculations of shear stresses and cautious predictions of the capacity of slab-column connection deemed necessary to prevent punching shear failure.

The brittle punching shear failure in flat plates is a major drawback. Therefore, it has been of special interest to researchers to investigate the behaviour of steel-RC slab-column connections under different parameters (Richart 1984; Elstner and Hognestad 1956; Whitney 1957; Moe 1961; Zaghlool and De Pavia 1973; Hawkins et al. 1974; Alexander and Simmonds 1986; Gardner 1990; Marzouk et al. 1996; Menétrey 1998; Ghannoum 1998; El-Salakawy et al. 2000; Dilger et al. 2005; Mitchell et al. 2005; Stein et al. 2007; Gayed and Ghali 2008). As a result, different codes and guidelines have included provisions and guidelines for the design of slab-column connections (European Standard EN 1992-1-1:2004; JSCE 2007; CSA 2014a; ACI Committee 318 2014).

On the other hand, few research has been carried out to investigate the punching shear behaviour of FRP-RC slabs. The majority of these researches, if not all, have been focused on concentric punching, mainly pushing a steel plate through the center of a square slab (Banthia et al. 1995; El-Ghandour et al. 1999; Matthys and Taerwe 2000; Ospina et al. 2003; El-Gamal et al. 2005; Zhang et al. 2005; Lee et al. 2009; Dulude et al. 2013; Nguyen-Minh and Rovňák 2013; Hassan et al.

2014a) these studies have demonstrated the differences between FRP and steel and proposed new design equations for FRP-RC two-way slabs.

To the author's best knowledge, only two research studies investigated the punching shear behaviour of slab-column interior connections under eccentric loading (shear force and unbalanced moment). Zaghloul (2002, 2007) tested half-scale specimens reinforced with carbon (C) FRP grids and Gouda and El-Salakawy (2016a; b) tested full-scale GFRP slab-column interior connections.

1.3. SCOPE OF WORK

In a typical flat plate system, there are three types of slab-column connections depending on their location; interior, edge and corner connection. This work deals with punching shear behaviour of slab-column interior connections reinforced with GFRP and subjected to a moment-to-shear ratio of 0.15 m. Compared to most commonly available FRPs, GFRP, in particular, is gaining popularity as internal reinforcement for concrete structures due to its lower cost and its ability to develop high tensile strains, hence, GFRP bars are used as flexural reinforcement in this study. Also. High strength concrete (HSC) is being utilised widely in the construction industry nowadays and it exhibits a different behaviour from normal strength concrete (NSC), for this reason, both HSC and NSC are used in this study. Another parameter that can significantly prevent the punching shear failure of RC slab-column connections is shear reinforcement. Shear studs, specially, have proved to be effective in increasing the shear strength of steel-RC slab-column connections (Dilger and Ghali 1981; Mokhtar et al. 1985; El-Salakawy et al. 2000; Stein et al. 2007; Birkle and Dilger 2008; Heinzmann et al. 2012). This study focuses on slab-column interior connections, subjected to shear force and unbalanced moment, with HSC and shear reinforcement.

1.4. OBJECTIVES

The main objectives of this study are to:

- Investigate the punching shear behaviour of GFRP-RC slab-column interior connections subjected to a combination of shear forces and unbalanced moment simulating a real structure under gravity loads.
- Verify the punching shear provisions in the Canadian Standards Association code CSA/S806-12 (CSA 2012), the American Concrete Institute guideline ACI 440.1R-15 (ACI Committee 440 2015) and the Japan Society of Civil Engineers code (JSCE 1997).
- Provide recommendations for designers and researchers to predict the punching shear capacity of GFRP-RC slab-column interior connections with and without GFRP shear reinforcement.

In order to achieve these objectives, the effects of the following parameters on the punching shear behaviour of slab-column interior connections have been studied:

- The effect of flexural reinforcement ratio on connections made of HSC
- The effect of shear reinforcement on connections made of NSC

1.5. WORK METHODOLOGY

Experimental work was designed and conducted in the W. R. McQuade Heavy Structures Laboratory at the University of Manitoba in order to achieve the aforementioned objectives. In this work a total of six full-scale GFRP-RC slab-column interior connections were constructed and tested under shear and unbalanced moment up to failure. All slabs were 2800 × 2800 mm with 200 mm thickness, simply supported along all four edges with the corners free to lift. The connections were isolated from a parking structure to simulate an interior supporting column of a flat plat

system consisting of three 6.5-m long bays in both directions and bounded by the lines of contra-flexure.

1.6. THESIS ORGANIZATION

The thesis consists of five chapters as follows:

- Chapter one: Introduces the problem definition, the scope and objectives of the research, and the methodology followed to achieve these objectives.
- Chapter two: Provides information about FRP composites and their constituent materials, the behaviour of RC flat plate system, an overview of the existing design provisions regarding punching shear in different codes and guidelines for both steel- RC and FRP-RC structures and a critical review of previous research pertaining to punching shear behaviour of both steel-RC and FRP-RC slab-column connections.
- Chapter three: Provides a detailed description of the experimental program including test connections (dimensions, properties of constituent materials and reinforcement detailing), the instrumentations used for real time monitoring of the connections during the test (LVDTs, reinforcement and concrete strain gauges, and PI gauges) and the test setup and test procedure (test frame and hydraulic machines applying the loads).
- Chapter four: Provides the analysis and discussion of the experimental test results in terms of mode of failure and cracking pattern, strains in the reinforcement and concrete, deflections, the ultimate capacity and comparisons to different code predictions.
- Chapter five: Presents a summary of the work, derived conclusions and recommendations for future research.

Also, further details regarding the analysis and the design of the tested connections are presented in three appendices.

CHAPTER 2: LITERATURE REVIEW

2.1. INTRODUCTION

The use of FRP in the reinforced concrete structures instead of steel reinforcement has proved to be an effective solution to the corrosion problem. However, there is still a need for research to better understand the behaviour of FRP-RC elements in general, and for flat plate structures in particular. The concept of having the slab supported directly on columns, makes it susceptible to punching shear failure, regardless of the reinforcement type. Due to difference in properties between FRP and conventional steel reinforcement, codes and guidelines for steel-RC structures cannot be directly applied to FRP-RC structures. As a result, several design guidelines and codes have been developed and published to address the design of FRP-RC elements.

This chapter presents brief information on physical and mechanical properties of FRP reinforcing bars and the previous research available on both steel-RC and FRP-RC slab-column connections with and without shear reinforcement. In addition, the punching shear design provisions and guidelines in the current codes in North America, Europe and Japan are presented.

2.2. FRP REINFORCING MATERIAL FOR CONCRETE STRUCTURES

The FRP reinforcing materials for concrete structures are made with different types of fibres, including aramid, carbon, glass and basalt fibres. They are available in several forms, such as bars, tendons, 2D grids, wraps and laminates for strengthening of existing structures. In this section, a brief overview of FRP materials, as well as the physical and mechanical properties are provided.

2.2.1 Constituents

Fibre-reinforced polymer products are composite materials consist of continuous fibres embedded in a polymer matrix (resin) in addition to some fillers and additives. The fibres are responsible for

providing mechanical strength and stiffness to the composite, however, they are able to carry loads only if they are oriented in the direction of the load. On the other hand, the resin is responsible for protecting the fibres from mechanical and environmental damage, transfer stresses between the fibres and prevent the fibres from buckling as well. The selection of a proper resin is very important in the manufacture of composites since the final physical and mechanical properties of FRP bars are influenced by the physical and thermal properties of the resin. Also, other factors such as fibre-volume, fibre type, fibre orientation, and quality control during manufacturing all play a major role in defining the characteristics of an FRP bar.

2.2.2. Properties of FRP Composite Bars

Unlike steel, FRP bars are anisotropic in nature, which means, the transverse direction has a lower strength and modulus of elasticity than the longitudinal direction. Also, the mechanical properties of FRP composites vary significantly from one product to another (ACI Committee 440 2015).

2.2.2.1. Physical Properties

2.2.2.1.1. Density

FRP bars have a considerably lower density in comparison with the steel, ranging from one-sixth to one-fourth that of steel reinforcement. The reduced weight lowers the transportation and storage costs, in addition, decreases handling and installation time. The densities of different types of reinforcing bars given by the ACI 440.1R-15 (ACI Committee 440 2015) are listed in Table 2.1.

Table 2.1: Typical densities of reinforcing bars (ACI Committee 440 2015)

Reinforcement type	Steel	GFRP	CFRP	AFRP
Density (gm/cm^3)	7.9	1.25 to 2.1	1.5 to 1.6	1.25 to 1.4

2.2.2.1.2. Coefficient of thermal expansion

The coefficient of thermal expansion (CTE) represents the change in unit length of a material due to unit change in temperature. FRP bars have different thermal expansion in the longitudinal and transverse directions. The longitudinal coefficient of thermal expansion is governed by the type of fibre, while the transverse coefficient of thermal expansion is dominated by the type of resin (ACI Committee 440 2015). The coefficients of thermal expansion of different types of reinforcing bars given by ACI 440-1R-15 (ACI Committee 440 2015) are shown in Table 2.2. In case of composite material (i.e. reinforced concrete), the behaviour of its constituents under thermal stresses has to be similar in order to minimize the differential deformations. However, the transverse thermal expansion of FRP is different of that of concrete, which may lead to cracking, and eventually, failure of the concrete cover (Kodur and Baingo 1998; Gentry and Husain 1999). Experimental results on slabs reinforced with GFRP bars showed that a ratio of concrete cover thickness to FRP bar diameter greater than 1.6 is sufficient to avoid cracking of concrete under high temperature up to 80 ℃ (Zaidi and Masmoudi 2008).

Table 2.2: Typical coefficient of thermal expansion (ACI Committee 440 2015)

Reinforcement type		Steel	GFRP	CFRP	AFRP
Coefficient ($\times 10^{-6}/℃$)	Longitudinal	11.7	6 to 10	-9 to 0	-6 to -2
	Transverse	11.7	21 to 23	74 to 104	60 to 80

2.2.2.2. Mechanical Properties

2.2.2.2.1. Tensile behaviour

FRP bars, when loaded in tension, they do not exhibit a yielding plateau before rupture. Instead, they exhibit a linear-elastic stress-strain relationship until failure as shown in Figure 2.1. The

tensile properties of different types of reinforcing bars given by the ACI 440.1R-15 (ACI Committee 440 2015) are listed in Table 2.3. As the resin has a lower strength than the fibres, the tensile properties significantly affected by the fibre-volume fraction and the diameter of the bar. Thus, the tensile properties of FRP composite bars should be obtained directly from the manufacturer. Moreover, except for FRP bars with thermoplastic resins, FRPs cannot be reshaped or bent after being manufactured. FRP bent bars can be done only during the manufacturing process, however, a strength reduction of 40% to 50% in the bend portion compared with the strength of a straight bar is expected due to stress concentrations.

Table 2.3: Typical tensile properties for reinforcing bars (ACI Committee 440 2015)

Reinforcement type	Steel	GFRP	CFRP	AFRP
Tensile strength (MPa)	276 to 517*	483 to 690	600 to 3,690	1,720 to 2,540
Tensile modulus (GPa)	200	35-51	120-580	41-125

*yield strength

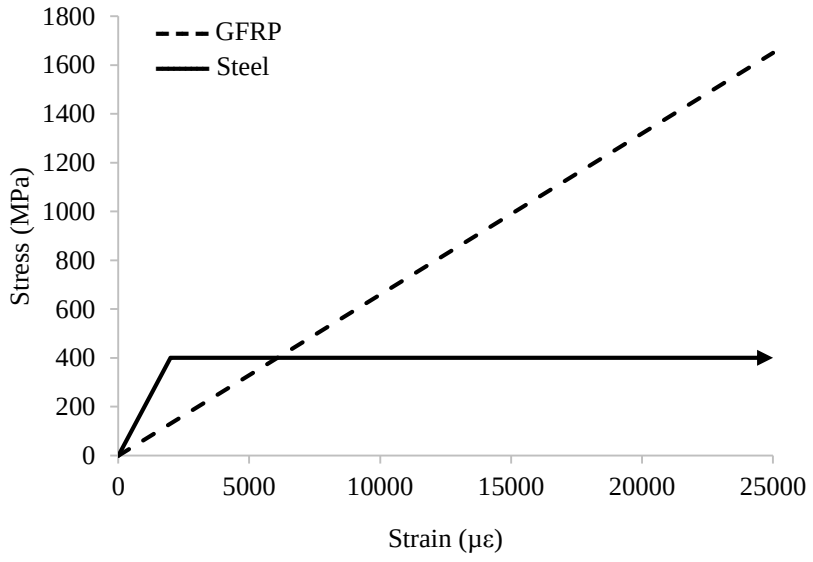

Figure 2.1: Typical stress-strain relationship

2.2.2.2.2. Compressive behaviour

Generally, the compressive strength and compressive modulus of FRP bars is less than the tensile strength and modulus of the same product. The failure mode for FRP bars subjected to axial compression may include transverse tensile failure, fibre microbuckling, or shear failure depending upon type of fibres and resin and the fibre-volume fraction. Compressive strengths of 55, 78, and 20 percent of the tensile strength have been reported for GFRP, CFRP, and AFRP, respectively.

2.2.2.2.3. Shear behaviour

FRP bars are weak in interlaminar shear because the resin is usually unreinforced in the transverse direction of the bar and, consequently, interlaminar shear strength depends on the weak resin. Placing fibres in the transverse direction across the axial fibres will increase the shear resistance.

2.2.2.2.4. Bond behaviour

The effectiveness of a reinforced concrete system depends on the transfer mechanisms of stresses between the concrete substrate and the reinforcing bars (i.e. bonding behaviour). Bond stresses between FRP bars and concrete can be transferred by adhesion (chemical bond), frictional resistance of the interface against slip and mechanical interlock due to irregularity of the bar interface. Bond properties of FRP bars is a function of the surface preparation of the bar, mechanical properties and environmental conditions.

2.3. BEHAVIOUR OF RC FLAT PLATES

Besides being cost-ineffective to test a full slab floor system to determine the shear strength of slab-column connections, the punching shear failure is a localized failure mode associated with only a portion of the slab around loaded area, thus, interior slab-column test specimens have generally been square with column stub at the centre of the slab (ACI-ASCE Committee 326 1962).

Generally, square test slab specimens are more similar to a conditions in footings, however, smaller thickness to span ratios and higher moment to shear ratios are more related to slabs than to footings (Elstner and Hognestad 1956). Test specimens are roughly representing the critical case for shear in a multi-panel floor system, however, the continuity of the slab and its consequences, such as in-plane forces and shifting the contraflexure lines around the column due to cracking, yielding or moment transfer, cannot be accurately modeled (Criswell and Hawkins 1974). In this work, the column stub extends above and below the slab to simulate the unbalanced moment and the slab is simply supported on all four edges at the assumed lines of contra-flexure with the corner free to left. These boundary conditions were selected to represent the most critical case, as the behaviour of the slab with fixed edges is different from simply supported ones and it can cause considerable increase in the shear capacity (Hawkins et al. 1974).

2.3.1. Flexural Behaviour

According to Elstner and Hognestad (1956), the behaviour of test square slab supported on all four edges in flexure can be divided into four stages. First, the uncracked stage, then developing of flexural cracks, followed by yielding of the tension reinforcement from the column area towards the slab edges and finally, plastic stage and increasing deflection which can be regarded as flexural failure. The flexural strength of the slab depends on the ultimate bending moment capacity developed along critical lines of yielding (known as yield lines) and the boundary conditions, in addition, redistribution of moments, due to the decrease in flexural rigidity at the cracked section, may be necessary to develop the failure mechanism. Thus, it is required that the slab section to be ductile enough to allow for the rotations which can occur at the slab-column connection. On the other hand, the ductility concept cannot be exhibited by FRP as it does not have a yielding point. FRP-RC elements exhibited substantial deflection before failure, as a result, deformability concept

replaced ductility, which quantifies the deformation characteristic by providing a comparison between the level of safety between ultimate and service states (ISIS canada 2007).

2.3.2. Shear Behaviour

In general, Shear is not critical when slabs are supported by beams or walls and subjected to line or distributed loads. However, shear can be critical in the vicinity of concentrated loads, where the maximum shear force per unit length is relatively high, this is particularly true of slab-column connection in flat plate systems. The shear strength of slabs in such cases is governed by either one-way shear (beam action) or two-way action (punching shear). In one-way shear mechanism, the slab fails as a wide rectangular beam where the failure occurs at an inclined crack extending across the entire width of the slab. Therefore, for this type of shear failure, conventional theory of beams applies. This type of shear failure is normally not critical and rarely happens in flat plate systems.

2.3.2.1. Two-Way Action - Punching Shear

As mentioned earlier, punching shear failure is a local failure of slab-column connection, in which the column together with a portion of the slab push through the remainder of the slab, resulting in a sloping surface along the diagonal tension cracks which extends from face of the column at the compression side of the slab to some distance from the column at the tension side of the slab and it usually takes the form of a truncated cone or a pyramid, this behaviour is very complex due to the multidimensional geometry of the connection.

Unlike beams where the diagonal cracks can be seen, the entire diagonal crack patterns take place inside the slab and cannot be seen and/or distinguished from flexural cracks at the tension face of the slab except at discontinuous edges. Hence, it is practically not possible to visually classify the failure mode as flexure or shear. Moreover, The critical sections for maximum moment and shear,

both occur at the perimeter of the loaded area, however, the shearing strength of a slab subjected to concentrated load is different from the four stages of slab behaviour in flexure stated earlier (Section 2.3.1). Consequently, interaction between shear and flexure is very strong and punching shear failures are a combined shear and flexure problem, i.e., the shear strength is dependent on the stiffness of the connection (Hawkins and Mitchell 1979).

Therefore, it is important to define the shear failure and flexural failure clearly. Masterson and Long (1974) described the punching failure process of a slab-column connection in the following four basic stages:

- Flexural and shear cracks form in the tension zone near the column periphery.
- Slab tension steel close to the column yields.
- Flexural and shear cracks propagate into what was the compression zone.
- Finally, punching failure occurs before yielding can extend beyond vicinity of the column by rupture of the reduced compression zone in the slab.

This agrees with Elstner and Hognestad (1956), who stated that punching of the column stub is always a shear failure, unless such punching occurs after the full flexural strength exhibited by rapidly increasing deflection. A failure by punching shear is undesirable, since an overall yield line mechanism will not have developed before punching.

Usually when flat plate system is subjected to gravity loads, unbalanced moments occur due to the discontinuity of the slab in the case of exterior connections and due to unequal span lengths and/or uneven loading conditions in the case of interior ones. The value of the unbalanced moment transferred at a connection is increased with the presence of lateral loading. Therefore, torsions develop at the side faces of the column while the front and back faces of the column have the same strength as for a connection transferring shear only. Consequently, the shear stress distribution

around the column becomes nonuniform and the punched region is confined to the area at the heavier-loaded side of the column, while the opposite face may show little or no distress as shown in Figure 2.2.

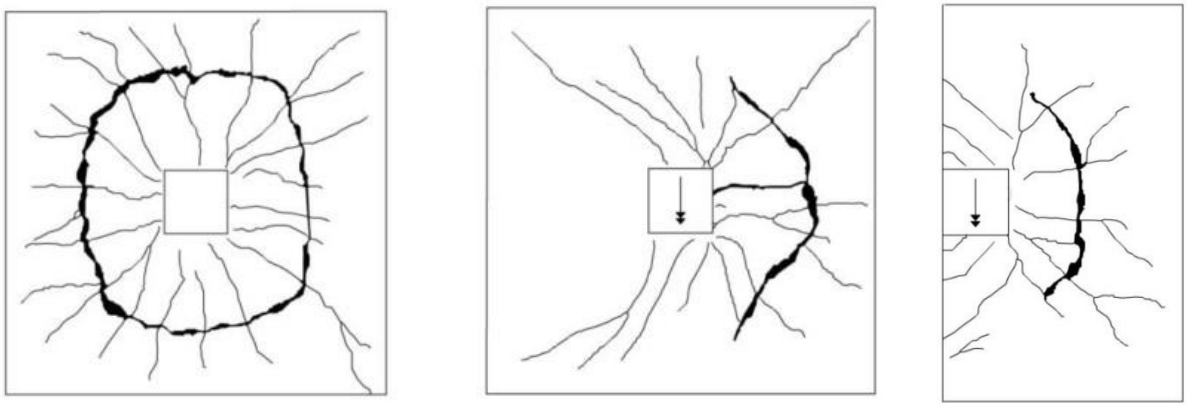

a) Interior – shear only b) Interior – shear and moment c) Edge

Figure 2.2: Different punching failures (reproduced from Alexander and Simmonds 1986)

Many solutions have been used to avoid punching shear failure in a flat plate system, such as increasing the slab thickness, using larger column cross-sections, increasing the flexural reinforcement ratio, providing concrete of higher shear strength and using shear reinforcement around the column.

- Increasing the slab thickness increases the self-weight of the slab as well, which increases the shear stresses applied to the connections and the overall cost of the concrete structure.
- Using larger column cross-sections is often architecturally undesirable.
- Increasing the flexural reinforcement ratio does increase the punching shear capacity but not ductility of the connection.
- Providing concrete of higher shear strength can be done by utilizing HSC. The change in behaviour of concrete with increasing the compressive strength should be assessed. It was

found that the stress-strain relationship of HSC is more linear and steeper compared to NSC resulting in a more brittle failure (Ramdane 1996; Ozden et al. 2006).

It seems that all of these methods can provide an increase in the punching shear capacity, however, only the use of well-anchored shear reinforcement has the advantage of increasing ductility. The choice of the type of shear reinforcement should be based on performance, simplicity, ease of installation and availability. Nevertheless, shear reinforcement must be properly placed to ensure that the crack does not form in-between the two transverse reinforcing bars, and properly anchored to develop its yield strength at punching failure, especially when the slab is thin and there is not much space for anchoring the bars (Polak et al. 2005). The current Canadian standard CSA/A23.3-14 (CSA 2014a) and American standard ACI 318-14 (ACI Committee 318 2014) include provisions for the design of steel-RC slab-column connections with and without shear reinforcement. They permit the use of shear reinforcement in the form of structural steel sections (shearheads), bars, wires, single- or multiple-leg stirrups and headed studs. Shearheads were introduced in the 1930s by Wheeler (1936), but it was not incorporated into the ACI code until the 1971 edition (ACI Committee 318 1971) based on the work by Corley and Hawkins (1968). However, besides being expensive to fabricate, shearheads may interfere with the column reinforcement and they cannot be used in relatively thin slabs (Dilger and Ghali 1981). On the other hand, although considerably effective in increasing the punching shear capacity, bent bars and stirrups are difficult to install in practice and their anchorage cannot be easily achieved in thin slabs. Dilger and Ghali (1981) introduced the headed studs, which seem to overcome all these issues. In order to form stud rails, headed studs are usually arranged in the form of single-headed studs welded to a thin steel base plate or double-headed studs mechanically crimped into a steel channel. Because of their simple geometry, they can be anchored as close as possible to the

surfaces of the slab, which ensures optimum anchorage, and can be easily fitted in-between the longitudinal bars. Moreover, compared to a leg of a stirrup with bends, a headed stud exhibits smaller slip, which results in smaller shear crack width (ACI Committee 421 2008).

2.4. BUILDING CODE PROVISIONS FOR PUNCHING SHEAR

The evaluation of punching shear capacity of slab-column connection depends on many variables such as concrete strength, flexural reinforcement type and ratio, column aspect ratio, the effective depth of the slab and the presence of shear reinforcement, in addition, the design model used in the analysis. Most design codes calculate the punching shear capacity on a control perimeter located at some distant from the column face, however, the effect of these variables differ considerably in each code. In this section, the details of formulae and provisions of different design codes and guidelines in North America, Europe and Japan for both steel-RC and FRP-RC slab-column connection reinforced with shear reinforcement are presented.

2.4.1. Steel-RC Slab-Column Connections

The formulae adopted by the North American codes (CSA 2014a; ACI Committee 318 2014) and the European standard (EN 1992-1-1:2004) are presented. The punching shear resistance is calculated on a critical perimeter which is located at $0.5\,d$ and $2.0\,d$ for North American codes and European standards, respectively. The European standard accounts for the reinforcement ratio and the concrete strength to express the ultimate shearing stress along the critical perimeter, while the North American codes depend solely on the concrete strength.

2.4.1.1. Canadian Standards Association (CSA) A23.3-14 (CSA 2014a)

The Canadian code adopt the theory of linear variation of shear stresses acting along a critical perimeter. Shear stresses utilized by this method are induced by vertical shearing force and a

portion of the unbalanced moment transferred through the connection (Figure 2.3). The remainder portion of the unbalanced moment is assumed to be resisted by flexure in the slab. The maximum shear stress, v_f, is calculated by Equation 2.1.

$$v_f = \frac{V_f}{b_o d} + \frac{\gamma_v M_f}{j} e \qquad \text{Eq. [2.1]}$$

$$\gamma_v = 1 - \frac{1}{1 + \frac{2}{3}\sqrt{\frac{b_1}{b_2}}} \qquad \text{Eq. [2.2]}$$

$$j = \frac{b_1^3 d + d^3 b_1}{6} + \frac{b_2 d b_1^2}{2} \qquad \text{Eq. [2.3]}$$

Where V_f is the factored shear force, $b_\circ$ is the perimeter of the critical section, d is the slab average effective depth, γ_v is the fraction of the unbalanced moment transferred between slab and column (Equation 2.2), M_f, and resisted by shear, e is the distance from centroid of section for critical shear perimeter to point where shear stress is being calculated, j is a property of the critical shear section analogous to the polar moment of inertia for interior connections (Equation 2.3), b_1 and b_2 are the widths of the critical perimeter measured in the direction of the span for which moments are determined and the perpendicular direction, respectively.

The CSA/A23.3-14 (CSA 2014a) requires that the factored shear stress resistance, v_r, shall be equal to or greater than the maximum factored shear stress, v_f, due to factored shear force and unbalanced moments.

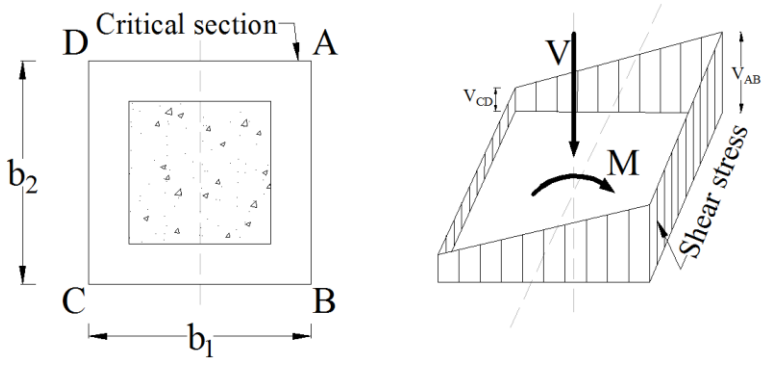

Figure 2.3: Assumed linear shear stress distribution for interior connections

Shear stress resistance without shear reinforcement

In absence of shear reinforcement, $v_r = v_c$; where v_c is the factored shear resistance provided by concrete at a critical shear section located at *d/2* from the column's face or the concentrated load, and it shall be the smallest of Equations 2.4 to 2.6:

$$v_r = v_c = 0.19\left(1+\frac{2}{\beta_c}\right)\lambda\varphi_c\sqrt{f_c'} \qquad \text{Eq. [2.4]}$$

$$v_r = v_c = \left(0.19+\frac{\alpha_s d}{b_o}\right)\lambda\varphi_c\sqrt{f_c'} \qquad \text{Eq. [2.5]}$$

$$v_r = v_c = 0.38\lambda\varphi_c\sqrt{f_c'} \qquad \text{Eq. [2.6]}$$

Where β_c is the ratio of long side to short side of the column, λ is a factor to account for low-density concrete, φ_c is the resistance factor for concrete, f_c' is the specified compressive strength of concrete ($\sqrt{f_c'}$ shall not exceed 8 MPa), α_s is a factor takes into account the support condition ($\alpha_s = 4$ for interior columns) and b_o is the perimeter of critical section for shear in slabs.

Also, CSA/A23.3-14 (CSA 2014a) accounts for the size effect when the slab effective depth exceeds 300 mm, by multiplying the value of v_c obtained from the above three equations by $1300/(1000 + d)$.

Shear stress resistance with shear reinforcement

Generally, shear reinforcement may be used to increase the shear capacity of the slabs, in this case, the shear resistance v_r, within the shear-reinforced area, shall be computed as $(v_c + v_s)$, where v_s is the factored shear resistance provided by the shear reinforcement.

Shear reinforcement shall be extended to the greater of, a distance of *2d* from the column face, or the section where the factored shear stress is not greater than the specified value in Equation 2.7.

$$v_r = v_c = 0.19\lambda\varphi_c\sqrt{f_c'} \qquad \text{Eq. [2.7]}$$

Headed shear reinforcement shall be mechanically anchored and properly detailed in order to be capable of developing the yield strength of the bar. When it is provided is such way, the factored shear stress v_f, the factored shear stress resistance by concrete v_c, and the factored shear resistance by shear reinforcement v_s, shall be as follows:

$$v_f \le 0.75\lambda\varphi_c\sqrt{f_c'} \qquad \text{Eq. [2.8]}$$

$$v_c = 0.28\lambda\varphi_c\sqrt{f_c'} \qquad \text{Eq. [2.9]}$$

$$v_s = \frac{\varphi_s A_{vs} f_{yv}}{b_o s} \qquad \text{Eq. [2.10]}$$

Where, φ_s is the resistance factor of steel, A_{vs} is the cross-sectional area of the headed shear reinforcement on a concentric line parallel to the perimeter of the column, f_{yv} is the specified yield strength of headed shear reinforcement, and s is the spacing of headed shear reinforcement measured perpendicular to b_o.

The distance between the column face and the first line of headed shear reinforcement shall be 0.4*d*. The spacing between lines of headed shear reinforcement shall be based on the value of v_f at a critical section 0.5*d* from the column face as follows:

$s \le 0.75d$ when $v_f \le 0.56\lambda\varphi_c\sqrt{f_c'}$ $\quad$ $s \le 0.5d$ when $v_f > 0.56\lambda\varphi_c\sqrt{f_c'}$

When stirrups are provided, the factored shear resistance by shear reinforcement v_s, shall be computed from Equation 2.10. The factored shear stress, v_f, and the factored shear stress resistance by concrete, v_c, shall be as follows:

$$v_f \le 0.55\lambda\varphi_c\sqrt{f_c'} \qquad \text{Eq. [2.11]}$$

$$v_c = 0.19\lambda\varphi_c\sqrt{f_c'} \qquad \text{Eq. [2.12]}$$

2.4.1.2. American Concrete Institute (ACI) 318-14 (ACI Committee 318 2014)

Similar to the Canadian standard, the ACI 318-14 (ACI Committee 318 2014) is based on linear variation of stresses along a critical perimeter, where the maximum shear stress, v_u, due to a combination of factored shear force, V_u, and the fraction of unbalanced moment, $\gamma_v M_u$, should not exceed the reduced nominal shear strength, φv_n, where φ is a strength reduction factor ($\varphi = 0.75$).

Shear stress resistance without shear reinforcement

The shear strength provided by concrete, v_c, shall be the smallest of Equations 2.13 to 2.15:

$$v_r = v_c = 0.083\left(2 + \frac{4}{\beta_c}\right)\lambda\sqrt{f_c'} \qquad \text{Eq. [2.13]}$$

$$v_r = v_c = 0.083\left(2 + \frac{\alpha_s d}{b_o}\right)\lambda\sqrt{f_c'} \qquad \text{Eq. [2.14]}$$

$$v_r = v_c = 0.33\lambda\sqrt{f_c'} \qquad \text{Eq. [2.15]}$$

Where v_c is the nominal shear strength provided by concrete and α_s is a factor takes into account the support condition (40 for interior connections), also, the value of $\sqrt{f_c'}$ shall not exceed 8.3 MPa.

Shear stress resistance with shear reinforcement

Shear stress due to factored shear force and moment shall not exceed the following value (Equation 2.16) at the critical section located *0.5d* outside the outermost peripheral line of shear reinforcement.

$$v_f \leq 0.17\lambda\varphi\sqrt{f_c'} \qquad \text{Eq. [2.16]}$$

Headed shear reinforcement when properly anchored and detailed, v_c and v_r shall not exceed the following values:

$$v_c \leq 0.25\lambda\sqrt{f_c'} \qquad \text{Eq. [2.17]}$$

$$v_r \leq 0.66\lambda\sqrt{f_c'} \qquad \text{Eq. [2.18]}$$

And the nominal shear resistance provided by the stud shear reinforcement, v_s, shall be calculated according to the following equations:

$$V_s = \frac{A_v f_{yt} d}{s} \qquad \text{Eq. [2.19]}$$

$$v_s = \frac{A_v f_{yt}}{b_o s} \geq 0.17\lambda\sqrt{f_c'} \qquad \text{Eq. [2.20]}$$

Where A_v is the cross-sectional area of all the shear reinforcement on one peripheral line that is approximately parallel to the perimeter of the column section, and f_{yt} is the specified yield strength of the headed shear reinforcement.

The distance between the column face and the first line of headed shear reinforcement shall not exceed *0.5d*, and the spacing, *s*, shall be based on the value of the shear stress due to factored shear force and unbalanced moment at the critical section as follows:

$s \le 0.75d$ when $v_f \le 0.50\lambda\varphi\sqrt{f_c'}$ $\qquad$ $s \le 0.5d$ when $v_f > 0.50\lambda\varphi\sqrt{f_c'}$

When stirrups are provided, the factored shear resistance by shear reinforcement v_s, shall be computed from Equation 2.19. The factored shear stress, v_n, and the factored shear stress resistance by concrete, v_c, shall be as follows:

$$v_n \le 0.50\lambda\sqrt{f_c'} \qquad \text{Eq. [2.21]}$$

$$v_c \le 0.17\lambda\sqrt{f_c'} \qquad \text{Eq. [2.22]}$$

2.4.1.3. The European Standard (EN 1992-1-1:2004)

The Eurocode calculates the maximum applied shear stress, v_{Ed}, from the following equation:

$$v_{Ed} = \beta\frac{V_{Ed}}{u_i d} \qquad \text{Eq. [2.23]}$$

Where V_{Ed} is the design value of the applied shear force at the section considered due to factored loads, u_i is the length of the control perimeter being considered and d is the mean effective depth of the slab. For a rectangular column where the load is eccentric along one axis:

$$\beta = 1 + k\frac{M_{Ed}u_1}{V_{Ed}W_1} \qquad \text{Eq. [2.24]}$$

Where M_{Ed} is the applied unbalanced moment at the section considered due to factored loads, u_1 is the length of the basic control perimeter (at a distance 2.0 d from the loaded area), k is a coefficient dependant on the ratio between the column dimensions c_1 and c_2 which is a function

of the proportions of the unbalanced moment transmitted by uneven shear, bending and torsion (Table 2.4).

Table 2.4: Values of *k* for rectangular loaded areas (EN 1992-1-1:2004)

c_1/c_2	≤ 0.5	1.0	2.0	$\gg 3.0$
k	0.45	0.6	0.7	0.8

And, W_1 correspond to a distribution of shear and is a function of the basic control perimeter, u_1, as shown in Figure 2.4.

$$W_1 = \int_o^{u_i} |e| \, dl \qquad \text{Eq. [2.25]}$$

Where *dl* is a length increment of the perimeter and *e* is the distance of *dl* from the axis about which the moment M_{Ed} acts. W_1 could be calculated from Equation (2.26) for a rectangular column

$$W_1 = \frac{c_1^2}{2} + c_1 c_2 + 4c_2 d + 16d^2 + 2\pi d c_1 \qquad \text{Eq. [2.26]}$$

Where c_1 and c_2 are the column dimensions parallel and perpendicular to the eccentricity of the load, respectively.

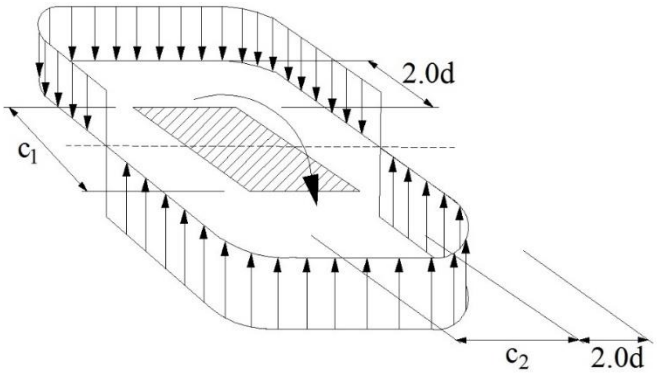

Figure 2.4: Shear distribution due to an unbalanced moment at a slab-column interior connection (EN 1992-1-1:2004)

Shear stress resistance without shear reinforcement

According to the Eurocode, the design of punching shear resistance of a slab without shear reinforcement may be calculated as:

$$v_{Rd,c} = \frac{0.18}{\gamma_c} K \left(100 \rho f_{ck}\right)^{1/3} + 0.1\sigma_{cp} \geq \left(v_{\min} + 0.1\sigma_{cp}\right) \quad \text{Eq. [2.27]}$$

$$K = \left(1 + \sqrt{\frac{200}{d}}\right) \leq 2.0 \quad \text{Eq. [2.28]}$$

$$v_{\min} = 0.035 K^{3/2} f_{ck}^{1/2} \quad \text{Eq. [2.29]}$$

$$\rho = \sqrt{\rho_y + \rho_z} \leq 0.02 \quad \text{Eq. [2.30]}$$

Where $v_{Rd,c}$ the design value of the punching shear resistance of a slab is without punching shear reinforcement along the control section considered, γ_c is the concrete partial safety factor (1.5), K is a size effect parameter (Equation 2.28), ρ is the flexural reinforcement ratio (Equation 2.30), f_{ck} is characteristic compressive cylinder strength of concrete at 28 days, σ_{cp} is the compressive stress in the concrete from axial load

$$\sigma_{cp} = \left(\sigma_{c,y} + \sigma_{c,z}\right)/2 \quad \text{Eq. [2.31]}$$

Where $\sigma_{c,y}$, , $\sigma_{c,z}$ are the normal concrete stresses in the critical section in *y* and *z* directions, respectively.

$$\sigma_{c,y} = \frac{N_{Ed,y}}{A_{cy}} \text{ and } \sigma_{c,z} = \frac{N_{Ed,z}}{A_{cz}} \quad \text{Eq. [2.32]}$$

Where $N_{Ed,y}$, $N_{Ed,z}$ are the longitudinal forces across the full bay for interior columns and the longitudinal force across the control section for edge columns, respectively (the force may be from a load or prestressing action) and A_c is the area of concrete according to the definition of N_{Ed}.

Shear stress resistance with stud shear reinforcement

The Eurocode calculates the design value of the punching shear resistance of a slab with shear reinforcement, $v_{Rd,cs}$, by the following equation:

$$v_{Rd,cs} = 0.75v_{Rd,c} + 1.5\left(\frac{d}{s_r}\right)A_{sw} f_{ywd,ef}\left(\frac{1}{u_1 d}\right)\sin\alpha \qquad \text{Eq. [2.33]}$$

$$f_{ywd,ef} = 250 + 0.25d \le f_{ywd} \qquad \text{Eq. [2.34]}$$

Where s_r is the radial spacing of perimeters of shear reinforcement, A_{sw} is the area of one perimeter of shear reinforcement around the column, $f_{ywd,ef}$ is the effective design strength of the punching shear reinforcement (Equation 2.34), α is the angle between the shear reinforcement and the plane of the slab and , f_{ywd} is the design yield of shear reinforcement.

2.4.2. FRP-RC Slab-Column Connections

The North American codes (CSA 2012; ACI Committee 440 2015) and the Japan Society of Civil Engineers code (JSCE 1997) consider the critical section for shear to be located at a distance $0.5\,d$ from the column face. Yet, no provisions for designing slab-column connections with any type of shear reinforcement.

2.4.2.1. Canadian Standards Association (CSA) S806 (CSA 2012)

The CSA/S806-12 (CSA 2012) accounts for the flexural reinforcement stiffness in calculating the punching shear resistance of FRP-RC slab-column connections and it shall be the smallest of the following:

$$v_r = v_c = 0.028\left(1 + \frac{2}{\beta_c}\right)\lambda\varphi_c\left(E_F\rho_F f_c'\right)^{\frac{1}{3}} \qquad \text{Eq. [2.35]}$$

$$v_r = v_c = 0.147\left(0.19 + \frac{\alpha_s d}{b_o}\right)\lambda\varphi_c\left(E_F\rho_F f_c'\right)^{\frac{1}{3}} \qquad \text{Eq. [2.36]}$$

$$v_r = v_c = 0.056\lambda\varphi_c \left(E_F \rho_F f_c^{'}\right)^{\frac{1}{3}} \quad \text{Eq. [2.37]}$$

Where E_F and ρ_F are the elastic modulus and the flexural reinforcement ratio for the FRP reinforcement, respectively, f_c' is the concrete compressive strength (shall not exceed 60 MPa) and α_s is a factor takes into account the support condition ($\alpha_s = 4$ for interior columns).

If the effective depth of the slab exceeds 300 mm, then the size effect should be considered by multiplying the value of v_c obtained from the above equations by $(300/d)^{0.25}$

2.4.2.2. American Concrete Institute (ACI) 440.1R (ACI Committee 440 2015)

The nominal shear strength provided by concrete, V_c, is calculated as:

$$V_n = V_c = \frac{4}{5}\sqrt{f_c^{'}} b_o c \quad \text{Eq. [2.38]}$$

Where c is the cracked transformed section neutral axis depth, and may computed as,

$$c = kd \quad \text{Eq. [2.39]}$$

$$k = \sqrt{2\rho_F n_F + \left(\rho_F n_F\right)^2} - \rho_F n_F \quad \text{Eq. [2.40]}$$

Where n_F is the ratio of modulus of elasticity of FRP bars to modulus of elasticity of concrete.

2.4.2.3. Japan Society of Civil Engineers (JSCE 1997)

The design punching shear capacity, V_{pcd}, may be determined by the following equations:

$$V_{pcd} = \beta_d \beta_p \beta_r \frac{f_{pcd} u_p d}{\gamma_b} \times \frac{1}{\alpha} \quad \text{Eq. [2.41]}$$

$$\beta_d = \sqrt[4]{\frac{1{,}000}{d}} \leq 1.5 \quad \text{Eq. [2.42]}$$

$$\beta_p = \sqrt[3]{100\rho \frac{E_f}{E_s}} \leq 1.5 \quad \text{Eq. [2.43]}$$

$$\beta_r = 1 + \frac{1}{1 + 0.25(u/d)} \quad \text{Eq. [2.44]}$$

$$f_{pcd} = 0.2\sqrt{f_{cd}^{'}} \leq 1.2 \quad \text{Eq. [2.45]}$$

$$\alpha = 1 + 1.5 * \frac{e_x + e_y}{\sqrt{b_x b_y}} \quad \text{Eq. [2.46]}$$

where, f_{pcd} is the design compressive strength of concrete, u_p is the peripheral length of the design cross-section at $d/2$ from the column face, d is the average effective depth of both orthogonal directions, γ_b is a partial safety factor, α is a factor takes into account the eccentricity of the shearing force, ρ is the average flexural reinforcement ratio in both orthogonal direction, E_f and E_s are the elastic modulus for the FRP and steel reinforcement, respectively, u is the peripheral length of the column, e_x and e_y are the load eccentricity in the two orthogonal directions, and b_x and b_y are the dimensions of the critical section in the two orthogonal directions.

2.5. RESEARCH ON STEEL-RC SLAB-COLUMN CONNECTIONS

2.5.1. Effect of Flexural Reinforcement Ratio

Extensive research has been done to investigate the effect of flexural reinforcement ratio on the punching shear capacity of slab-column connections. Increasing the flexural reinforcement ratio increases the punching capacity and the post-cracking stiffness (Marzouk and Hussein 1991; Osman et al. 2000; Dilger et al. 2005; Ozden et al. 2006; Stein 2006; Rizk et al. 2011b). In addition, increasing the reinforcement ratio tend to decrease the proportion of moment transferred through shear, the number and width of cracks, and the ductility of the connection (Luo and Durrani 1995; Marzouk et al. 1998; Rizk et al. 2011a). Thus, punching failure occurred before the yield stress is reached in the steel. On the other hand for under-reinforced slabs, crack width increases which lead to a reduction in aggregate interlock and dowel action. The flexural capacity of the slab in

this case governs the strength and the failure mode will be ductile (Stein et al. 2007; Guandalini et al. 2009; Ghali et al. 2013)

2.5.2. Effect of Shear Reinforcement

As mentioned in Section 2.3.2.1, there are many types of shear reinforcements have been proposed over the past years for slab-column connections. Seible et al. (1980) tested the use of headed shear studs welded with a welding gun to a steel strip, among other types of preassembled shear reinforcement units (I-beam segments and welded wire fabric). They concluded that, all the three types of shear reinforcement can be used to increase strength and ductility of slab-column connections. Dilger and Ghali (1981) proposed a procedure for the design of stud shear reinforcement of slab-column connections. The headed ends provide anchorage to concrete allowing the bar to develop the yield strength. Also, due to its simple design, studs are easier to place and arrange in thin slabs during construction than traditional stirrups and bent bars (Mokhtar et al. 1985; Elgabry and Ghali 1987; Robertson et al. 2002).

All tests done on slabs with headed shear studs showed increase ductility and the strength of the slab-column connection (Megally and Ghali 1994; El-Salakawy et al. 1998, 2000; Birkle and Dilger 2008; Heinzmann et al. 2012). Shear stud reinforcement can transform the failure mode from punching shear failure to a more ductile flexure failure, deflections at failure in specimens containing shear studs were two to three times greater than those observed in specimens containing no shear studs (Mokhtar et al. 1985; Mortin and Ghali 1991).

2.5.3. Effect of Concrete Compressive Strength

Concrete strength has a direct influence on the punching behaviour and punching capacity of concrete slabs, thus, it is essential to investigate how the shear strength is related to concrete strength. Moe (1961) reported that shear failure is a function of tensile-splitting strength, which is

assumed to be proportional to $\sqrt{f_c'}$. However, the behaviour of HSC, which is defined as concrete with compressive strength of at least 55 MPa (ACI Committee 363 2010), differs from NSC. It was found that increasing the compressive strength increased the ultimate punching load, but at a rate less than the square root of the slab compressive strength. In addition, using the square root of the concrete strength results in an overestimate of the influence of this parameter, and may result in some reduction in the safety margins. The cubic root of concrete compressive strength is a better assumption for predicting punching shear of high strength concrete (Gardner 1990; Marzouk and Hussein 1991, 1992; Gardner and Shao 1996; Sherif and Dilger 1996).

It was demonstrated that, although the contribution of aggregate interlock to the punching shear strength is reduced (Hallgren and Kinnunen 1996), increasing the concrete strength increased the overall punching shear capacity and stiffness of the connections (Ghannoum 1998; Ozden et al. 2006) and delayed the formation of flexural cracks (Ramdane 1996). For NSC connections the failure angle was found to be between 26° and 30°, while for HSC slabs the observed angle of failure surface varied between 32° and 38° (Marzouk and Hussein 1991, 1992). In general, HSC slabs exhibits a more brittle failure than normal strength concrete slabs (Ramdane 1996; Marzouk and Hussein 1992; Ozden et al. 2006).

2.5.4. Effect of Moment-to-Shear Ratio

The ultimate shearing strength of a reinforced concrete slab is a function of the distribution and magnitude of shearing and normal stresses on the critical section. Since normal stresses in slabs are produced by flexural action, therefore the shearing strength is a function of the moment-to-shear ratio. Furthermore, determination of the available net area to resist shear is difficult as it is dependent on the amount and location of flexural cracks that take place prior to ultimate failure, and certainly, for slabs with high moment-to-shear ratio the amount of flexural cracking will be

greater than for slabs with low moment-to-shear ratio (Scordelis et al. 1958). With increasing eccentricity, a reduction in the punching capacity was observed regardless of concrete strength, and slab reinforcement ratio (Zaghlool and De Pavia 1973; Marzouk et al. 1996, 2000; El-Salakawy et al. 1998; Ozden et al. 2006). Also, it was found that the high moment-to-shear ratio increased the zone of the slab around the column that was affected by the shear stresses (El-Salakawy et al. 1998; Marzouk et al. 2000).

2.6. YIELD LINE THEORY

The yield line theory is based on plastic behaviour represented by pattern of yield lines, and it is an efficient tool to estimate the ultimate flexural strength of a reinforced concrete slab. The basic assumption is that a reinforced concrete slab, analogous to continuous beam or frame, will develop yield hinges under overload, the hinges in a slab must be in form of a long line, along with the maximum moment and as the loading continues the lines spread into a pattern referred to as yield-line pattern. The crack pattern which the yield lines will form depends primarily on loading and boundary condition and may be deduced logically from geometry. The theory intended for the prediction of the ultimate flexural strength, it provides upper-bound values of the shearing force and the unbalanced moment that can be transferred between the column and the slab, which depends on the crack pattern, thus, it is necessary to investigate all possible crack patterns to find the least value of the ultimate load (Hsueh 1966). The theory has been efficiently used to estimate the ultimate flexural capacities of steel- RC slab-column connections (Mortin 1989; Mortin and Ghali 1991; El-Salakawy et al. 2000; Ritchie et al. 2006; Stein 2006).

On the other hand, it is difficult to find a similar method of analysis to predict the ultimate flexural strength of FRP reinforced slabs. Unlike steel reinforcement, FRP behaves linearly till failure and does not exhibit a yield hinges, however, due to the relatively low modulus of elasticity of FRP, it

develops post-cracking deformations before flexural failure. Gar et al. (2014) suggested that the flexural behaviour of FRP-RC sections can be idealized into a trilinear behaviour as shown in Figure 2.5, where EI_g and EI_{cr} are the flexural stiffness before and after cracking, respectively. They replaced the conventional yielding moment of steel-RC slabs with an equivalent plastic moment, M_p, by simplifying the trilinear behaviour into and energy equivalent bilinear behaviour, such that, the area beneath the idealized trilinear and the simplified bi-linear responses are the same (Equation 2.47).

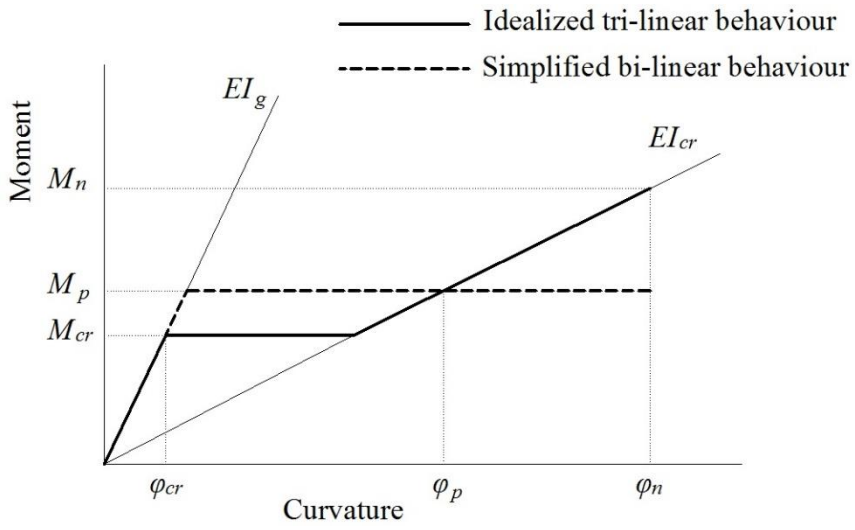

Figure 2.5: Moment curvature response of FRP-RC sections (reproduced from Gar et al. 2014)

$$M_p = 0.5M_n + 0.5\left(1 - \frac{I_{cr}}{2I_g}\right)\left(\frac{M_{cr}}{M_n}\right)M_{cr} \qquad \text{Eq. [2.47]}$$

Where M_n and M_{cr} are the nominal and cracking moment capacities of the section, respectively, and I_g and I_{cr} are the gross and cracked moment of inertia of the section, respectively.

The previous equation was used by Gouda and El-Salakawy (2016a) and El-Gendy and El-Salakawy (2016a) to estimate the flexure capacity of GFRP-RC slab-column interior and edge connections, respectively, using the following patterns (Figure 2.6).

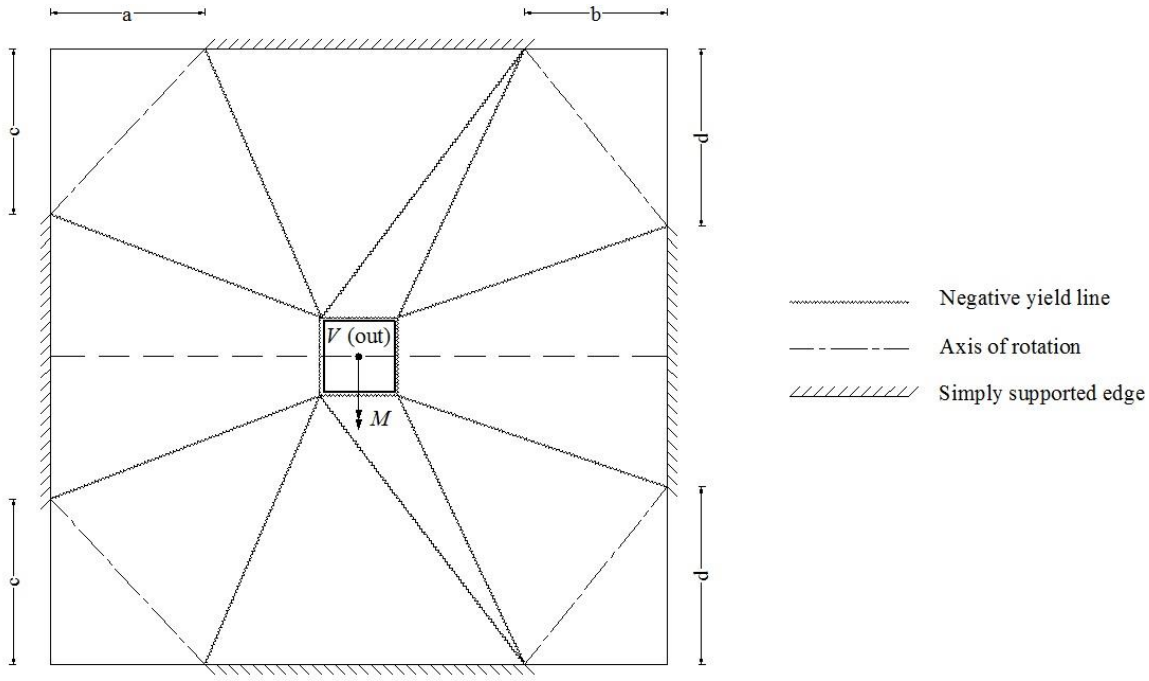

a) Gouda and El-Salakawy (2016a)

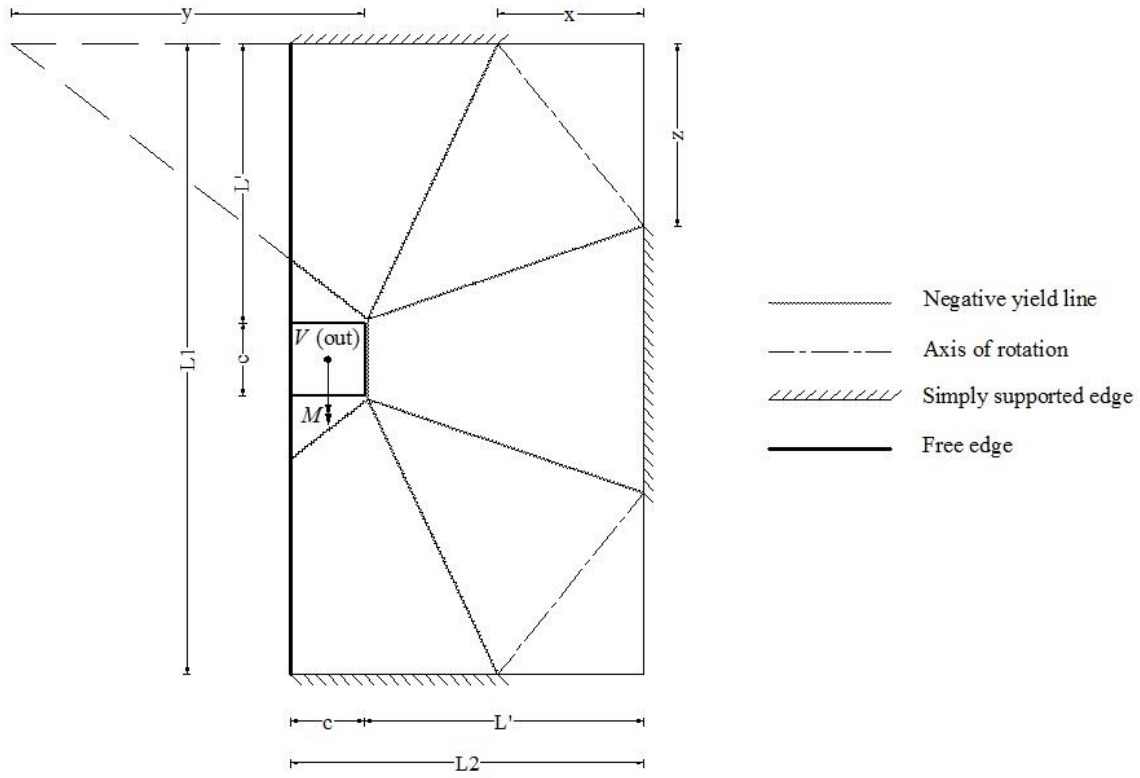

b) El-Gendy and El-Salakawy (2016a)

Figure 2.6: Different yield line patterns for FRP-RC slab-column connections

2.7. RESEARCH ON PUNCHING SHEAR OF FRP-RC SLABS

2.7.1. Previously Proposed Design Models

El-Ghandour et al. (1999) proposed a new equation based on the ACI 318-95 (ACI Committee 318 1995) equation for the punching shear capacity of steel-RC flat slabs without shear reinforcement (Equation 2.48). When using FRP reinforcement with low modulus of elasticity, unlike steel reinforcement, the concrete shear resistance becomes more sensitive to the reinforcement stiffness, as the neutral axis depth reduces significantly with low reinforcement ratios, in this case, the ACI 318-95 (ACI Committee 318 1995) overestimates the slab capacities. In order to incorporate the FRP reinforcement stiffness, they multiplied the code's equation by the term $\left(\frac{E_f}{E_s}\right)^{1/3}$, and it was found to accurately predict the punching shear capacity of the tested slabs.

$$v_{c,\,El} = v_{c,\,ACI\ 318} \times \left(\frac{E_f}{E_s}\right)^{1/3} = 0.33\sqrt{f_c'}\left(\frac{E_f}{E_s}\right)^{1/3} \qquad \text{Eq. [2.48]}$$

Matthys and Taerwe (2000) introduced the equivalent reinforcement ratio $\rho_f \frac{E_f}{E_s}$ to account for the axial rigidity of the FRP reinforcement as shown in Equation 2.49, which is a modification of the BS 8110-97 (British Standards Institution 1997) equation for steel-reinforced slabs (Equation 2.50).

$$v_{c,\,MT} = 1.36\frac{\left(100\rho_f \frac{E_f}{E_s} f_c'\right)^{1/3}}{d^{1/4}} \qquad \text{Eq. [2.49]}$$

$$v_{c,\,BS} = 0.79\left(100\rho_s\right)^{1/3}\left(\frac{400}{d}\right)^{1/4}\left(\frac{f_{ck}}{25}\right)^{1/3} \qquad \text{Eq. [2.50]}$$

Where ρ_s is the steel reinforcement ratio and f_{ck} is the characteristic compressive strength of concrete.

Ospina et al. (2003) found that, based on test results reported by other researchers, the equation proposed by El-Ghandour et al. (1999) tend to overestimate the punching capacity and produces scatter results. On the other hand, the equation proposed by Matthys and Taerwe (2000) is a reliable predictor of the punching capacity for slabs with FRP reinforcing bars or grids. However, they presented a further modification to it which leads to a slight reduction in the coefficient of variation of test-to-predicted ratios (Equation 2.51).

$$v_{c,\,Osp} = 2.77\left(\rho_f f_c^{'}\right)^{1/3}\sqrt{\frac{E_f}{E_s}} \qquad \text{Eq. [2.51]}$$

Moreover, Ospina (2005) extended the one-way shear design model proposed by Tureyen and Frosch (2003) which accounts for reinforcement stiffness (Equation 2.52), to account for the increased confinement provided by the two-way action in concrete slabs as shown in Equation 2.53, which was adopted by the ACI 440.1R-06 (ACI Committee 440 2006).

$$v_{c,\,TF} = \frac{2}{5}\sqrt{f_c^{'}}k \qquad \text{Eq. [2.52]}$$

$$v_{c,\,Osp2} = \frac{4}{5}\sqrt{f_c^{'}}k \qquad \text{Eq. [2.53]}$$

El-Gamal et al. (2005) presented a new model to predict the punching shear capacity, modified from ACI 318-05 (ACI Committee 318 2005) equation, as shown in Equations 2.54 and 2.55.

$$v_{c,\,GEB} = 0.33\sqrt{f_c^{'}}\alpha\left(1.2\right)^{N} \qquad \text{Eq. [2.54]}$$

$$\alpha = 0.5(\rho E)^{1/3}\left(1+8d/b_o\right) \quad \text{Eq. [2.55]}$$

Where N is the continuity factor taken as 0, 1, and 2 depending on the continuity of the slab along its axes and α is a parameter which is a function of the flexural stiffness of the tensile reinforcement (ρE), the perimeter of the applied load, and the effective depth of the slab.

Hassan et al. (2014a) proposed an equation for evaluating the FRP stirrup contribution, v_s, to the punching shear capacity in two-way slabs (Equation 2.56), the proposed equation is an adaptation of the shear design equation for steel in CSA/A23.3-04 (CSA 2004) as follows:

$$v_{s,\,Hass} = \frac{0.7\phi_f A_{vs} f_{fs}}{b_o s} \quad \text{Eq. [2.56]}$$

Where ϕ_f is the resistance factor for FRP reinforcement, A_{vs} is the cross-sectional area of shear reinforcement and f_{fs} is the smallest stress in the shear reinforcement from Equations 2.57 and 2.58.

$$f_{fs} = 0.004E_{fs} \quad \text{Eq. [2.57]}$$

$$f_{fs} = \frac{(0.05r_b/d_b + 0.3)\, f_{fu}}{1.5} \le f_{bend} \quad \text{Eq. [2.58]}$$

Where E_{fs} is the modulus of elasticity of FRP shear reinforcement, r_b is the radius of bend, d_b is the bar diameter, f_{fu} is the tensile strength of the straight portion of the stirrup and f_{bend} is the bend capacity of FRP stirrup.

Gouda and El-Salakawy (2016b) and El-Gendy and El-Salakawy (2016a) proposed equations to calculate the inner, $v_{c,inner(Studs)}$, and the outer, $v_{c,outer}$, punching capacity of connections with studs shear reinforcement. Equations 2.59 to 2.61 and 2.62 to 2.64 are based on the relationship between

the provisions regarding steel-RC slab-column connections with and without stud shear reinforcement in the CSA/A23.3-14 (CSA 2014a) and the ACI 318-14 (ACI Committee 318 2014), respectively.

CSA/S806-12 Provisions (Modified)

$$v_{c,inner(Studs)} = 0.041\lambda\phi_c\left(E_f\rho_f f_c^{'}\right)^{1/3} \quad \text{Eq. [2.59]}$$

$$v_{c,outer} = 0.028\lambda\phi_c\left(E_f\rho_f f_c^{'}\right)^{1/3} \quad \text{Eq. [2.60]}$$

$$v_s = \frac{\phi_f A_{vs} f_{fs}}{b_o s} \quad \text{Eq. [2.61]}$$

ACI 440.1R-15 Provisions (Modified)

$$v_{c,inner(Studs)} = 0.6\sqrt{f_c^{'}}k \quad \text{Eq. [2.62]}$$

$$v_{c,outer} = 0.4\sqrt{f_c^{'}}k \quad \text{Eq. [2.63]}$$

$$v_s = \frac{A_{vs} f_{fs}}{b_o s} \quad \text{Eq. [2.64]}$$

2.7.2. Effect of Different Parameters

2.7.2.1. Effect of Flexural Reinforcement Ratio

Under concentric loading

Lee et al. (2009) tested six slab-column interior connections, with 300 mm extension of the column stub above and below the slab. Four slabs reinforced with GFRP bars and the other two connections were reinforced with steel reinforcement. The reinforcement in all connections was distributed either uniformly or in a banded manner. All the slabs failed in punching and all behaved similarly in the uncracked state, but the GFRP slabs had much lower stiffness after first cracking compared to steel reinforced slabs, as the stiffness of the slab is a function of elastic modulus and

reinforcement ratio. The punching capacity of GFRP slabs were 26% and 22% lower than reference slabs for uniformly and banded distribution, respectively, due to the lower modulus of elasticity of GFRP bars. The banded distribution resulted in a slightly higher punching strength, smaller crack widths and more uniform distribution of strains, however, excessive concentrations of slab reinforcement was found to be not effective in improving the punching strength.

Hassan et al. (2013) tested ten full-scale square slab-column interior connections with a side length of 2,500 mm and thickness of 200 and 350 mm. The connections were divided into two series based on the slab thickness, four connections in each series were reinforced with GFRP with reinforcement ratio ranging from 0.71%-1.56%, and 0.34%-1.61% for series I and series II, respectively, and one connection reinforced with conventional steel reinforcement as a reference slab for each series. Due to the lower modulus of elasticity of FRP reinforcement compared to steel reinforcement, the punching capacity of GFRP connections was 33% and 38% lower in series I and series II, respectively, compared to the steel connection. Test results showed that increasing the reinforcement ratio from 0.71%-1.56% for series I and from 0.34%-1.61% for series II, increased the ultimate capacity by 35% and 81%, respectively

Nguyen-Minh and Rovňák (2013) tested six full-scale slab-column interior connections, three GFRP reinforced connections and three steel reinforced connections were tested, the only parameter was the reinforcement ratio, varying from 0.4%, 0.6% and 0.8%. All connections failed in punching, however, the failure of GFRP connections was more brittle and the cracks growth was faster, also, the punching capacity of GFRP reinforced connections was lower in comparison with steel reinforced connections at the same reinforcement ratio. Increasing the reinforcement ratio led to increase in the punching capacity and the post-cracking stiffness.

Under eccentric loading

Gouda and El-Salakawy (2016a) tested four full-scale slab-column interior connections. One connection was reinforced with steel reinforcement and the other three were reinforced with GFRP reinforcement with reinforcement ratio of 0.65%, 0.98% and 1.30%. Test results showed that the GFRP connection had 25% lower capacity than its counterpart steel connection at the same reinforcement ratio. Increasing the reinforcement ratio by 50 and 100% increased the punching capacity by 8.0 and 20%, respectively.

El-Gendy and El-Salakawy (2016b) tested four full-scale slab-column edge connections. Three connections reinforced with GFRP with different flexural reinforcemet ratio (0.9%, 1.35% and 1.8%), and one slab reinforced with steel with a reinforcement ratio of 0.9%. Comparsion between the reference slab and GFRP slab at the same reinforcement ratio showed that, the steel connection had 35% higher capacity than the GFRP connection due to lower modulus of elasticity of the GFRP bars, which led to larger and wider cracks, consequently, decreasing the aggregate interlock and the depth of the uncracked concrete. Also, the steel connection exhibited 51% less deflection at failure for the same reason. Increasing the rinforcement ratio in GFRP connections by 50 and 100% increased the capacity by 14 and 21%, respectively.

2.7.2.2. Effect of Shear Reinforcement

Under concentric loading

El-Ghandour et al. (2003) tested eight circular slab-column interior connections, in which three connections were reinforced with CFRP shearbands as shear reinforcement with different flexural reinforcement ratio. The shear-reinforced slabs showed larger deformability compared to slabs without shear reinforcement. The use of CFRP shearbands in a slab with GFRP flexural reinforcement of 0.38% resulted in 13.9% increase in the punching capacity. The authors proposed

the value 0.0045 as a strain limit for the shear reinforcement, as well, 0.5*d* for the maximum spacing for shear reinforcement. In addition, they assume that only 50% of the concrete resistance can be relied upon, which agrees with the ACI 318-95 (ACI Committee 318 1995) code.

Hassan et al. (2014b) tested ten full-scale slab-column interior connections. The connections were divided into two series based on the thickness, 200 mm or 350 mm. All the slabs had GFRP flexural reinforcement but only seven slabs had GFRP or CFRP closed, spiral or bundled spiral stirrups as shear reinforcement. Test results showed enhancement in the performance by reducing the brittleness of the failure when FRP stirrups were used as shear reinforcement. Furthermore, it increased the shear capacity of the specimens by an average of 29% and 23% for series I and series II, respectively. However, for specimens with low reinforcement ratio, the author concluded that, the punching shear capacity is governed by the flexural reinforcement rather than shear reinforcement, and the use of FRP stirrups may not exhibit a significant increase in punching shear capacity.

Under eccentric loading

Zaghloul (2007) tested half-scale interior and edge connections reinforced with GFRP bars. CFRP shear reinforcement in form of rails similar to steel stud reinforcement were used. Results showed a higher capacity for the shear-reinforced interior connections up to 30%, however, the increase was only 9% for the edge connections.

A new type of GFRP studs with headed ends was used by Gouda and El-Salakawy (2016b) as shear reinforcement in interior connections. They arranged the headed studs on eight lines around the central column (two orthogonal lines at each column corner) forming five and seven parallel peripheral rows of studs (eight studs in each row) in their Connections R-15-75 and R-15-50, respectively, with spacing between studs' rows of 120 and 80 mm (0.75 *d* and 0.50 *d*), respectively.

As such, in both connections, the studs extended in the slab such that the critical section outside the shear-reinforced zone is located at 3.90 *d* from the column face. The authors reported an increase in both stiffness and capacity of the shear-reinforced connections; however, the GFRP studs were not able to prevent the brittle punching shear failure and both connections failed inside the shear-reinforced zone. Moreover, the heads of the shear studs were also damaged.

Similar arrangement of the same type of GFRP shear reinforcement was used in GFRP-RC slab-column edge connections by El-Gendy and El-Salakawy (2016a). They demonstrated that the connection with seven parallel peripheral rows of studs (studs spaced at 0.50 *d*) experienced a flexural mode of failure with substantial deformability; however, the connection with only five parallel peripheral rows of studs (studs spaced at 0.75 *d*) failed in a mixed flexural/punching mode.

2.7.2.3. Effect of Concrete Compressive Strength

Under concentric loading

Zhang et al. (2005) carried out experimental study on a high strength concrete two-way square slabs reinforced with GFRP bars with a side length of 1,900 mm, the thickness of the slabs was 150 mm and the reinforcement ratio of the slabs was around 1.10%. They concluded that, the use of HSC increased the ultimate punching capacity but at a rate much less than a rate of the square root of the compressive concrete strength.

Hassan et al. (2013) tested ten full-scale interior slabs with a length of 2,500 mm and thickness of 200 and 350 mm, specimens were divided into two series based on the slab thickness (200 mm, or 350 mm). One slab in each series was fabricated with high strength concrete of 75.8 MPa to study the influence of HSC. Results showed improvement in the ultimate capacity by 27% and 7% increase for the HSC specimens with 200 mm and 350 mm thickness, respectively. Also, it showed

lower deflections at the same load level than other GFRP-RC with NSC. The author concluded that compressive strength had a significant effect on the initial stiffness, it showed increase by 22% and 51% for the HSC specimens with 200 mm and 350 mm thickness, respectively. However, the post-cracking stiffness was similar to that of NSC.

Under eccentric loading

Gouda and El-Salakawy (2016a) reported that increasing the concrete compressive strength from 42 MPa to 70 MPa (67% increase) resulted in a 5% and 21% increase in the punching capacity and deflection at failure of GFRP-RC slab-column interior connection, respectively.

2.7.2.4. Effect of Moment-to-Shear Ratio

Zaghloul and Razaqpur (2004) tested seven 1,760 mm square half-scale slab-column interior connection under eccentric loading. Three connections had different moment-to-shear ratio as the only parameter with the values of (0.0 m, 0.22 m, and 0.30 m). Test results showed that increasing the moment-to-shear ratio from 0.0 m to 0.22 m and 0.3 m causes a reduction of the punching capacity by 27 and 43%, respectively.

Gouda and El-Salakawy (2016b) tested three full-scale slab-column interior connections with flexural reinforcement ratio of 0.65% and subjected shear and unbalanced moment with different moment-to-shear ratio (0.0 m, 0.15 m and 0.3 m). Increasing the moment-to-shear ratio resulted in a reduction in the vertical load capacity. The vertical load reduced by approximately 17 and 32% when the moment-to-shear ratio was increased from 0.0 to 0.15 and 0.3 m, respectively

El-Gendy and El-Salakawy (2016a) tested three full-scale slab-column edge connection with flexural reinforcement ratio of 0.9% to investigate the effect of different moment-to-shear ratio (0.2, 0.4 and 0.6 m). Results showed that increasing the moment-to-shear ratio from 0.2 to 0.4 and

0.6 m resulted in a decrease in the punching capacity by 7% and 33%, respectively, due to the increased shear stresses at the critical shear perimeter. Also, it decrases the number of cracks at failure on the tension face of the slab, and pushed the failure surface away from the column face and led to a flatter angle of the diagonal crack with the horizontal level. Furthermore, it decreased the deflection at failure by 21% and 62%, respectively.

CHAPTER 3: EXPERIMENTAL PROGRAM

3.1. GENERAL

The purpose of the experimental work is to study the behaviour of RC slab-column interior connections under different parameters. Two variables were investigated; the flexural reinforcement ratio when HSC is used and the type of GFRP shear reinforcement (headed studs and corrugated bars) when NSC is used. This chapter presents the details of the experimental work through describing the test connections, the material properties, instrumentations, test set-up and test procedure.

3.2. TEST CONNECTIONS

Six full-scale slab-column interior connections were constructed and tested to failure. The dimensions and flexural reinforcement ratios of the connections were obtained by performing an elastic analysis of a multistory parking structure having three 6.5-m square bays, according to the Canadian standards (CSA 2014a; CSA 2012), where applicable (Appendix A). The specified loads were obtained in accordance with the National Building Code of Canada (NRCC 2015). The structure was designed to carry specified dead and live loads of 5.8 and 2.4 kN/m^2, respectively, resulting in a moment-to-shear ratio of 0.15 m and a service load of 295 kN. The resulting dimensions of the slab were 2,600×2,600×200 mm for all connections. These dimensions represent, with a proper approximation, the region of negative moment around interior column and bounded by the lines of contra-flexure. The lines of contra-flexure are assumed to be at a distance of 0.2l away from the centrelines of the columns, where l is the span between centrelines of columns. However, 2,800×2,800×200 mm slabs were cast for all connections, in order to allow for supporting clearance. The typical dimensions and flexural reinforcement layout for the test connections are shown in Figure 3.1. For all connections, the columns extended 1,000 mm above

and below the slab with 300-mm square cross-section. The columns were adequately reinforced with 4-20M conventional steel reinforcement and 10M steel stirrups to prevent any premature failure, as shown in Figure 3.2. The connections were divided into two series; each series consisted of three connections. Series 1 investigated the effect of flexural reinforcement ratio on connections made of HSC, while Series 2 investigated the effect of GFRP shear reinforcement type on connections made of NSC. In Series 1, the flexural reinforcement ratio resulting from the analysis (1.0%) was used in one connection and was multiplied by 1.5 (ρ_f = 1.5%) and 2.0 (ρ_f = 2.0%) and used for the two other connections to study the effect of flexural reinforcement ratio. The 1.0% flexural reinforcement ratio was then used for all connections in Series 2. The designation of the connections consists of three parts. The first part indicates the concrete strength ("N" for NSC and "H" for HSC), while the second part is a number reflecting the average flexural reinforcement ratio of the two orthogonal directions ("1.0" for ρ_f = 1.0%, "1.5" for ρ_f = 1.5% and "2.0" for ρ_f = 2.0%). The third part refers to the type and number of peripheral rows of shear reinforcement (XX for no shear reinforcement, S5 for five rows of headed studs, S6 for six rows of headed studs and C5 for 5 rows of vertical stems of corrugated bars). For example, N-1.0-S5 denotes a connection made of NSC with a flexural reinforcement ratio of 1.0% and five peripheral rows of headed studs. The details of the connections are listed in Table 3.1.

All connections were reinforced in flexure with a single orthogonal mesh of SC-GFRP bars in the tension side only. Series 1 connections (without shear reinforcement) were designed to fail in shear. On the other hand, based on the results of Gouda and El-Salakawy (2016b), it was decided to use twelve lines of shear reinforcement. Therefore, at each column corner, the shear reinforcement was arranged on three lines, two parallel to the column faces and one at 45°. In Connection N-1.0-S5 with shear studs, five peripheral rows of size No. 13 spaced at 0.75 *d* (120

mm) with the distance between the column face and the first peripheral studs' row of 0.40 *d* (64 mm) were used. For Connection N-1.0-C5, similar arrangement to that of the headed studs in Connection N-1.0-S5 was used, as shown in Figures 3.3 and 3.4. However, the spacing between the column face and the first vertical stems of the corrugated bars was 40 mm (0.25 *d*) and a smaller bar diameter (9.5 mm) was selected due to manufacturing constraints and to provide the longest practical vertical stem (between the two bends) with a reasonable capacity. A larger bar diameter will result in a shorter vertical stem and, consequently, a higher possibility of missing diagonal cracks (inadequate anchorage). Based on the results of Connection N-1.0-S5, which experienced punching failure outside the shear-reinforced zone as will be discussed later, it was decided to extend the critical shear section outside the shear-reinforced zone by adding another row of headed studs in Connection N-1.0-S6. Accordingly, as shown in Figure 3.3, the critical shear section outside the shear-reinforced zone was located at 624 mm (3.90 *d*), 600 mm (3.75 *d*) and 744 mm (4.65 *d*) from the column face for Connections N-1.0-S5, N-1.0-C5 and N-1.0-S6, respectively. The choice of the type of shear reinforcement should be based on performance, simplicity, ease of installation and availability. That being said, it is worth mentioning that, regarding the ease of installation, the individual headed studs were easily manipulated in the column vicinity with minimal interference with the longitudinal reinforcement. On the other hand, installing the corrugated bars was very challenging. The fixed spacing of the vertical stems and the horizontal portions of the corrugated bars makes it very difficult, if at all possible, to maintain a uniform spacing of the longitudinal reinforcement.

Table 3.1: Details of test connections

Series	Connection	Flexural reinforcement		Shear reinforcement		
		ρ_f [a] (%)	S (mm)	Type	No. of rows	Ratio (%)
1	H-1.0-XX	0.98	128	N/A	N/A	N/A
	H-1.5-XX	1.46	85			
	H-2.0-XX	1.93	64			
2	N-1.0-S5	0.98	128	Headed studs	5	0.69
	N-1.0-S6	0.98	128		6	0.69
	N-1.0-C5	0.98	128	Corrugated bars	5	0.39

[a] Average reinforcement ratio in both orthogonal directions

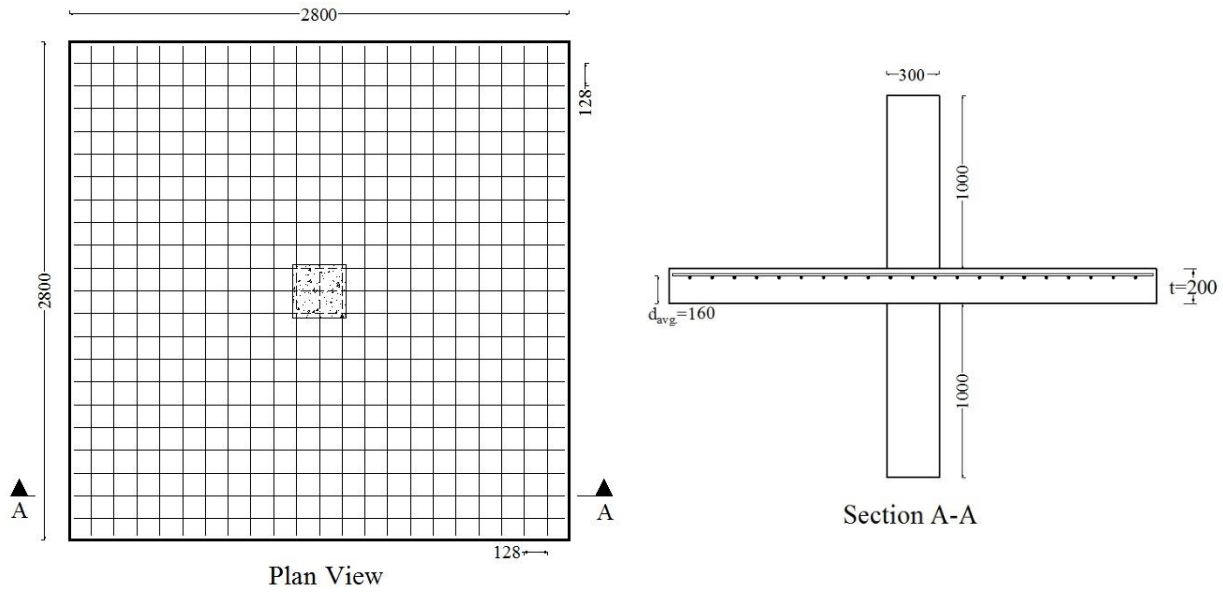

a) Connections H-1.0-XX, N-1.0-S5, N-1.0-S6 and N-1.0-C5

Figure 3.1: Dimensions and flexural reinforcement layouts (all dimensions are in mm)

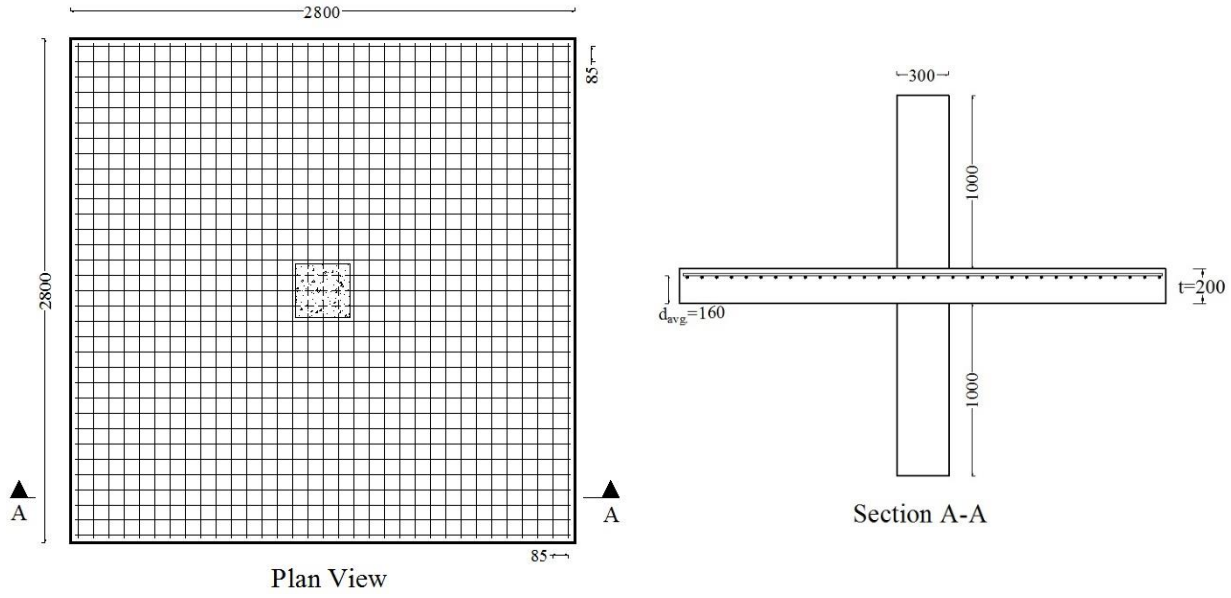

b) Connection H-1.5-XX

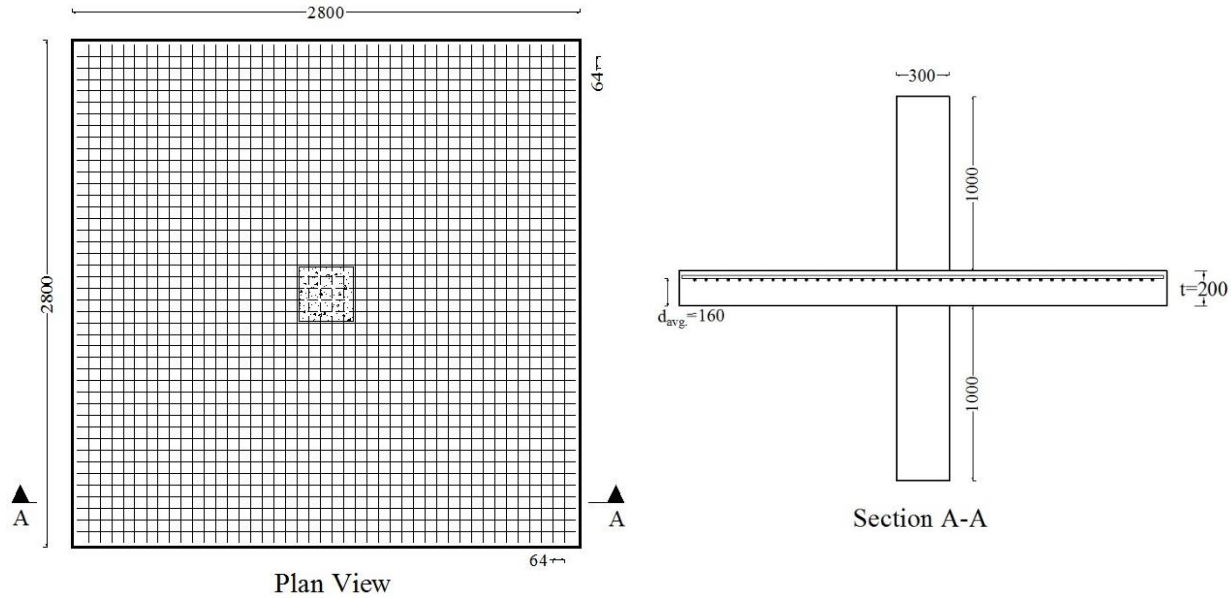

c) Connection H-2.0-XX

Figure 3.1: Dimensions and flexural reinforcement layouts - continued (all dimensions are in mm)

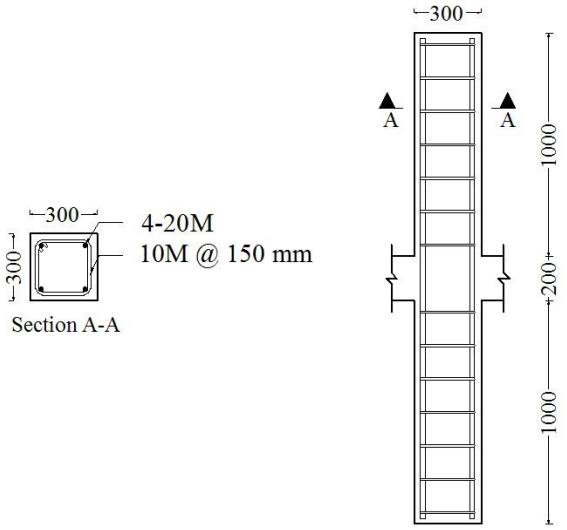

Figure 3.2: Typical column reinforcement (all dimensions are in mm)

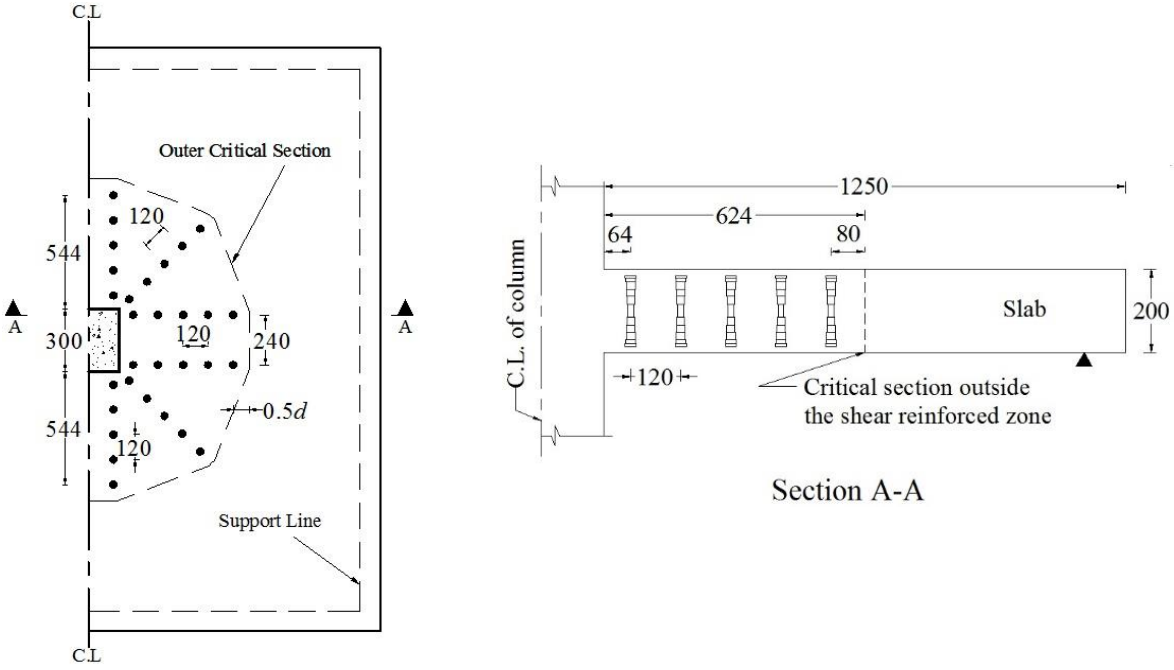

a) Connection N-1.0-S5

Figure 3.3: Shear reinforcement layout (all dimensions are in mm)

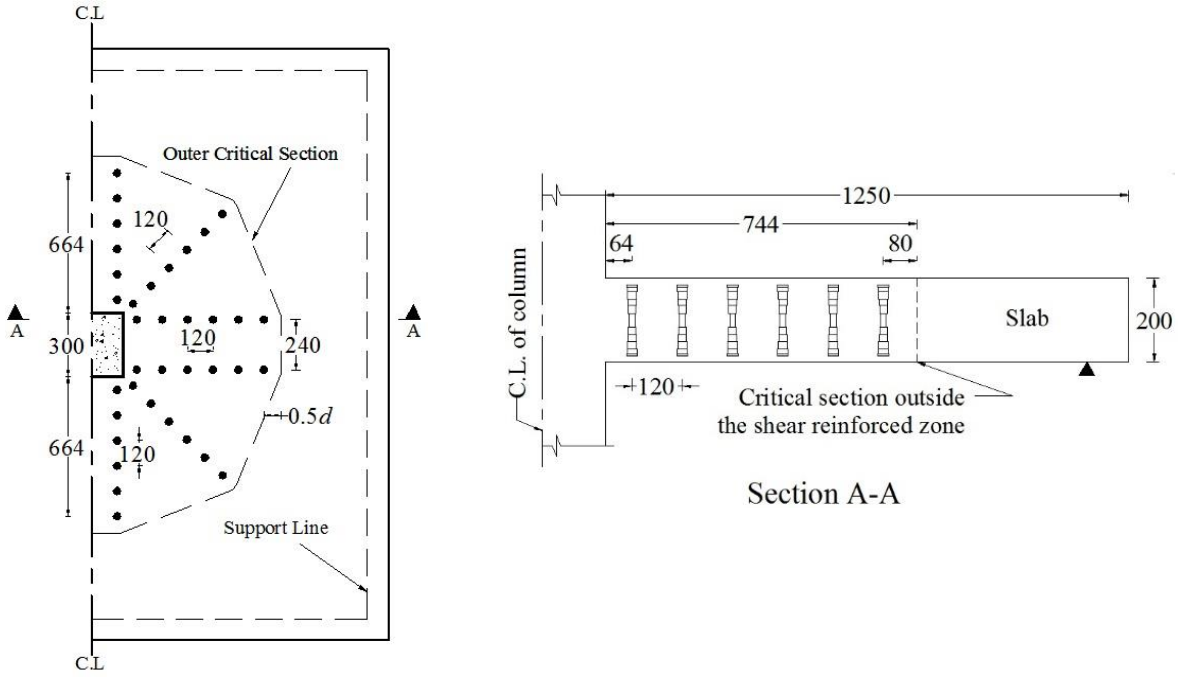

b) Connection N-1.0-S6

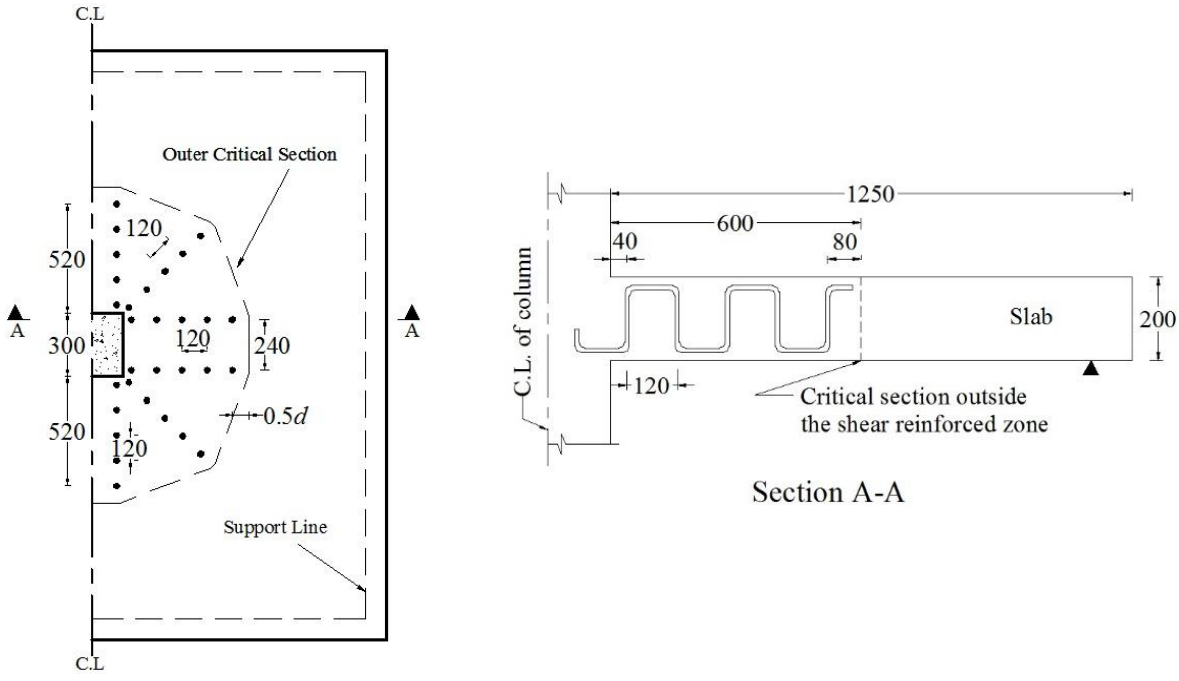

c) Connection N-1.0-C5

Figure 3.3: Shear reinforcement layout - continued (all dimensions are in mm)

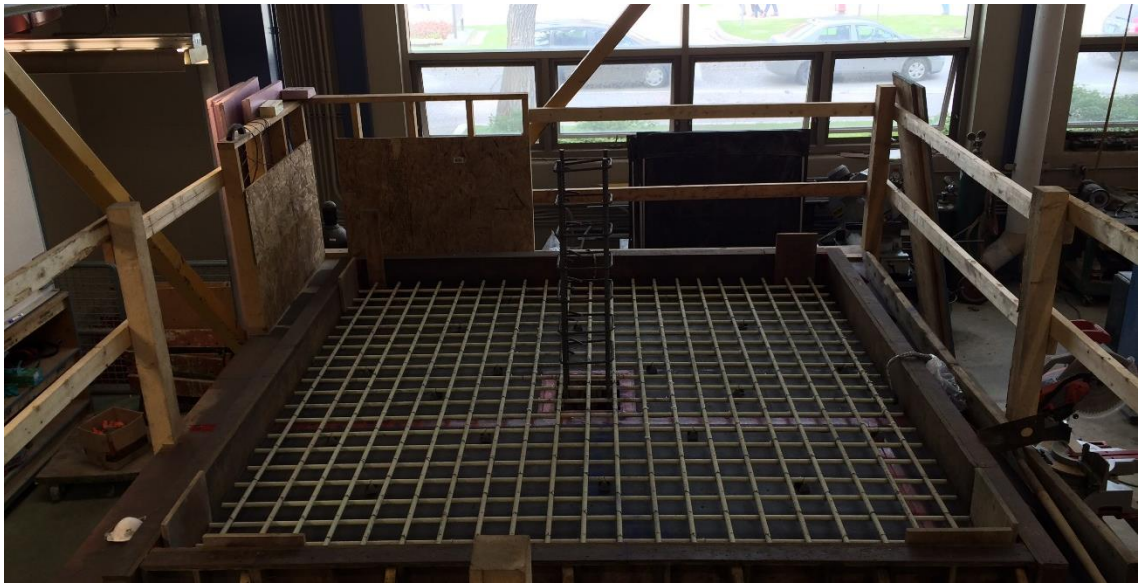

a) Connection H-1.0-XX

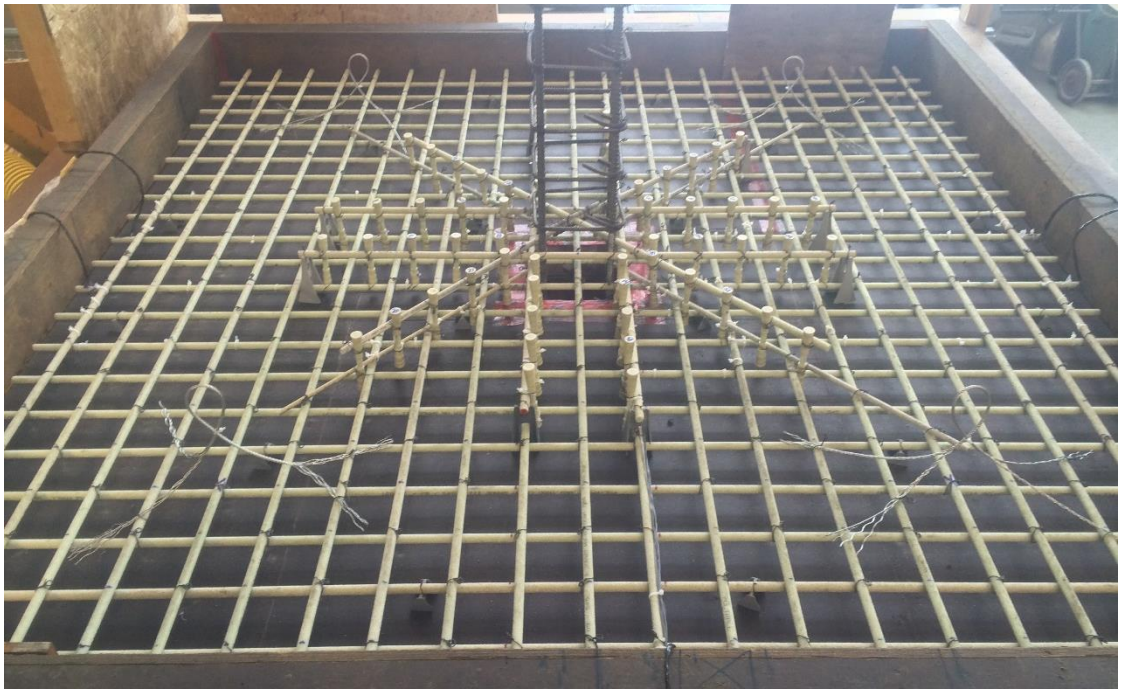

b) Connection N-1-0-S5

Figure 3.4: Reinforcement configuration

c) Connection N-1.0-S6

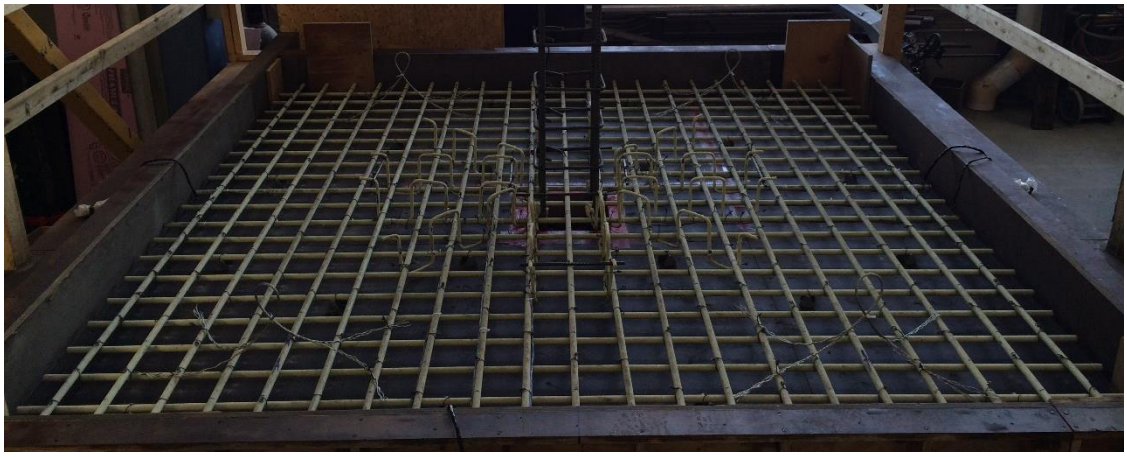

d) Connection N-1.0-C5

Figure 3.4: Reinforcement configuration - continued

3.3. MATERIALS

3.3.1. Concrete

All connections were designed and constructed using normal-weight, ready-mix concrete with a maximum aggregate size of 19 mm and a target compressive strength after 28 days of 40 and 80 MPa for normal and high strength concrete, respectively. All specimens were cast and wet-cured in the laboratory for 7 days. The actual concrete compressive and tensile strength was determined on the day of testing based on standard cylinders (100 × 200 mm and 150 × 300 mm for the compressive and tensile splitting tests, respectively) in accordance with the CSA A23.1/A23.2-14 (CSA 2014b). The obtained concrete strength for all connections is listed in Table 3.2.

Table 3.2: Concrete properties

Series	Connection	Concrete compressive strength, f'_c (MPa)	Concrete tensile strength, f_t (MPa)
1	H-1.0-XX	80	4.3
	H-1.5-XX	84	4.5
	H-2.0-XX	87	4.6
2	N-1.0-S5	43	3.5
	N-1.0-S6	43	3.7
	N-1.0-C5	43	3.7

3.3.2. Reinforcement

Straight No.16 sand-coated (SC) GFRP bars were used as longitudinal reinforcement for all connections. Moreover, No.20M and No.10M deformed steel bars and stirrups, respectively, were used to reinforce the column in all connections. Two newly-developed types of GFRP shear reinforcement were used: studs with headed ends and corrugated bars (Pultrall Inc. 2015). The studs with headed ends comprised 170-mm long No.13 GFRP bars with 70-mm long cast-on

headed ends. The heads were made of a thermoplastic matrix reinforced with short discrete glass fibres. The headed ends were tapered with an outer diameter of 26 mm (2 times the bar diameter) in steps towards the bar (Figure 3.5). The corrugated bars, on the other hand, were No.10 SC-GFRP bent bars with a 90° angle between the vertical stems and the horizontal portions. The total height of a corrugated bar was 160 mm, while the distance between the vertical stems was 120 mm (0.75 *d*) as shown in Figure 3.5. The properties of the flexural GFRP reinforcement were obtained according to ASTM D7205-16 (ASTM 2016), while those of the shear reinforcement were provided by the manufacturer as listed in Table 3.3.

Table 3.3: Mechanical properties of the used GFRP reinforcement

Bar material	Bar size	Nominal diameter (mm)	Nominal area (mm^2)	Tensile strength (MPa)	Tensile modulus (GPa)	Ultimate strain (%)
SC-GFRP (straight)	No.16	15.9	198.0	1,685	65	2.6
GFRP (headed studs)	No.13	12.7	126.7	552[a]	68	0.8[a]
SC-GFRP (corrugated bars)[b]	No.10	9.5	71.3	1,280	52	2.5

[a] Usable design stress/strain provided by the manufacturer (corresponds to a pull-out load capacity of 70 kN)
[b] Properties are for the straight portion of the bar

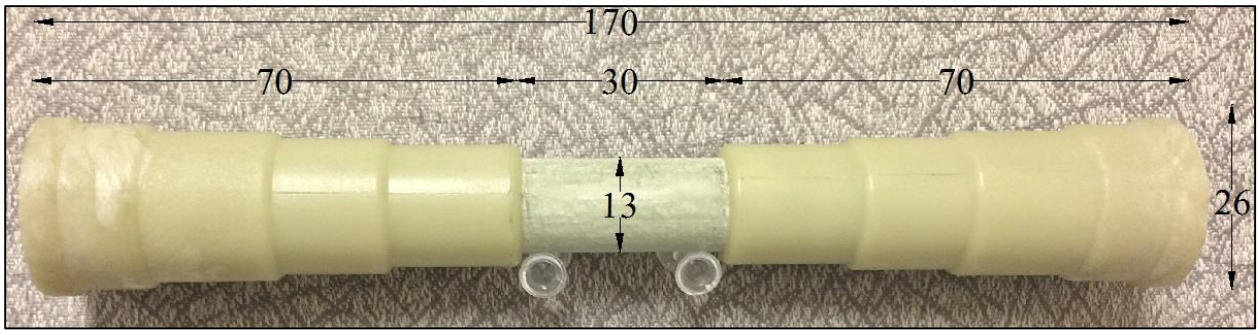

a) GFRP headed studs

Figure 3.5: Details of shear reinforcement (all dimensions are in mm)

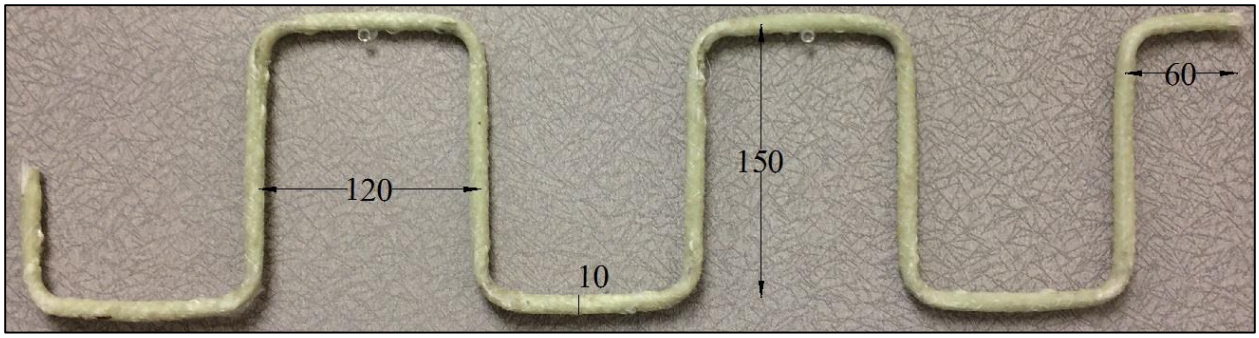

b) SC-GFRP corrugated bars

Figure 3.5: Details of shear reinforcement - continued (all dimensions are in mm)

3.4. TEST SET-UP AND PROCEDURE

Figure 3.6 shows the details of the test setup. All connections were tested in an upside-down position with respect to their position in a real structure. The slabs were simply supported (with their corners free to lift) on a rigid supporting frame consisting of four heavy steel I-beams. A 20-mm wide steel plate was used as a bearing plate between the slab and the supporting beams and neoprene strips were inserted on top of the supporting frame to ensure a uniform distribution of the loads along the edges. This arrangement allows the vertical shear force to be applied from top to bottom using a 1,000-kN hydraulic actuator; therefore, tension cracks appeared at the bottom surface of the slab. The unbalanced moment was simulated by two lateral forces applied near the tips of the upper and lower columns through two hydraulic jacks. A moment-to-shear ratio of 0.15 m was kept constant during the test for all connections. To allow for the horizontal and vertical movement of the column ends, three roller plates were placed between the loading equipment and the column tips. During the test, the propagation of cracks was carefully marked at 20 kN increments.

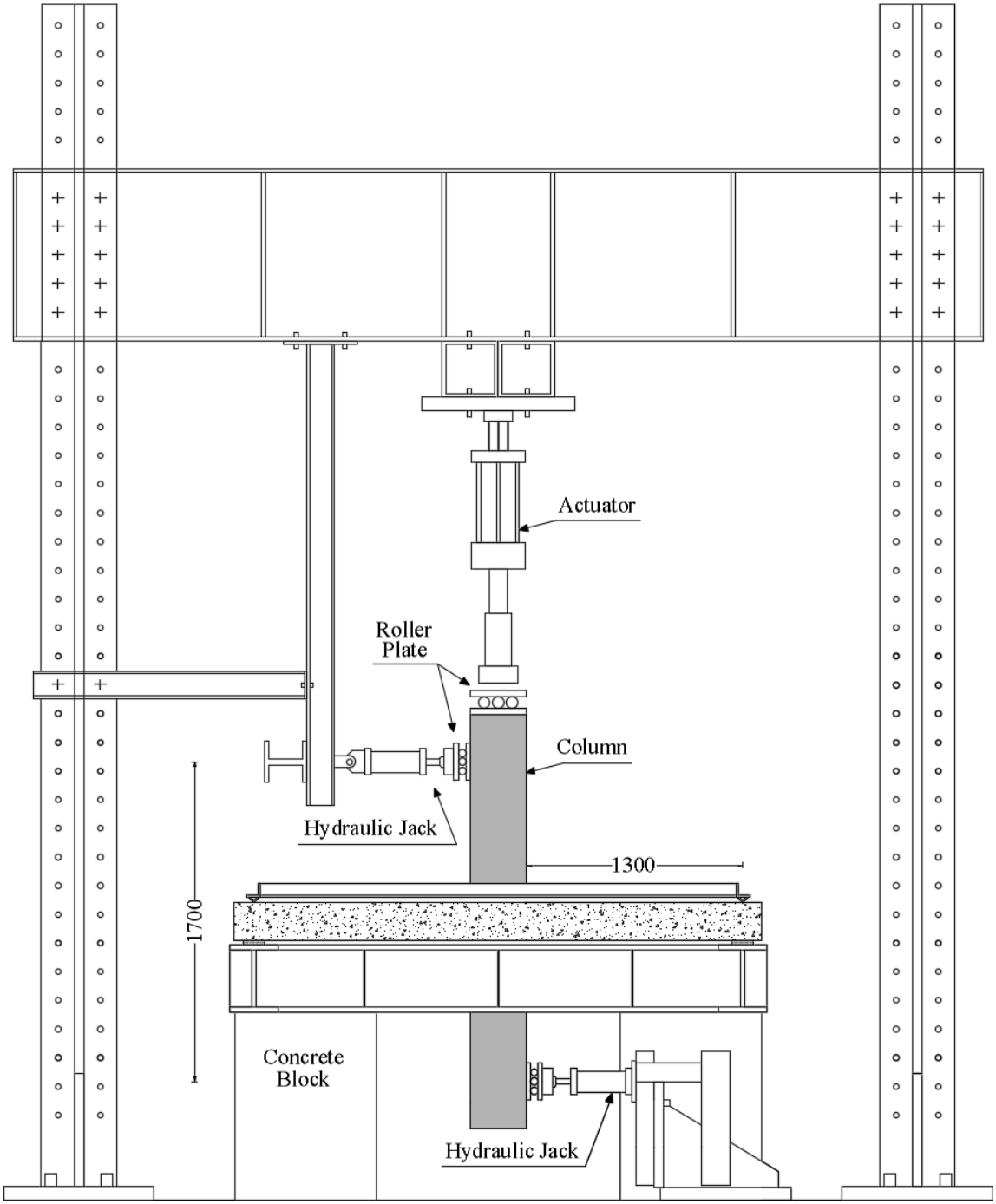

a) Schematic drawing of the set-up

Figure 3.6: Test setup (all dimensions are in mm)

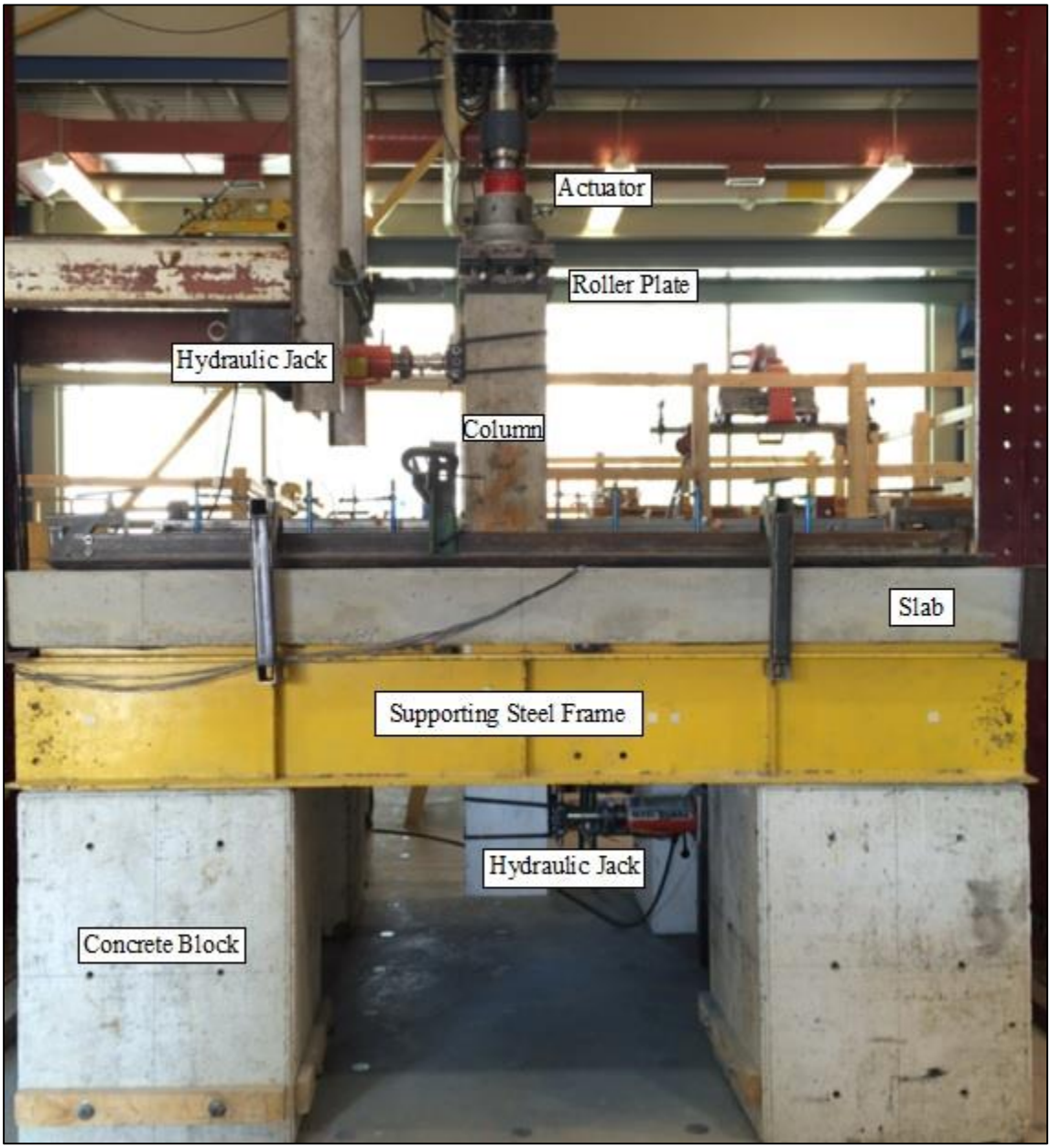

b) Photo of the set-up

Figure 3.6: Test setup - continued (all dimensions are in mm)

3.5. INSTRUMENTATION

To monitor the behaviour of all connections during the test, internal (reinforcement strain gauges) and external (load cells, PI-gauges, concrete strain gauges and linear variable displacement transducers) instrumentation provided a real-time recording of applied loads, strains and displacements. A data acquisition system (DAQ) was used to record all the readings for all instrumentation. Also, the propagation of cracks was monitored visually and marked carefully during the test. Details of instrumentations are discussed in the following section.

3.5.1. Reinforcement Strain Gauges

To measure the developed strains, electrical strain gauges (6-mm) were attached to the flexural reinforcing bars passing through the column in both directions at critical locations as shown in Figure 3.7. Moreover, electrical strain gauges were attached to the mid height of the stems for the shear reinforcement (studs and corrugated bars) as shown in Figure 3.8.

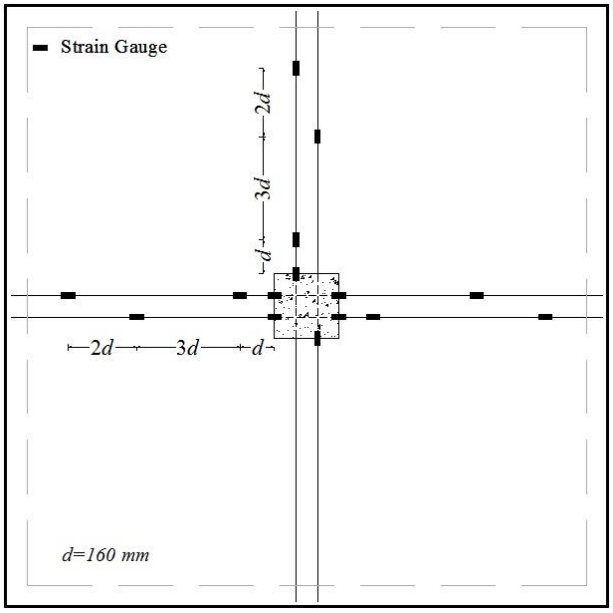

Figure 3.7: Typical strain gauges layout on the flexural reinforcement

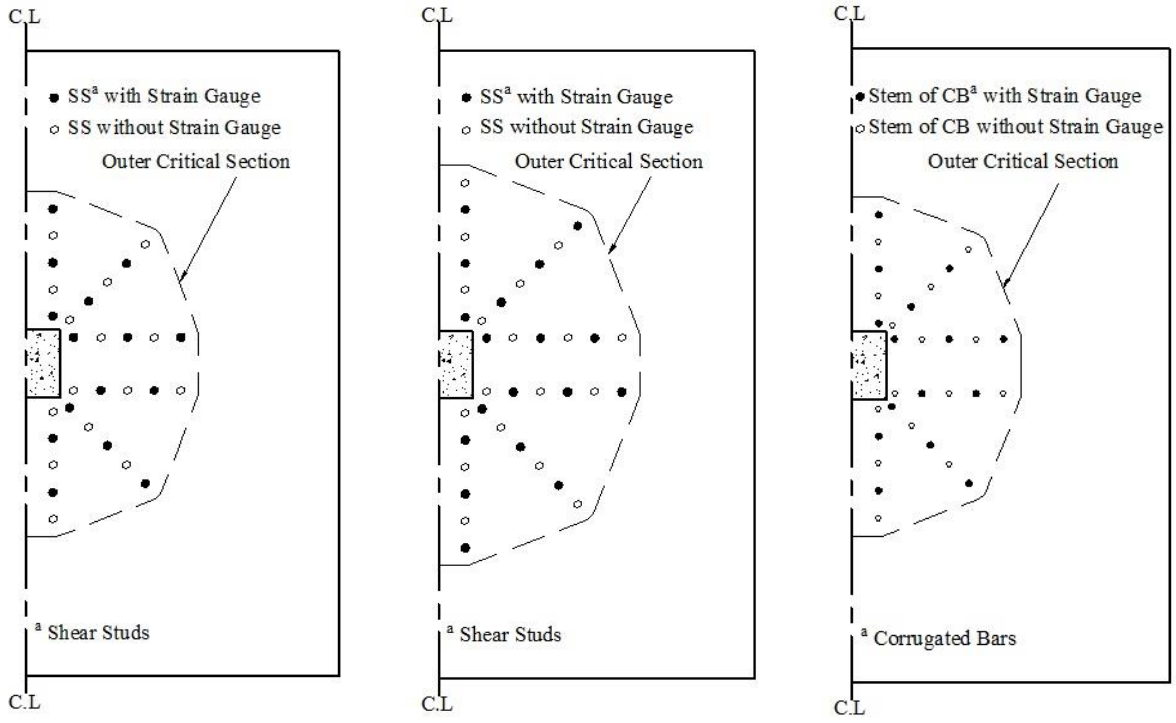

N-1.0-S5 N-1.0-S6 N-1.0-C5

Figure 3.8: Strain gauges layout on the shear reinforcement

3.5.2. PI-Gauges and Concrete Strain Gauges

Figure 3.9 shows the typical arrangement of PI-gauges/concrete strain gauges for all connections at the compression side of the slab near the column face in order to capture the maximum concrete strains in both orthogonal directions.

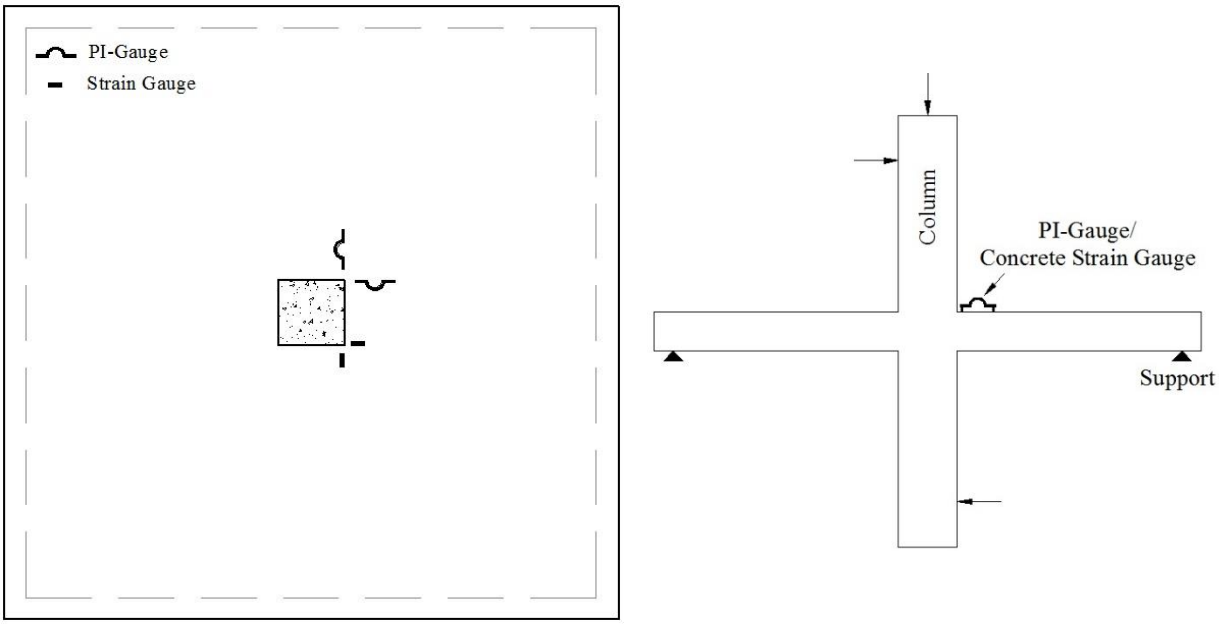

Figure 3.9: Typical PI-gauges/ concrete strain gauges arrangement

3.5.3. Load Cells

Three load cells were used in the test set-up; one was attached to the actuator to measure the column axial load and two were attached to the two hydraulic jacks to measure the lateral force at the column's tips

3.5.4. Linear Variable Displacement Transducers (LVDTs)

A group of eight LVDTs were used to capture the deflection profile in the direction of the applied moment, in addition to four LVDTs in the perpendicular direction as shown in Figure 3.10.

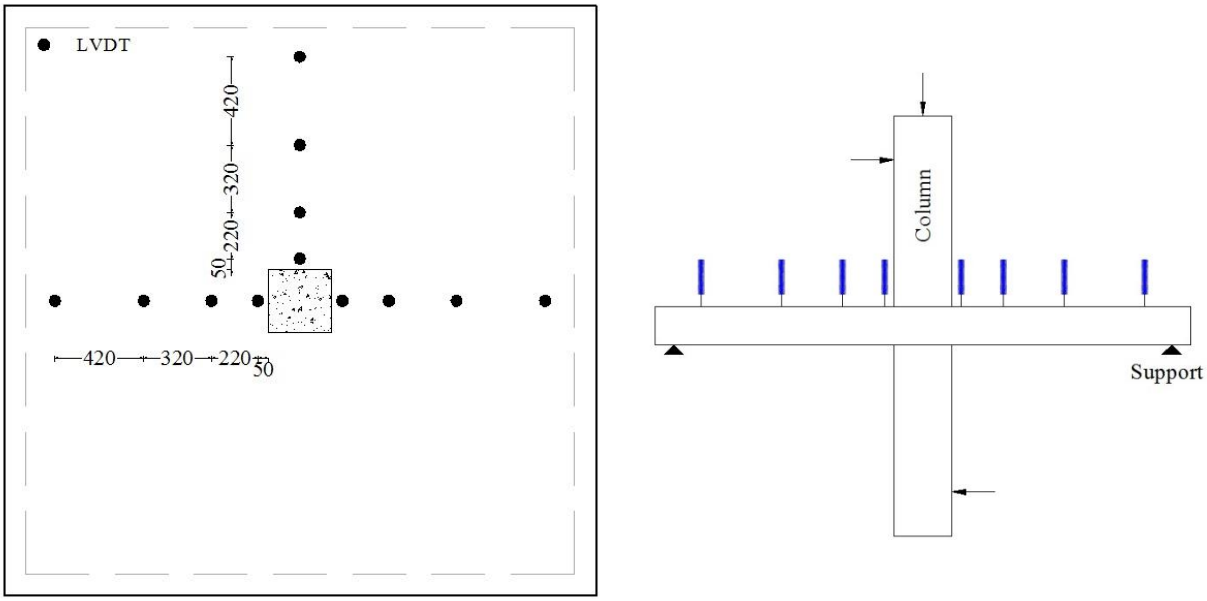

Figure 3.10: Typical arrangement of LVDTs (all dimensions are in mm)

CHAPTER 4: EXPERIMENTAL RESULTS AND DISCUSSION

4.1. GENERAL

This chapter presents the experimental results and discussion for all test connections. The behaviour of test connections is presented in terms of mode of failure and cracking pattern, deflections, strain measurements in both reinforcement and concrete, the ultimate capacity and the predictions of different codes. The test results are divided into two separate sections, each devoted to one of the series described in Chapter three.

4.2. SERIES 1: EFFECT OF FLEXURAL REINFORCEMENT RATIO

Three connections with three different reinforcement ratios of 1.0, 1.50 and 2.0% were constructed and tested to study the effect of GFRP flexural reinforcement ratio on slab-column interior connections made of HSC. Furthermore, the results of the three HSC connections were compared, when applicable, to the results of a similar slab-column interior connection made of NSC from a previous work (Gouda 2015), Connection G-0.98-N-15-XX, to investigate the effect of concrete compressive strength, and it will be referred to as Connection N-1.0-XX*.

4.2.1. Mode of Failure and Cracking Pattern

The three connections in Series 1 failed in a brittle punching shear mode, with no signs of flexural failure (no concrete crushing at the compression face of the slab). The punching failure was characterized by a sudden drop in the vertical load with the punching of the column through the slab. Figure 4.1 shows the cracking pattern on the tension face of Series 1 connections at failure. All connections exhibited similar cracking pattern and behaviour in terms of crack initiation and propagation. As the load progressed, several types of cracks were observed. The first crack was observed in the slab at the column corner, i.e., location of maximum bending moment, at the

vertical cracking loads listed in Table 4.1. As the load increased, radial cracks developed from the column vicinity and radiated in all directions towards the supports. At a relatively higher load, approximately 45-50% of the failure load, a series of circumferential cracks appeared connecting the radial cracks together in all connections. The behaviour is similar to that experienced by Connection N-1.0-XX* made of NSC. It was observed that, the average crack spacing is closely related to the spacing of slab flexural reinforcement; closer bar spacing resulted in higher crack density because of increasing the reinforcement ratio. On the other hand, although failed at a higher vertical load, Connection H-1.0-XX (made of HSC) showed less cracks at failure compared to Connection N-1.0-XX* (made of NSC). This may be attributed to the higher cracking load associated with the connection made of HSC, which delayed the initiation of flexural cracks. Increasing the concrete strength from 38 to 80 MPa (111% increase) increased the cracking load by 26%.This behaviour is similar to that reported by Marzouk et al. (1998) who tested steel-RC slab-column interior connections made of NSC and HSC and subjected to a combination of shear force and unbalanced moment.

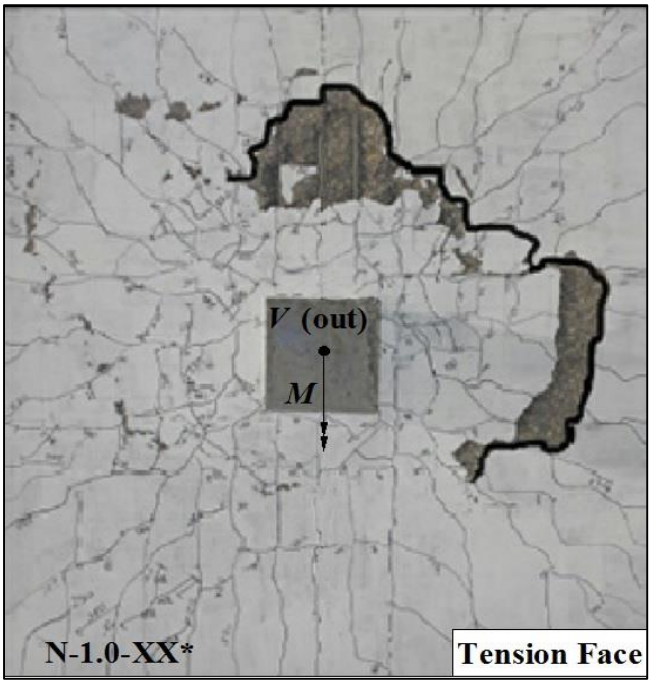

a) N-1.0-XX*

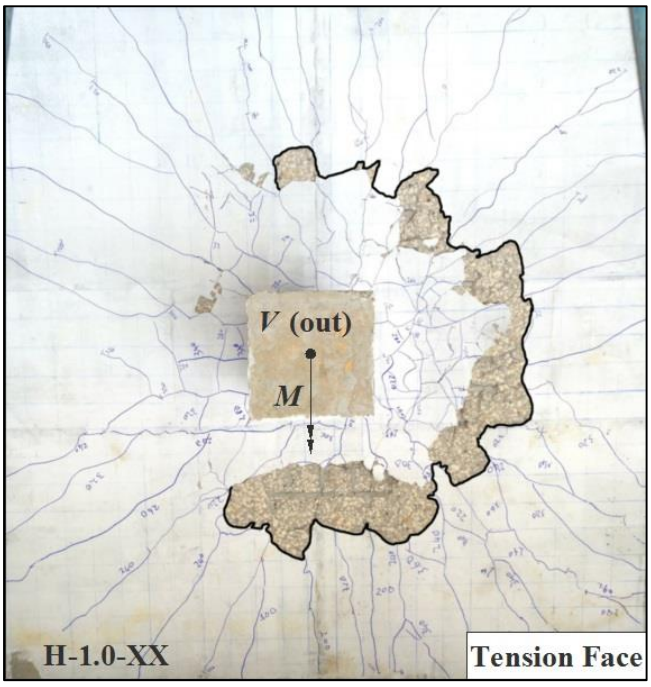

b) H-1.0-XX

Figure 4.1: Cracking pattern on the tension face of the slab at failure (Series 1)

c) H-1.5-XX

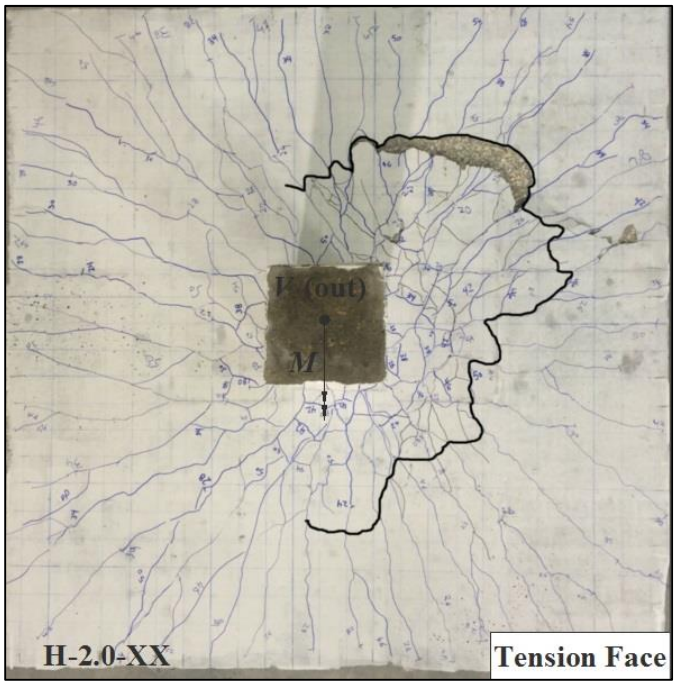

d) H-2.0-XX

Figure 4.1: Cracking pattern on the tension face of the slab at failure - continued (Series 1)

After the test, saw-cuts were made in the three slabs at the column face in the direction of the unbalanced moment to examine the diagonal cracking pattern inside the slabs. Figure 4.2 shows the cross-sections and schematic drawings of the cracks at failure in the three slabs. It is evident that the main shear crack is confined to the side of the slab where the unbalanced moment is acting in the same direction as the shear force (heavier-loaded side). The failure cone angle was calculated assuming a cone radius measured from the face of the column to the intersection of shear crack with the centre of the flexural reinforcement. It should be noted that, increasing the reinforcement ratio decreased the cone radius; consequently, increased the cone angle, i.e., led to a steeper inclination of the shear crack. The approximate measured cone radiuses were 1.72, 1.56, and 1.14 *d* and the corresponding cone angles were 30°, 33°, and 41° for connections H-1.0-XX, H-1.5-XX and H-2.0-XX, respectively. Similar behaviour was observed by Matthys and Taerwe (2000), who carried out punching tests on square FRP-RC slabs under concentric loading.

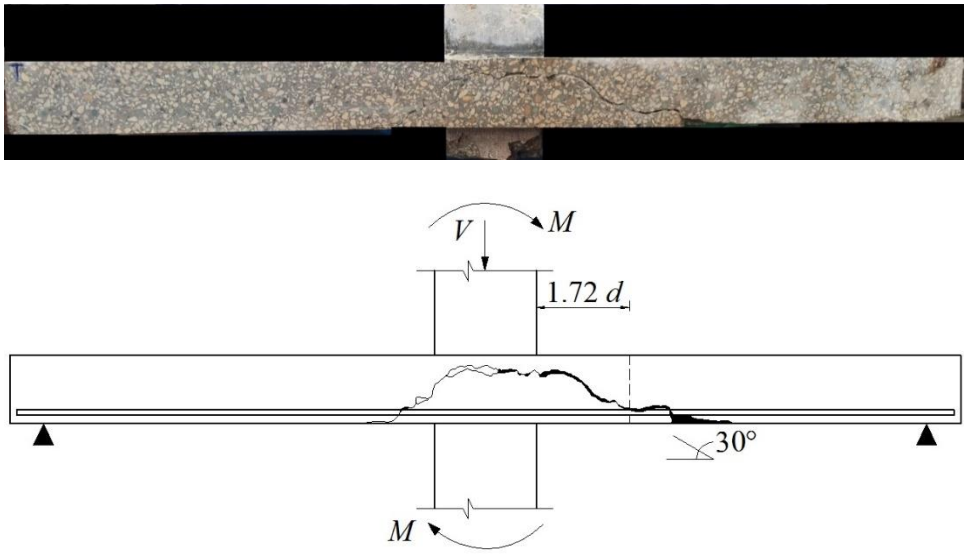

a) H-1.0-XX

Figure 4.2: Cross-section and schematic drawing of internal cracks (Series 1)

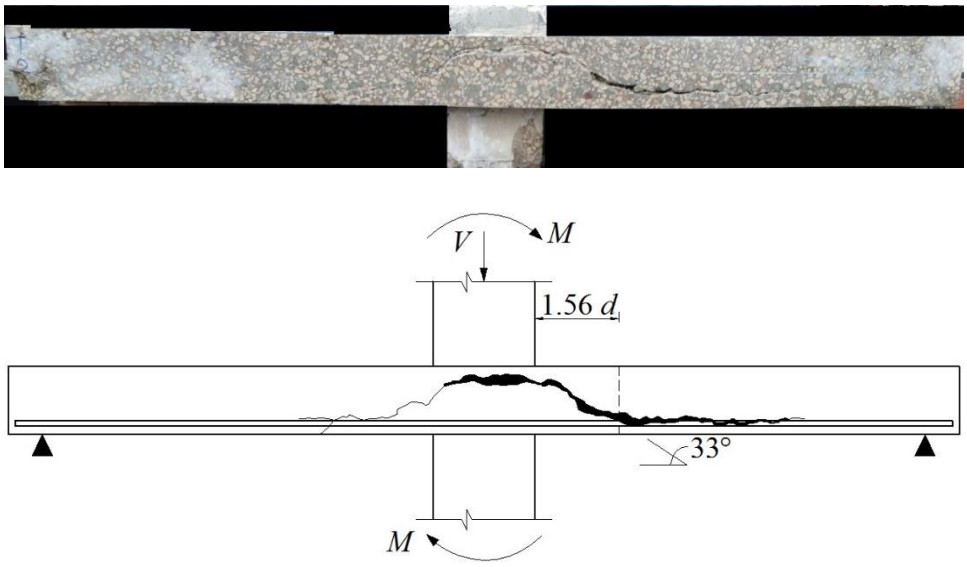

b) H-1.5-XX

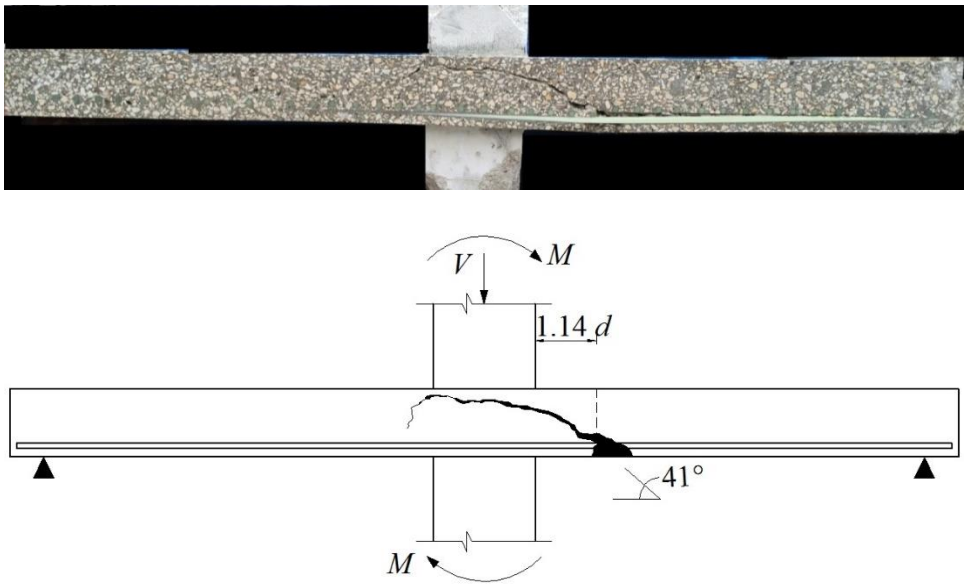

c) H-2.0-XX

Figure 4.2: Cross-section and schematic drawing of internal cracks (Series 1) – continued

Table 4.1: Test results for Series 1 connections

Connection	Cracking load (kN)	Deflection (mm)		Flexural reinforcement strain at column face [a] (με)		Concrete strain at failure (με)	Post-cracking stiffness, k_p (kN/mm)
		Service	Failure	Service	Failure		
H-1.0-XX	145	8.8	24.0	4,800	8,590	-610	11.3
H-1.5-XX	147	4.2	18.2	2,080	4,660	-780	16.5
H-2.0-XX	150	2.0	13.8	1,290	5,360	-440	22.6
N-1.0-XX*	115	13.7	22.0	-	6,790	-650	10.1

[a] Parallel to the direction of the applied moment

4.2.2. Deflections

The relationship between the vertical load and the deflection measured at a distance of 50 mm from the column face in the direction of unbalanced moment at the heavier-loaded side of the slab is shown in Figure 4.3 for Series 1 connections. Generally, before initiation of cracks, the behaviour of the three connections was comparable, as it depends on the mechanical properties of concrete. After cracking, the behaviour depends on the post-cracking stiffness up to failure, which is a function of the axial rigidity of the flexural reinforcement, $\rho_f E_f$.

Increasing the reinforcement ratio increased the post-cracking stiffness, which is quantified herein using the stiffness factor, k_p (the slope of the load-deflection curve after cracking), as shown in Figure 4.4, which shows an approximately linear increase in the post-cracking stiffness with increasing the flexural reinforcement ratio. This resulted in a reduction in the deflections at the same load level. Connections H-1.5-XX and H-2.0-XX exhibited 46 and 100% increase in the post-cracking stiffness factor and 52 and 77% reduction in the deflections at the service load level, respectively, compared to Connection H-1.0-XX. On the other hand, the use of HSC enhanced the pre-cracking stiffness (the slope of the load-deflection curve before cracking) and increased the

cracking load of Connection H-1.0-XX; thus, allowing the connection to experience 36% lower deflection at the service load level compared to Connection N-1.0-XX* made of NSC although they both had the same post-cracking stiffness.

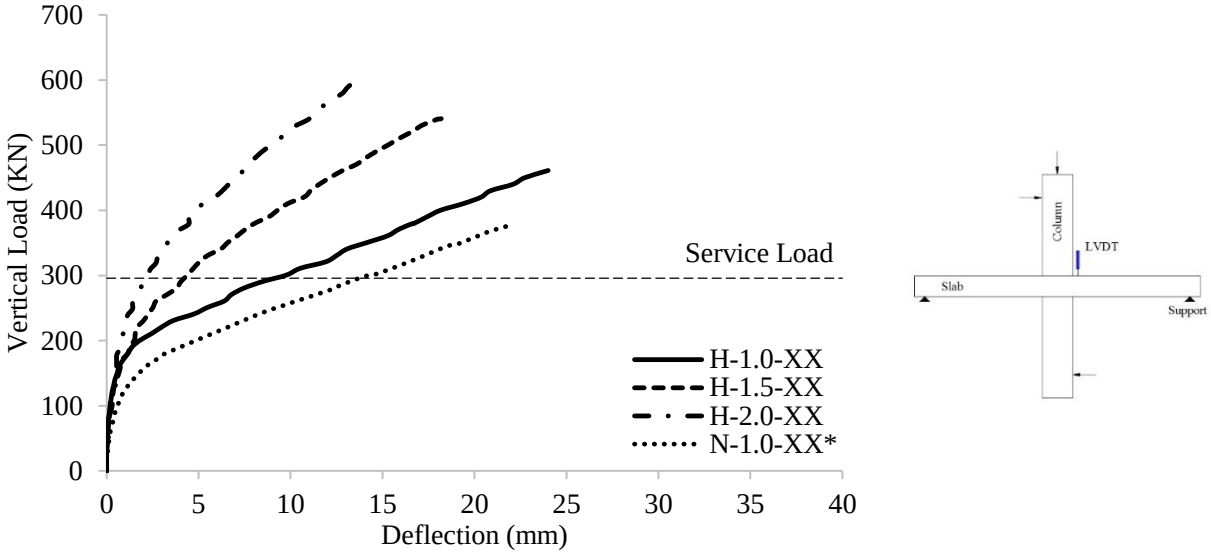

Figure 4.3: Vertical load-deflection relationship (Series 1)

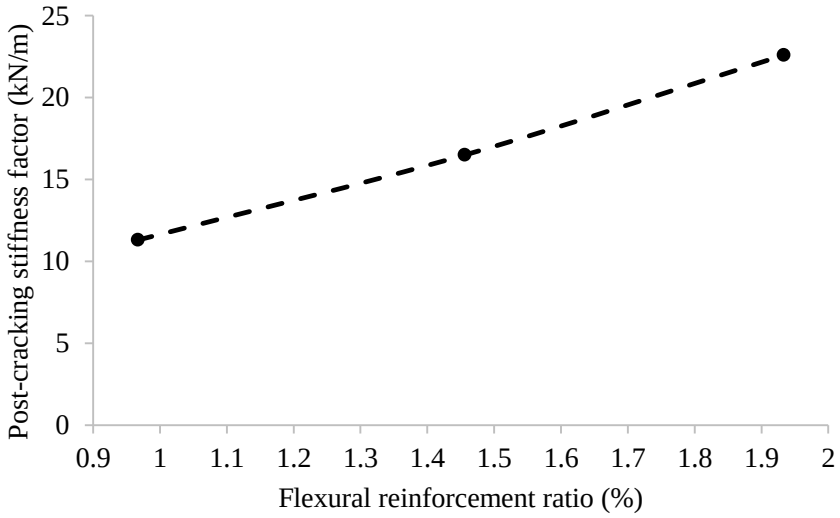

Figure 4.4: Post-cracking stiffness vs. flexural reinforcement ratio (Series 1)

4.2.3. Flexural Reinforcement and Concrete Strains

Figure 4.5 shows the relationship between the vertical load and the strains in flexural reinforcement and concrete measured at the column face in the direction of the unbalanced moment on the heavier-loaded side of the slab for all connections. Generally, strains in the reinforcing bars started to increase rapidly after the first crack in all connections. The rate of increase in the strains depends on the relative location of the crack and the strain gauge. For Series 1 connections, increasing the flexural reinforcement ratio decreased the reinforcement and concrete strains at the same load level. The maximum recorded reinforcement strain occurred in Connection H-1.0-XX (8,590 με), i.e. the one with the lowest GFRP flexural reinforcement ratio, this value represents 33% of the ultimate tensile strain of the GFRP bars. Also, the flexural reinforcement strain at the service level for Connection H-1.0-XX (4,800 με) is 26% less than the service strain limit specified by the CSA/S806-12 (CSA 2012), which is 25% of the rupture strain of the used GFRP bars (6,500 με). On the other hand, the maximum measured concrete strains for the three connections were below the theoretical crushing strain of concrete (3,500 με) specified by CSA/S806-12 (CSA 2012). This confirms that all connections exhibited punching failure before the slab reached its flexural capacity.

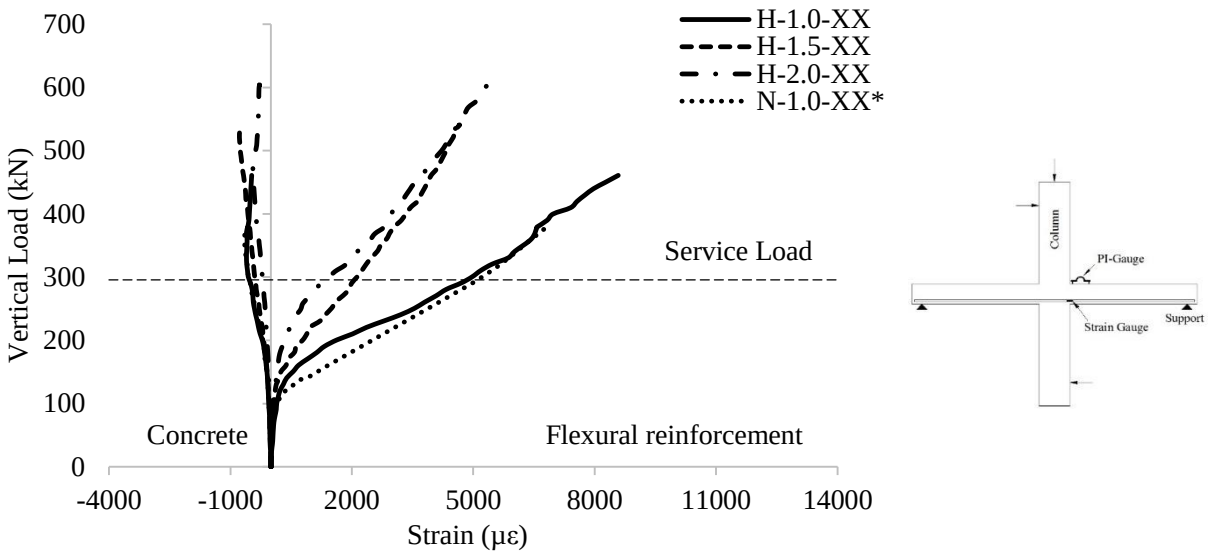

Figure 4.5: Vertical load-flexural strains relationship (Series 1)

For all connections, the flexural reinforcement running in the direction of the unbalanced moment experienced higher strains than those running in the perpendicular direction. Figures 4.6 and 4.7 show the flexural strain profiles in both orthogonal directions at increments of 25% of the failure load for all connections. It can be noticed that strains are decreasing as moving farther from the column face, which indicates that no bond slippage occurred during the test. Also, higher strains correspond to the direction of moment application, due to the unbalanced moment.

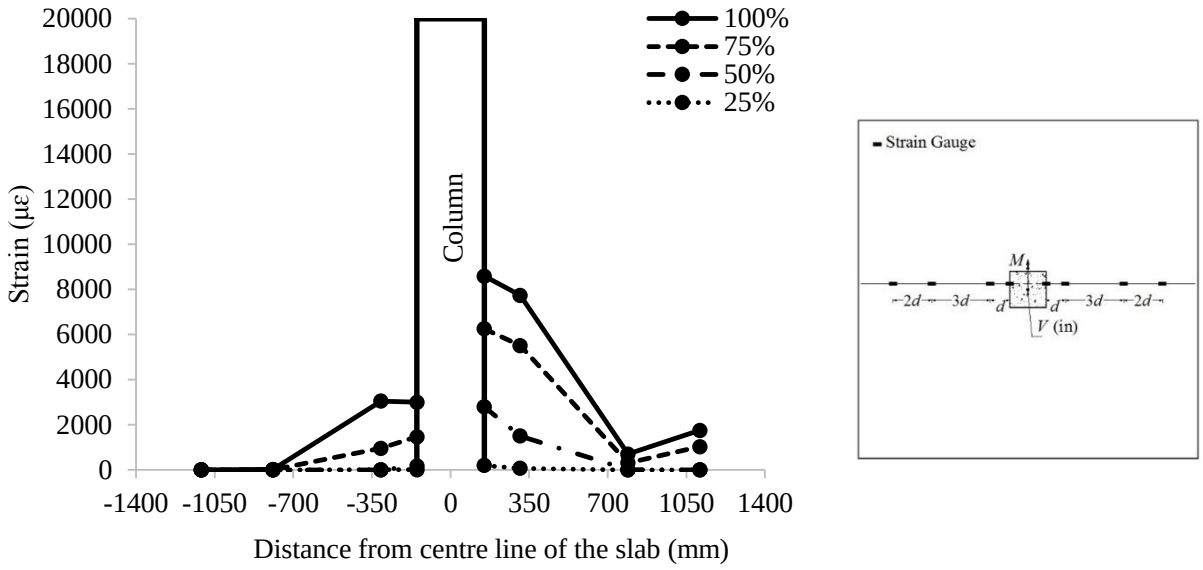

a) H-1.0-XX

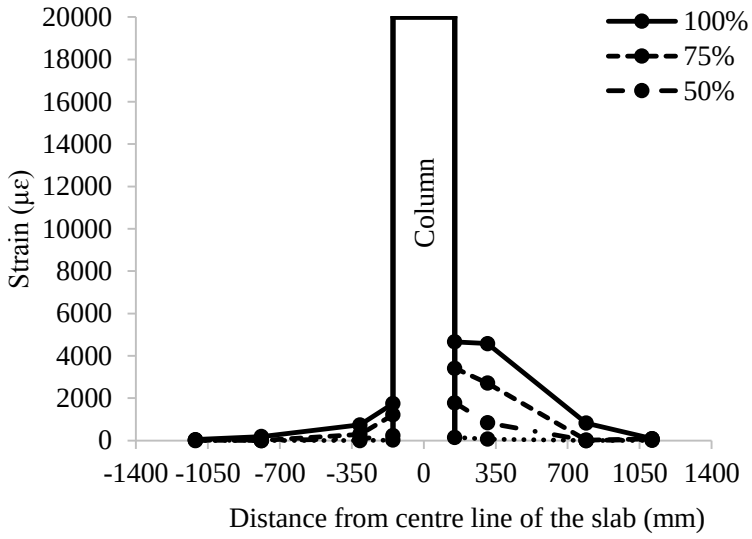

b) H-1.5-XX

Figure 4.6: Flexural reinforcement strain profile in direction parallel to the direction of the unbalanced moment for Series 1 connections

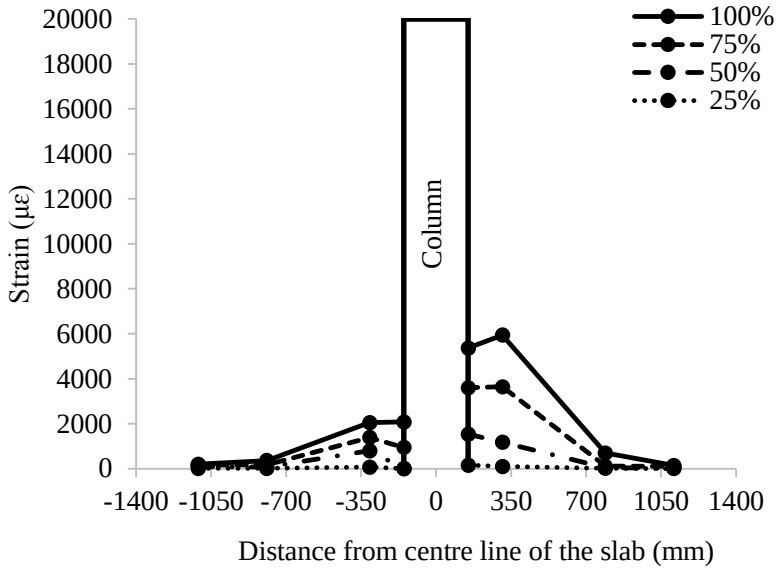

c) H-2.0-XX

Figure 4.6: Flexural reinforcement strain profile in direction parallel to the direction of the unbalanced moment for Series 1 connections - continued

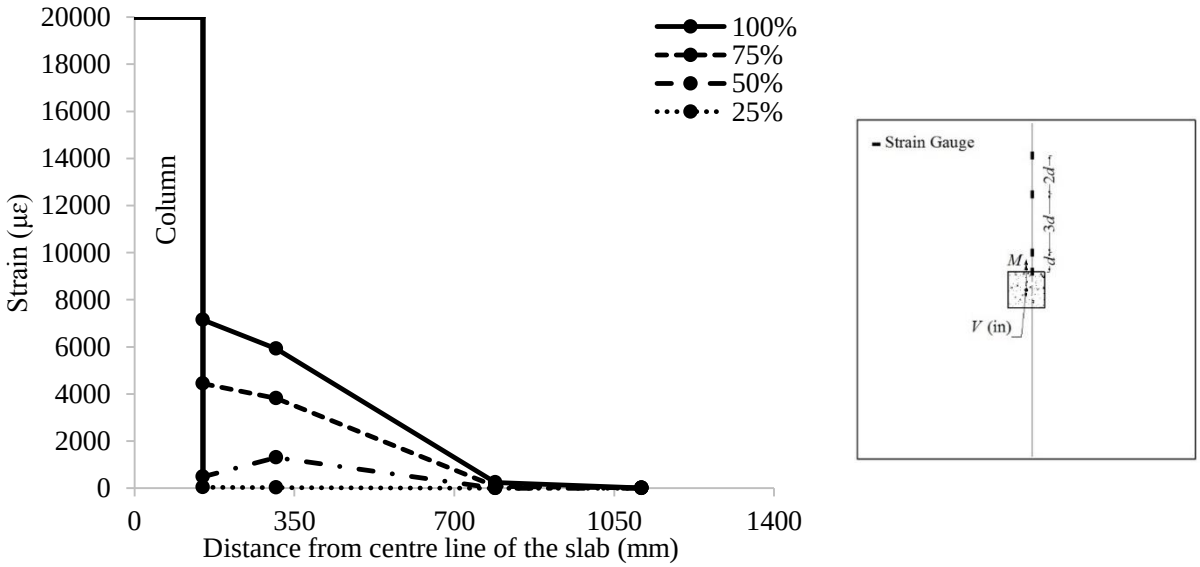

a) H-1.0-XX

Figure 4.7: Flexural reinforcement strain profile in direction perpendicular to the direction of the unbalanced moment for Series 1 connections

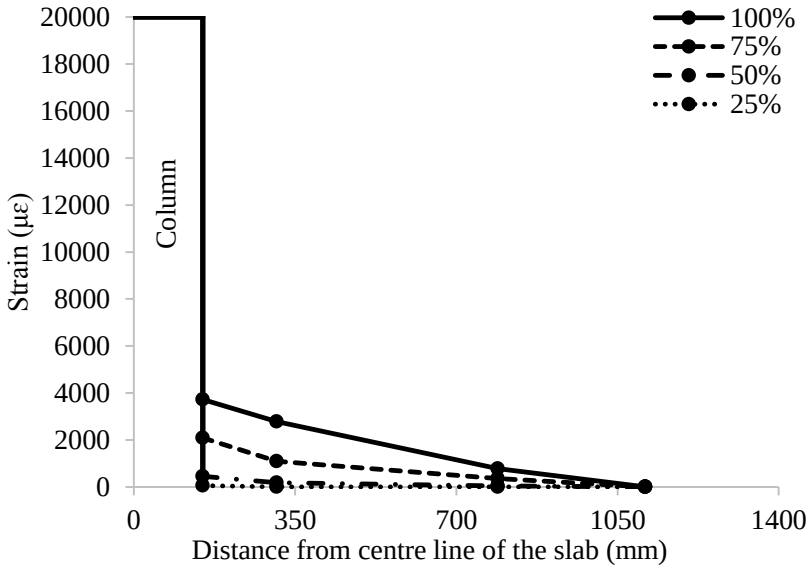

b) H-1.5-XX

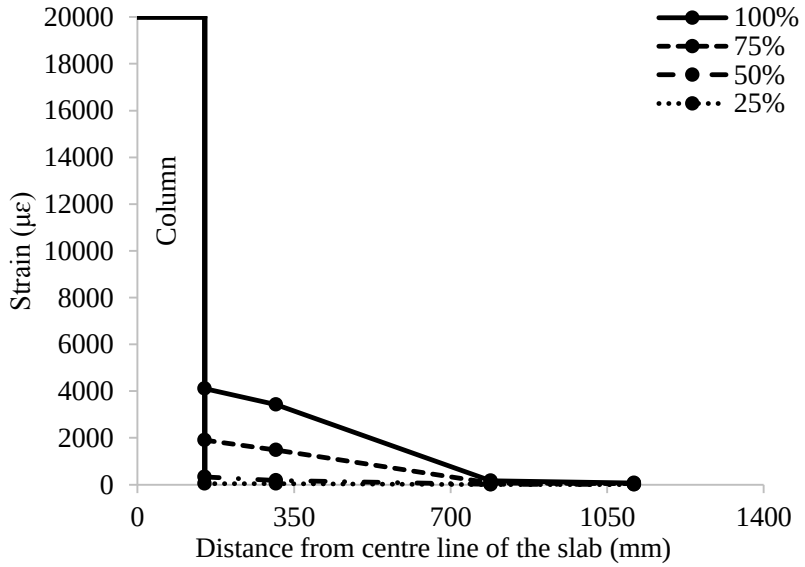

c) H-2.0-XX

Figure 4.7: Flexural reinforcement strain profile in direction perpendicular to the direction of the unbalanced moment for Series 1 connections - continued

4.2.4. Ultimate Strength

The ultimate capacities at failure were adjusted/normalized for varying concrete strength. The failure loads of Series 1 connections were multiplied by $\sqrt[3]{84/f_c'}$, where 84 MPa is the average concrete compressive strength for the three connections and f_c' is the concrete strength of each connection as given in Table 4.2. The cubic root of the concrete strength was used instead of the square root, which is commonly used in these cases, to follow the provisions of the Canadian standard CSA/S806-12 (CSA 2012). For Series 1 connections, it can be concluded that the normalized failure load is increased with increasing the flexural reinforcement ratio (Figure 4.8). This attributed to the role of the increased flexural reinforcement in controlling the widening of flexural cracks resulting in a reduction in the depth and width of cracks. This, in turn, will increase the contribution of the uncracked concrete and the aggregate interlock to the shear strength provided by concrete. In addition, increasing the reinforcement ratio increases the contribution of dowel action to the shear strength provided by concrete. Therefore, increasing the reinforcement ratio by 50 and 100% increased the normalized capacity by 15 and 27%, respectively. On the other hand, increasing the concrete strength enhanced the load carrying capacity. Compared to its counterpart Connection N-1.0-XX*, increasing the concrete strength from 38 to 80 MPa (111% increase) resulted in a 22% increase in the punching capacity of Connection H-1.0-XX. This is attributed to the role of HSC in increasing the cracking load and the uncracked concrete contribution to the shear strength provided by concrete. The flexural capacities of the connections were calculated using the yield line theory (Gar et al. 2014; Gouda and El-Salakawy 2016a). Table 4.2 shows a comparison between the actual failure loads, V_{Test}, and the predicted flexural capacities, V_{flex}. For Series 1 connections, the low V_{Test}/V_{flex} ratio with an average of 0.56 confirms the punching failure mode experienced by the connections.

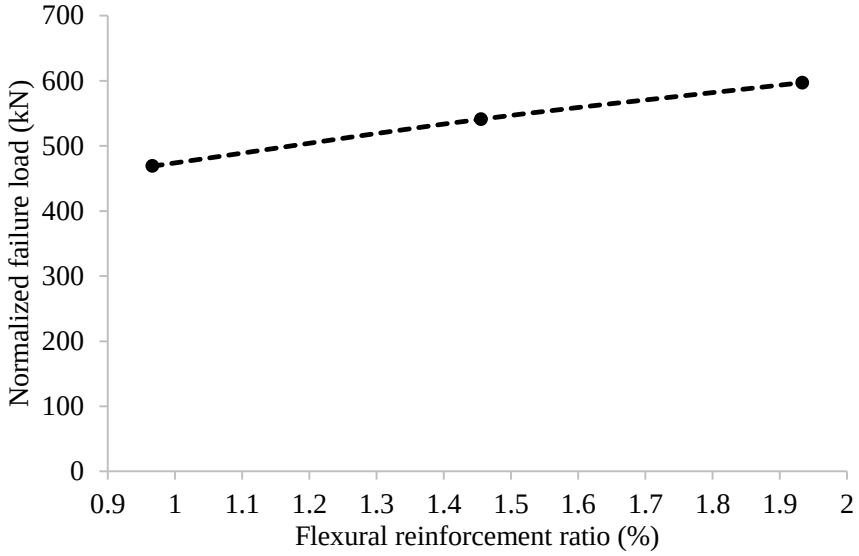

Figure 4.8: Normalized failure load vs. flexural reinforcement ratio (Series 1)

Table 4.2: Failure and normalized load and flexural capacities for Series 1 connections

Connection	Concrete strength, f'_c (MPa)	Failure load, V_{Test} (kN)	Normalized failure load (kN)	Flexural capacity		Failure mode
				V_{flex}[a] (kN)	V_{Test}/V_{flex}	
H-1.0-XX	80	461	469	816	0.56	Punching
H-1.5-XX	84	541	541	972	0.56	Punching
H-2.0-XX	87	604	597	1,094	0.55	Punching

[a] Calculated using actual f'_c

4.2.5. Code Comparisons

The actual capacities of Series 1 connections were compared to the predictions of the CSA/S806-12 (CSA 2012), the ACI 440.1R-15 (ACI Committee 440 2015) and the Japan Society of Civil Engineers code (JSCE 1997) as listed in Table 4.3. All the safety factors in the code equations were set to 1.0 to predict the nominal punching shear capacity (Appendix B). The CSA/S806-12 (CSA 2012) provisions provided reasonable predictions with an acceptable safety margin and an average V_{Test}/V_{Pred} of 1.18 ± 0.02 (COV = 2.0%). It should be noted that, the obtained average

V_{Test}/V_{Pred} will reduce to 1.05 ± 0.006 (COV = 0.6%) if the limit on the maximum concrete strength is waived and the actual concrete strengths are used. The predictions of the Japan Society of Civil Engineers code (JSCE 1997) were slightly conservative to the actual capacities with an average V_{Test}/V_{Pred} of 1.34 ± 0.03 (COV = 2.0%). On the other hand, the ACI 440.1R-15 (ACI Committee 440 2015) highly underestimated the capacities with an average V_{Test}/V_{Pred} of 1.80 ± 0.06 (COV = 3.4%). This is attributed to the fact that the punching shear equation of the ACI 440.1R-15 (ACI Committee 440 2015) only accounts for the uncracked concrete contribution to resist the applied shear stresses.

Table 4.3: Code comparisons for Series 1 connections

Connection	Failure load, V_{Test} (kN)	CSA/S806-12[a]		ACI 440.1R-15[b]		JSCE 1997[c]	
		V_{Pred} (kN)	V_{Test}/V_{Pred}	V_{Pred} (kN)	V_{Test}/V_{Pred}	V_{Pred} (kN)	V_{Test}/V_{Pred}
H-1.0-XX	461	401	1.15	248	1.86	352	1.31
H-1.5-XX	541	459	1.18	303	1.79	403	1.34
H-2.0-XX	604	505	1.20	347	1.74	443	1.36
Mean			1.18		1.80		1.34
SD			0.02		0.06		0.03
COV (%)			2.0		3.4		2.0

[a] Calculated using Equation [2.37]
[b] Calculated using Equation [2.38]
[c] Calculated using Equation [2.41]

4.3. SERIES 2: EFFECT OF SHEAR REINFORCMEENT

Three connections with flexural reinforcement ratio of 1.0% were assigned to study the effect of shear reinforcement on slab-column interior connections made of NSC. Also, the results of the three NSC connections were compared, when applicable, to the results of a similar slab-column interior connection made of NSC from a previous work (Gouda 2015), Connection G-0.98-N-15-XX, and it will be referred to as Connection N-1.0-XX*.

4.3.1. Mode of Failure and Cracking Pattern

Except for the final failure crack in Connection N-1.0-S5, all connections showed similar cracking behaviour to that of Series 1 connections. On the other hand, the punching capacity of shear-reinforced slab-column connections is governed by either the shear strength within the shear-reinforced zone or that outside the shear-reinforced zone. The headed studs used in Connection N-1.0-S5 (with five peripheral rows of studs) managed to control the propagation and widening of the shear cracks in the column vicinity and prevented the punching shear failure inside the shear-reinforced zone. Subsequently, as shown in Figure 4.9, the punching failure occurred outside the shear-reinforced zone simultaneously with flexural failure. This is also evident in the schematic drawing of the internal cracks in Series 2 connections as shown in Figure 4.10. It can be seen that, for Connection N-1.0-S5, multiple diagonal cracks intersect the headed studs, which managed to control the widening of these cracks forcing the punching failure to occur outside the shear-reinforced zone at an angle of 23^{o}. Normally, mild failure cracks are observed for connections failing outside the shear-reinforced zone (Dilger and Ghali 1981). However, Connection N-1.0-S6 (with six peripheral rows of studs) failed inside the shear-reinforced zone at approximately the same load of Connection N-1.0-S5. Adding another row of shear reinforcement increased the capacity outside the shear-reinforced zone, which caused the steeper crack to occur between the

first and second rows of studs (Figure 4.10). Even though Connection N-1.0-C5 failed inside the shear-reinforced zone as well, yet, this could be attributed to the excessive strains in the stems of the corrugated bars, considering the lower shear reinforcement ratio employed in that connection, which might cause a failure/slippage at the bend location. For both connections, the formation of a steep crack decreased the tendency of the shear reinforcement (spaced 0.75 *d*) to fully-control the shear crack. This addresses some concerns about the maximum practical spacing of the headed studs as will be discussed later.

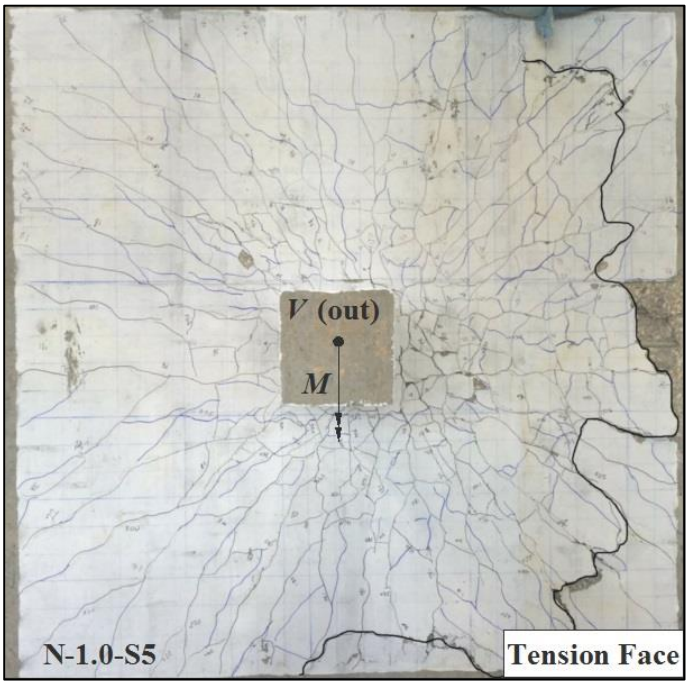

a) N-1.0-S5

Figure 4.9: Cracking pattern on the tension face of the slab at failure (Series 2)

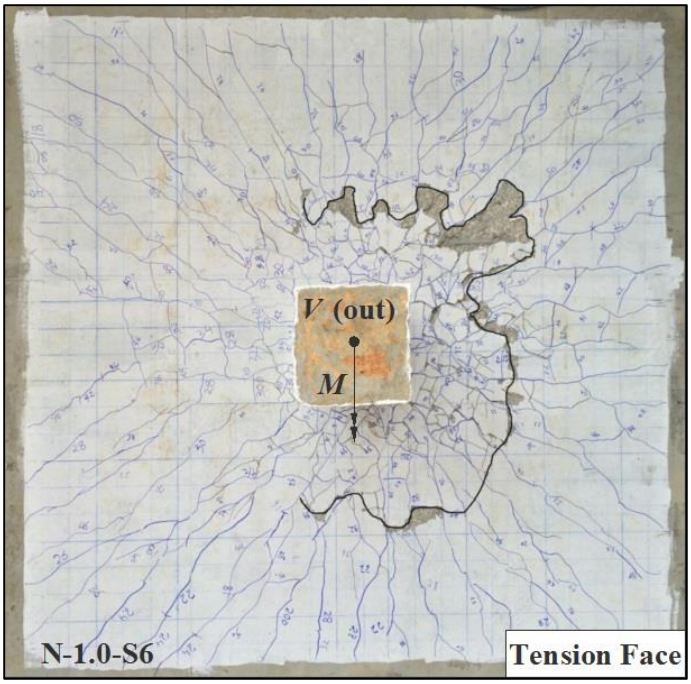

b) N-1.0-S6

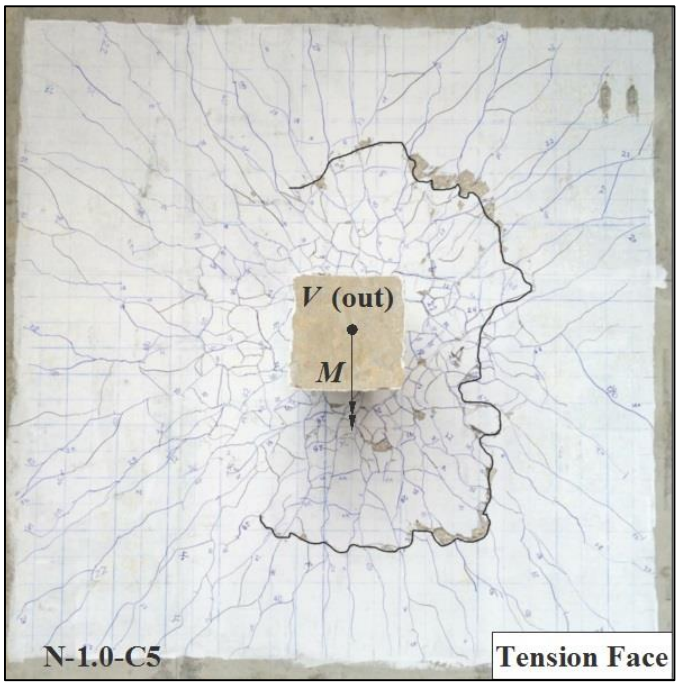

c) N-1.0-C5

Figure 4.9: Cracking pattern on the tension face of the slab at failure (Series 2) - continued

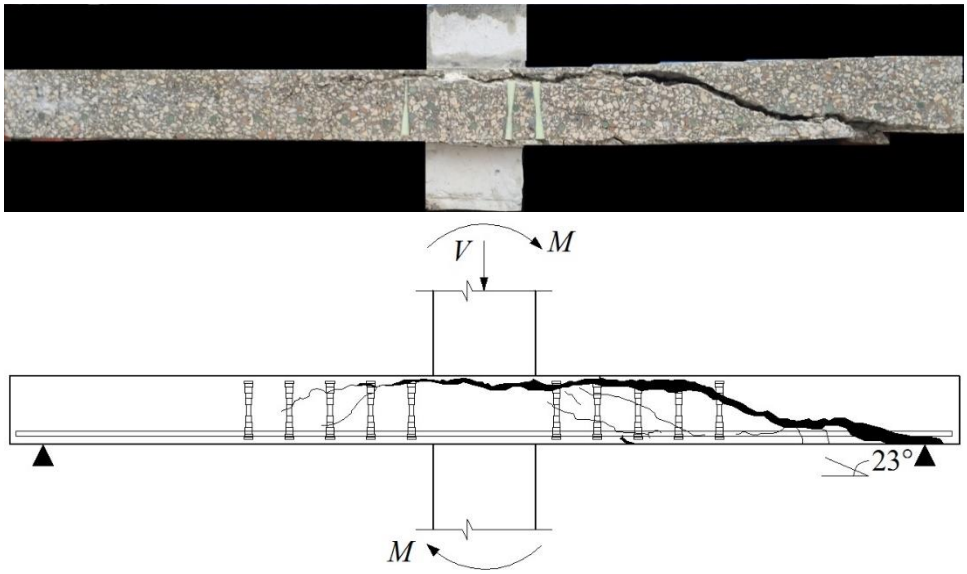

a) N-1.0-S5

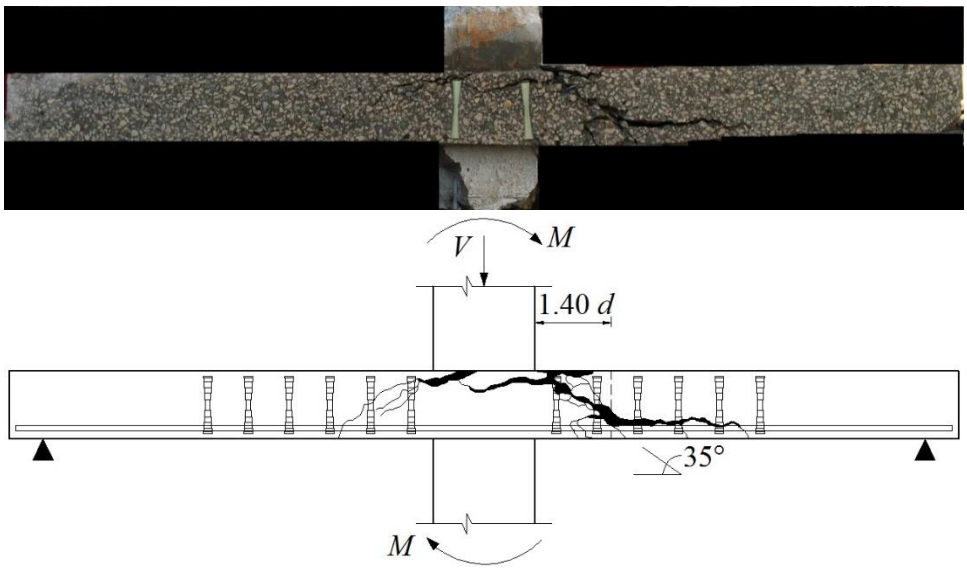

b) N-1.0-S6

Figure 4.10: Cross-section and schematic drawing of internal cracks (Series 2)

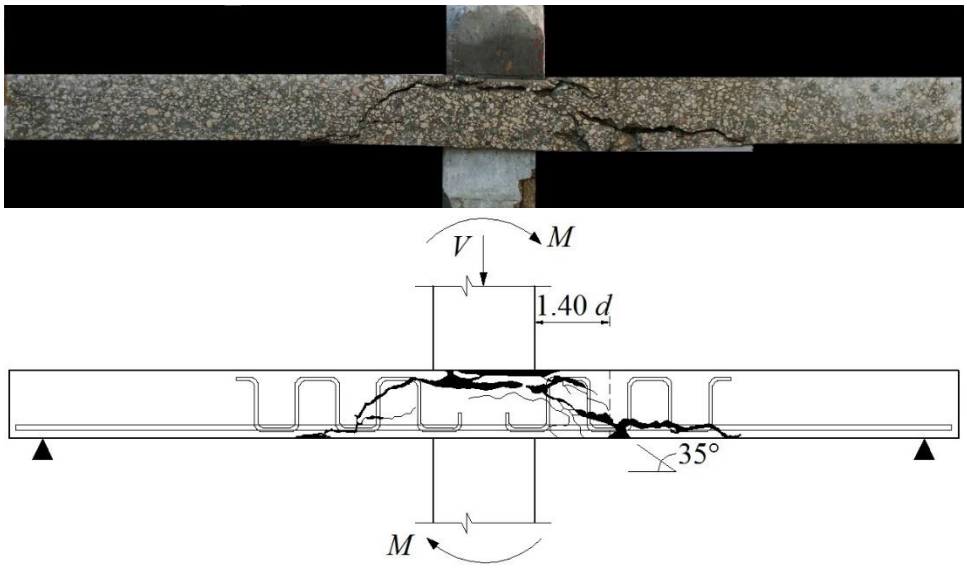

c) N-1.0-C5

Figure 4.10: Cross-section and schematic drawing of internal cracks (Series 2) - continued

Table 4.4: Test results for Series 2 connections

Connection	Cracking load (kN)	Deflection (mm)		Maximum strains at failure ($\mu\varepsilon$)			Post-cracking stiffness, k_p (kN/mm)
		Service	Failure	Flexural strain at column face [a]	Concrete	Shear reinforcement	
N-1.0-S5	120	10.4	36.5	8,830[b]	-1,920	4,420	13.7
N-1.0-S6	115	9.4	35.4	12,560	-1,880	5,340	13.3
N-1.0-C5	120	11.0	35.2	8,070	-1,230	5,850	11.5
N-1.0-XX*	115	13.7	22.0	6,790	-650	N/A	10.1

[a] Parallel to the direction of the applied moment
[b] Malfunctioned at 80% of the failure load

4.3.2. Deflections

The relationship between the vertical load and the deflections measured at 50 mm from the column face in the direction of unbalanced moment at the heavier-loaded side of the slab is shown in Figure 4.11. For Series 2 connections, the pre-cracking behaviour of the connections was similar; however, the presence of shear reinforcement slightly enhanced the post-cracking stiffness of the connections due to its ability to control the widening of diagonal shear cracks, which resulting in lower deflections at the same load level (Table 4.4). Connections N-1.0-S5, N-1.0-S6 (with headed studs) and N-1.0-C5 (with corrugated bars) had 36, 32 and 14% higher post-cracking stiffness factor than Connection N-1.0-XX* (without shear reinforcement), respectively. The lower enhancement in the post-cracking stiffness in the case of Connection N-1.0-C5 is attributed to the lower modulus of elasticity of the corrugated bars and the lower shear reinforcement ratio employed in the connection. Moreover, both types of shear reinforcement managed to increase the deflection at failure for the shear-reinforced connections. Connections N-1.0-S5, N-1.0-S6 (with headed studs) and N-1.0-C5 (with corrugated bars) experienced 66, 61 and 60% higher deflections at failure than Connection N-1.0-XX* (without shear reinforcement), respectively.

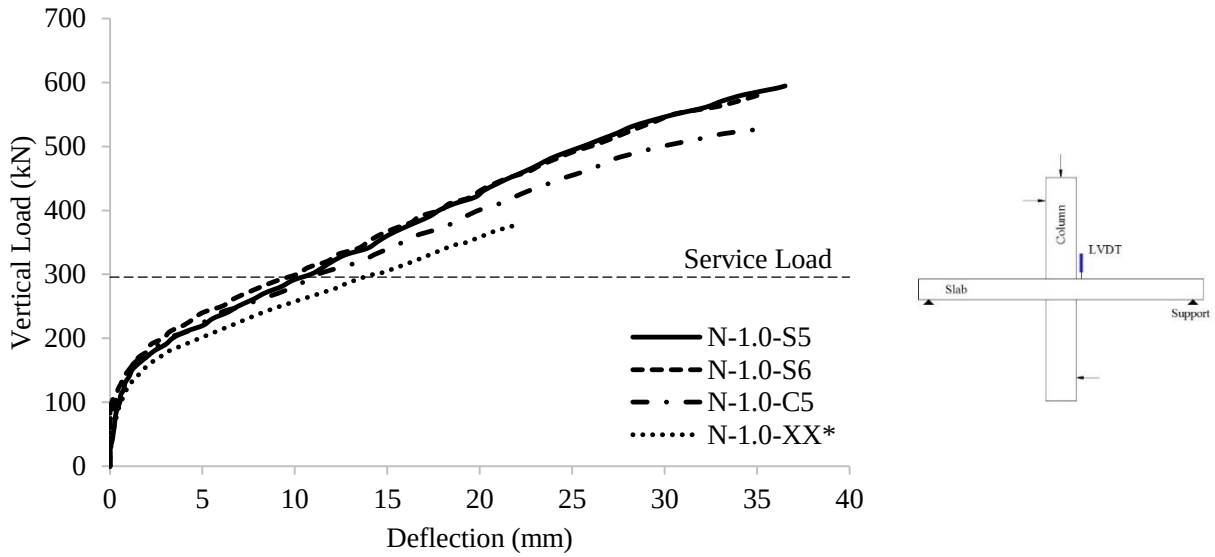

Figure 4.11: Vertical load-deflection relationship (Series 2)

4.3.3. Flexural Reinforcement and Concrete Strains

Figure 4.12 shows the relationship between the vertical load and the strains in flexural reinforcement and concrete measured at the column face in the direction of the unbalanced moment on the heavier-loaded side of the slab for all connections. For Series 2 connections, the maximum measured flexural reinforcement strain at the column face was recorded in Connection N-1.0-S6 (12,560 με), which represents 48% of the ultimate tensile strain of the GFRP bars. It is worth mentioning that the strain gauge in Connection N-1.0-S5 malfunctioned at 80% of the failure load (8,830 με). All Series 2 connections experienced higher concrete strains compared to Connection N-1.0-XX* with the maximum measured concrete strain of 1,920 με in Connection N-1.0-S5.

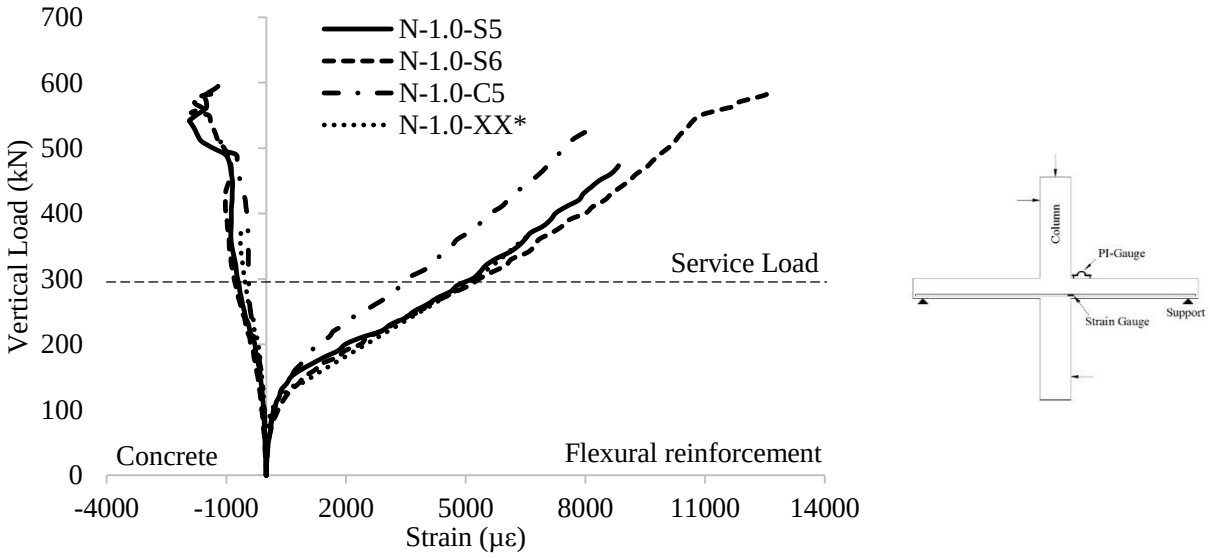

Figure 4.12: Vertical load-flexural strains relationship (Series 2)

Similar to Series 1 connections, the flexural reinforcement running in the direction of the unbalanced moment experienced higher strains than those running in the perpendicular direction. Figures 4.13 and 4.14 show the flexural strain profiles in both orthogonal directions at increments of 25% of the failure load for all connections. Again, it can be noticed that strains are decreasing as moving farther from the column face, which indicates that no bond slippage occurred during

the test. Also, higher strains correspond to the direction of moment application, due to the unbalanced moment.

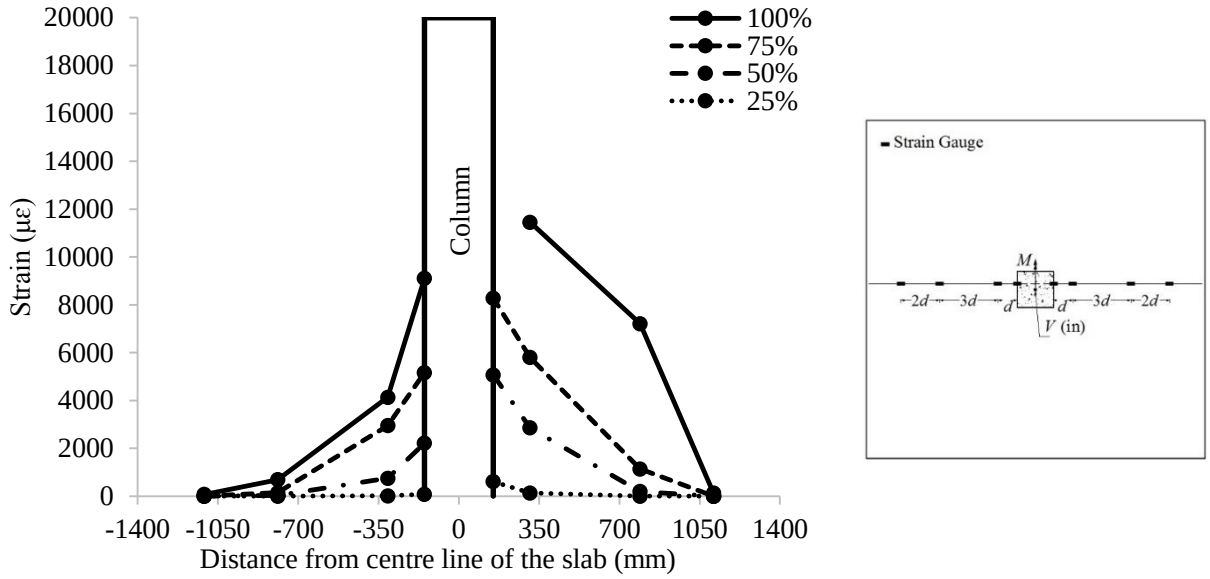

a) N-1.0-S5

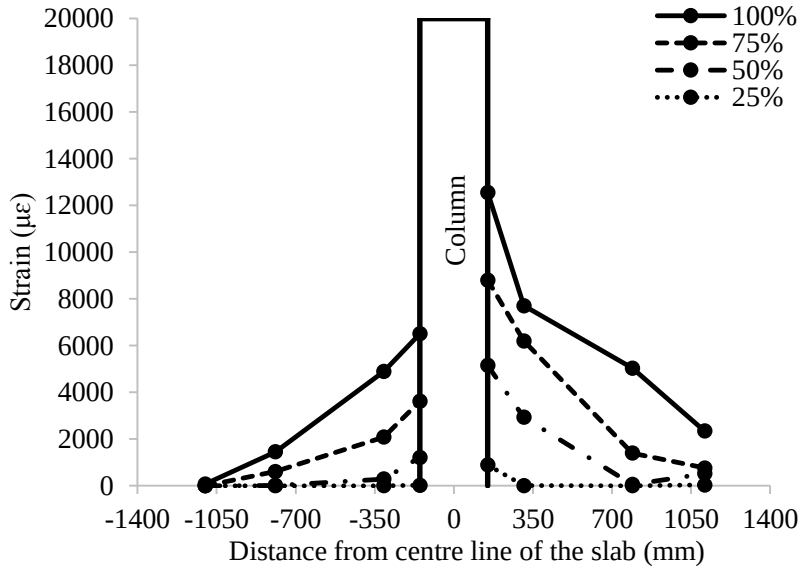

b) N-1.0-S6

Figure 4.13: Flexural reinforcement strain profile in direction parallel to the direction of the unbalanced moment for Series 2 connections

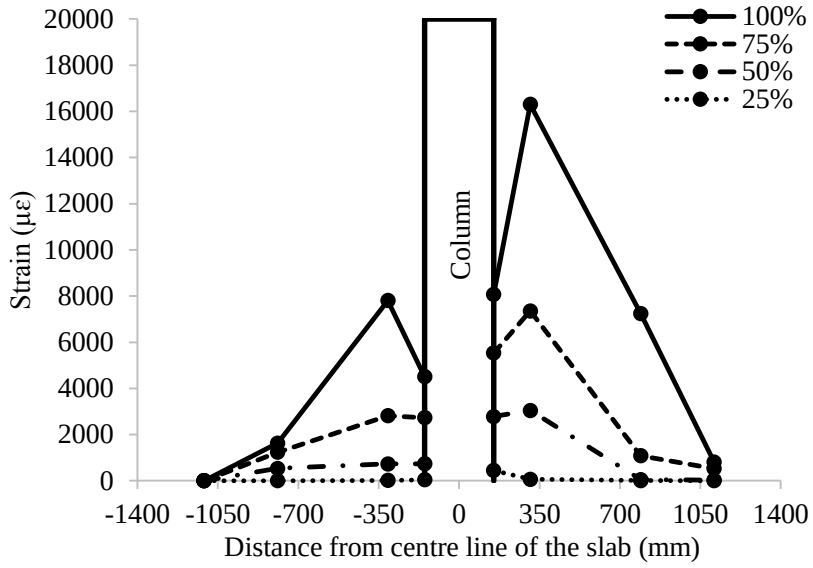

c) N-1.0-C5

Figure 4.13: Flexural reinforcement strain profile in direction parallel to the direction of the unbalanced moment for Series 2 connections - continued

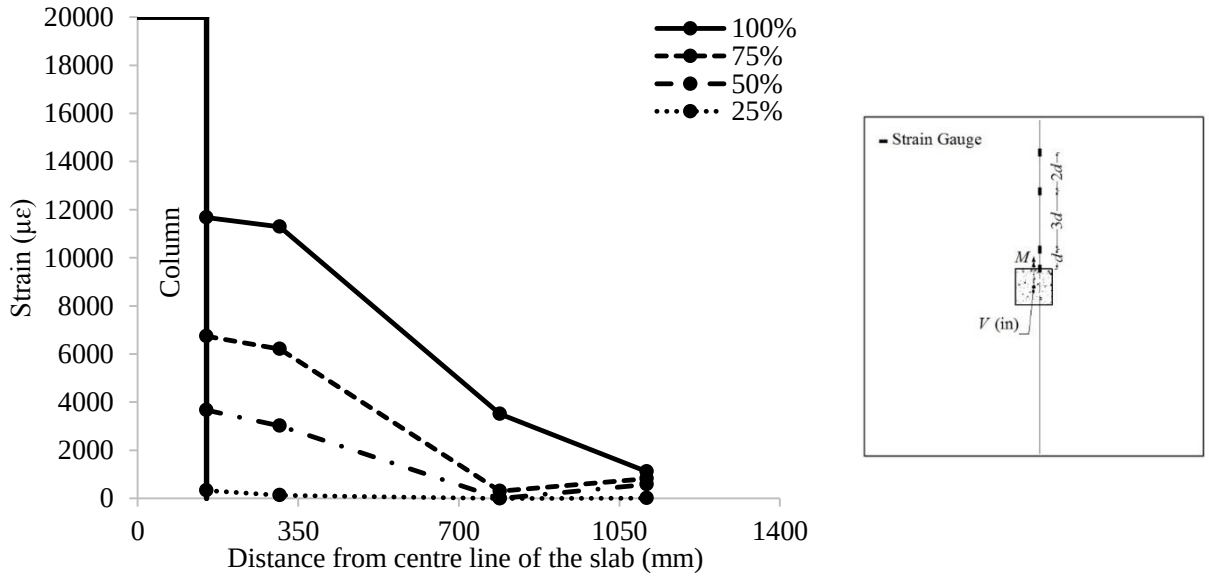

a) N-1.0-S5

Figure 4.14: Flexural reinforcement strain profile in direction perpendicular to the direction of the unbalanced moment for Series 2 connections

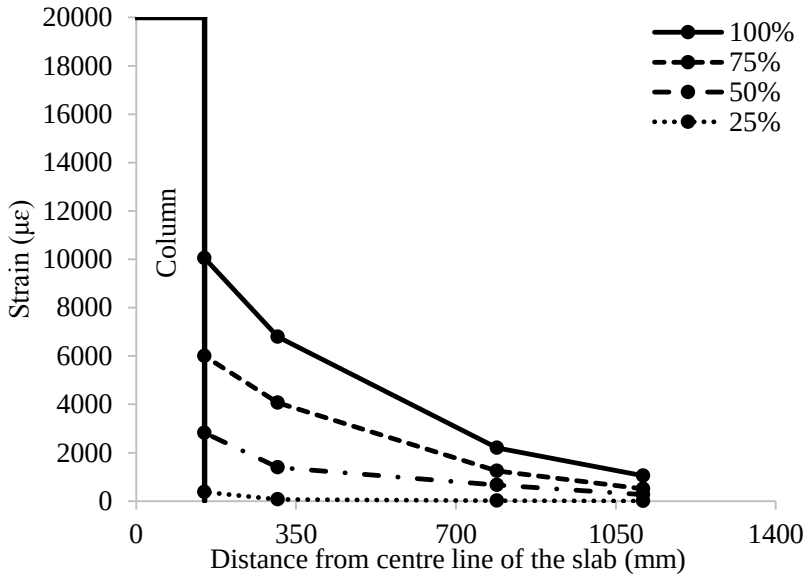

b) N-1.0-S6

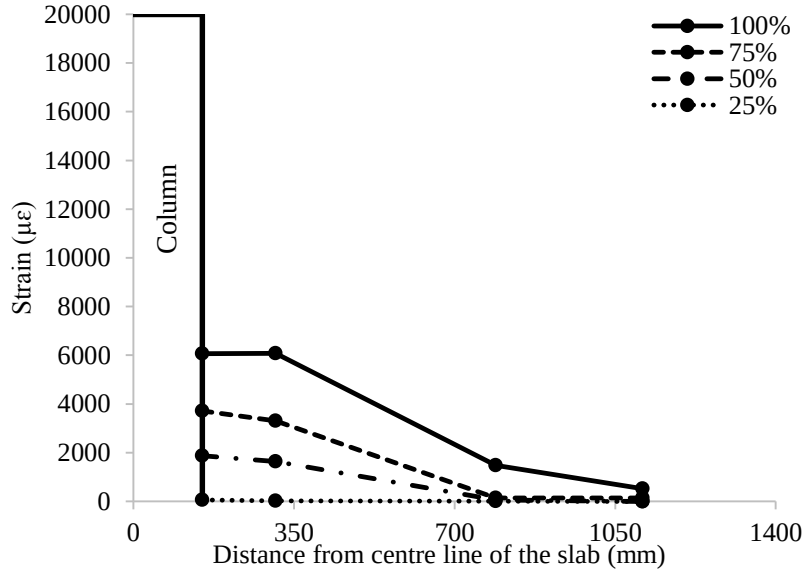

c) N-1.0-C5

Figure 4.14: Flexural reinforcement strain profile in direction perpendicular to the direction of the unbalanced moment for Series 2 connections - continued

4.3.4. Shear Reinforcement Strains

Figures 4.15, 4.16 and 4.17 show the shear reinforcement strains in the heavier-load side of the slabs for Series 2 connections, versus the distance from the column face divided by the average effective slab depth (d = 160 mm) at 25% increments of the failure load. For Connection N-1.0-S5 (with five peripheral rows of studs), the headed studs intersected diagonal shear cracks, the heads of the studs provided adequate anchorage, which enabled most of the studs to develop strains higher than 2,000 με with convergent values to all the studs before the punching failure occurs outside the shear-reinforced zone. Furthermore, one of the studs located at 0.40 d from the column face developed a strain of 4,420 με with no signs of apparent slippage or anchorage failure. This value is only 54% of the usable strain of the stud provided by the manufacturer; however, it is 88 and 111% of the CSA/S806-12 (CSA 2012) and ACI 440.1R-15 (ACI Committee 440 2015) strain limits of 5,000 με and 4,000 με, respectively. However, the strains in the rest of the studs were below the allowable limits. This indicates that all the studs performed as one system and managed to push the shear crack outside the shear-reinforced zone, i.e., the connection could have reached even higher capacity reaching flexure failure, if the punching failure outside the shear-reinforced zone was prevented. This was examined in Connection N-1.0-S6 (with six peripheral rows of studs). However, increasing the shear capacity outside the shear-reinforced zone caused the main diagonal shear crack near the column face to be steeper. This steeper crack resulted in higher strains in the first three studs in all directions compared to Connection N-1.0-S5. The propagation of a steep crack is reflected in the strains in the headed studs, these strains were close to 4,000 με with one of the studs reaching 5,340 με, while the strains in the rest of the studs are close to 1,000 με. The connection finally failed due to this steep crack, which suggests that, the provided stud spacing was inadequate and should be reduced.

Similarly, for Connection N-1.0-C5 (with five peripheral rows of corrugated bars), most of the vertical stems in the column vicinity developed strains higher than 4,000 με with two stems reaching 5,670 and 5,850 με at two different locations. These relatively higher strains compared to those in the headed studs in Connection N-1.0-S5 are attributed to the lower shear reinforcement ratio and modulus of elasticity of the corrugated bars compared to the headed studs. This considerably high strain in the vertical stem of the corrugated bar (5,850 με) is 17 and 46% higher than the CSA/S806-12 (CSA 2012) and ACI 440.1R-15 (ACI Committee 440 2015) strain limits, respectively, which indicates that the GFRP corrugated bars were able to reach their potential capacity without apparent anchorage failure. However, further investigation is required to examine the anchorage efficiency of the GFRP corrugated bars with larger bar diameters and/or less stem spacing, if their manufacturing is feasible.

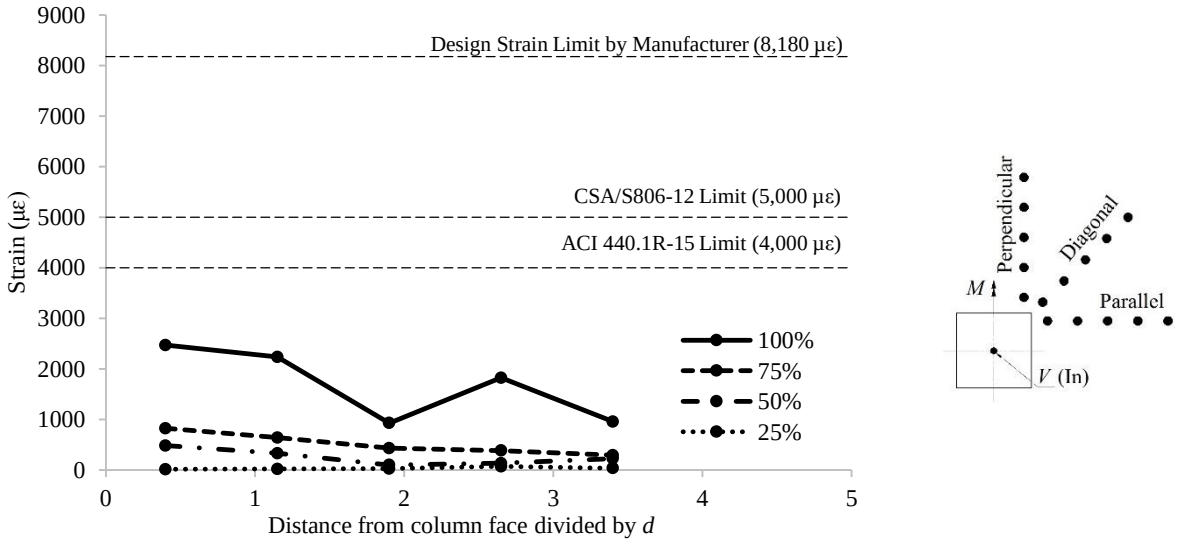

a) N-1.0-S5 (Parallel)

Figure 4.15: Shear reinforcement strains versus distance from column face for N-1.0-S5

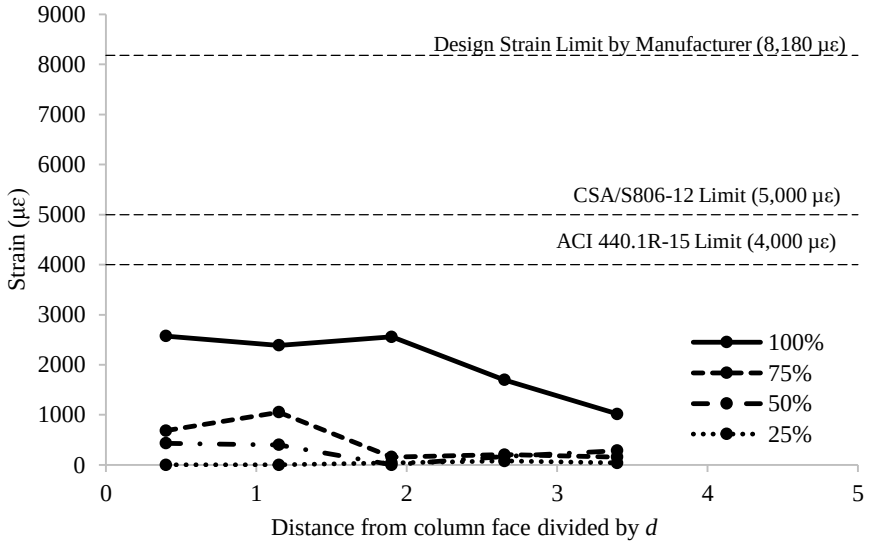

b) N-1.0-S5 (Diagonal)

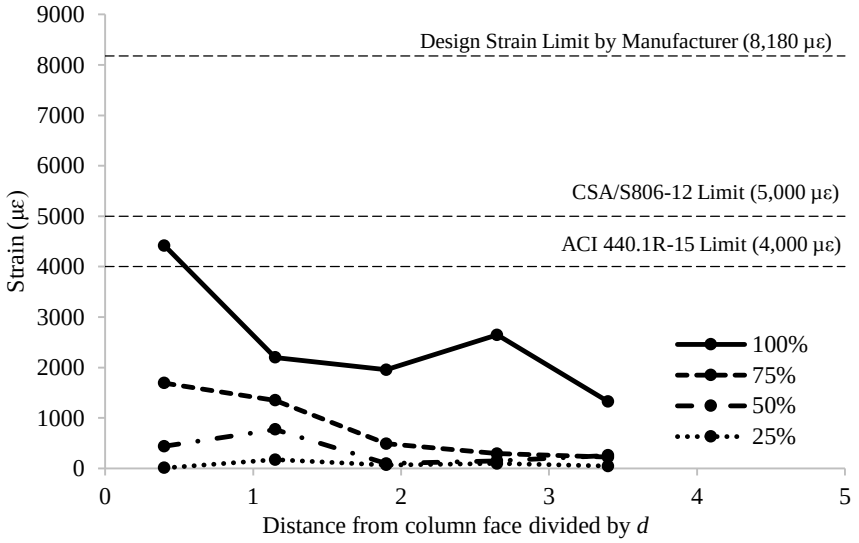

c) N-1.0-S5 (Perpendicular)

Figure 4.15: Shear reinforcement strains versus distance from column face for N-1.0-S5 - continued

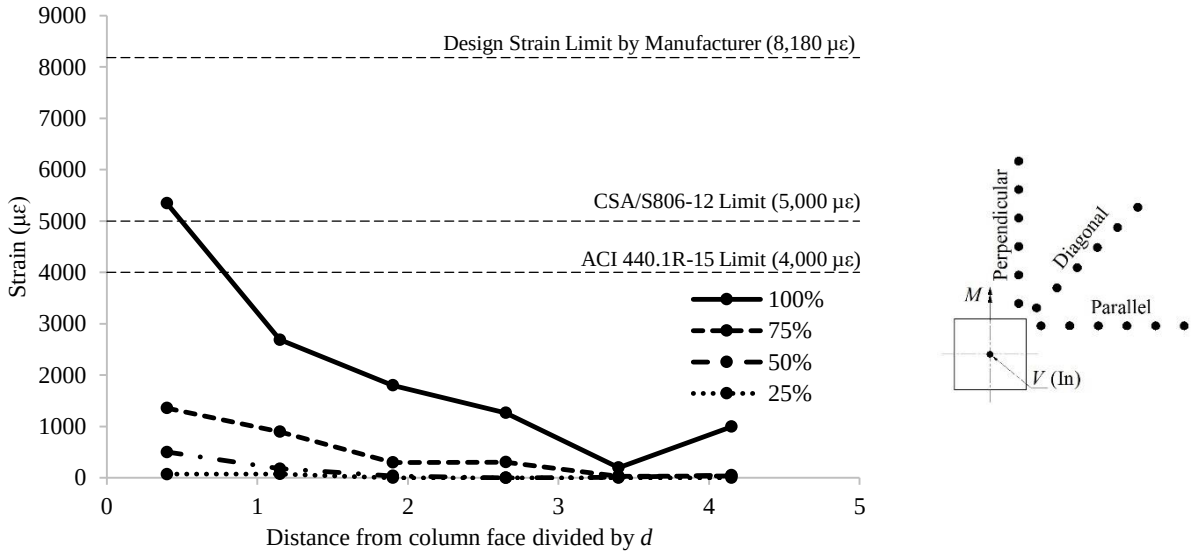

a) N-1.0-S6 (Parallel)

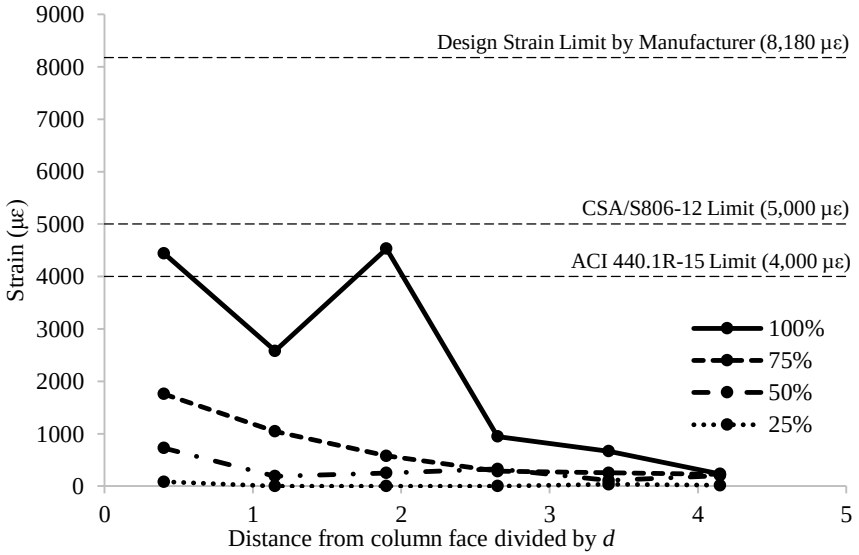

b) N-1.0-S6 (Diagonal)

Figure 4.16: Shear reinforcement strains versus distance from column face for N-1.0-S6

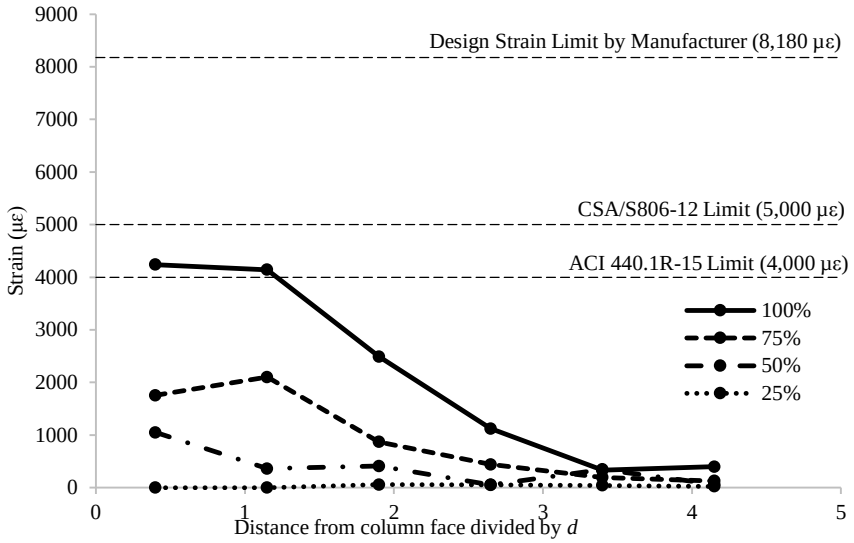

c) N-1.0-S6 (Perpendicular)

Figure 4.16: Shear reinforcement strains versus distance from column face for N-1.0-S6 - continued

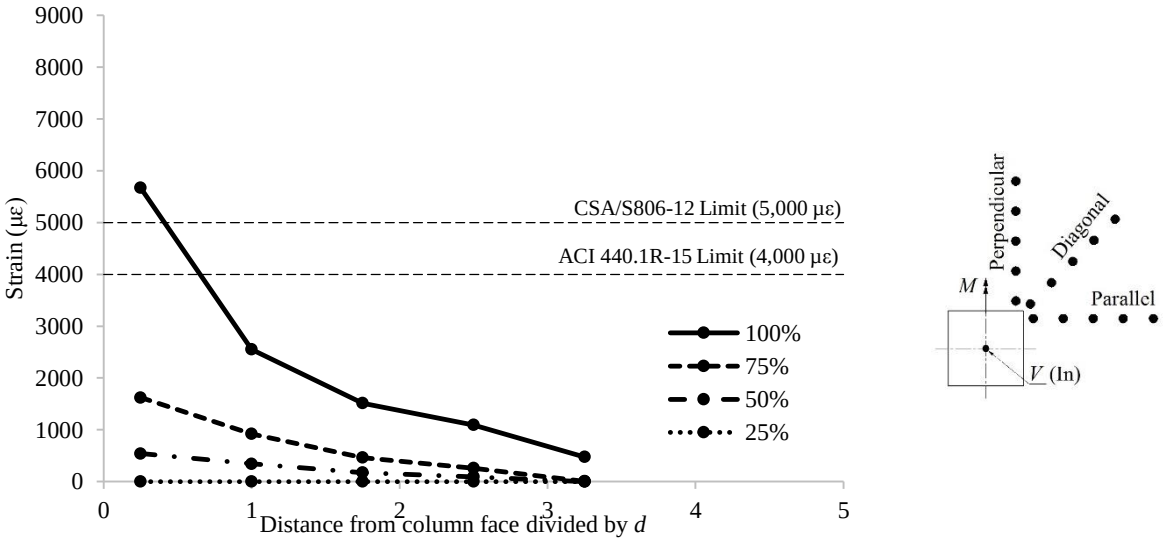

a) N-1.0-C5 (Parallel)

Figure 4.17: Shear reinforcement strains versus distance from column face for N-1.0-C5

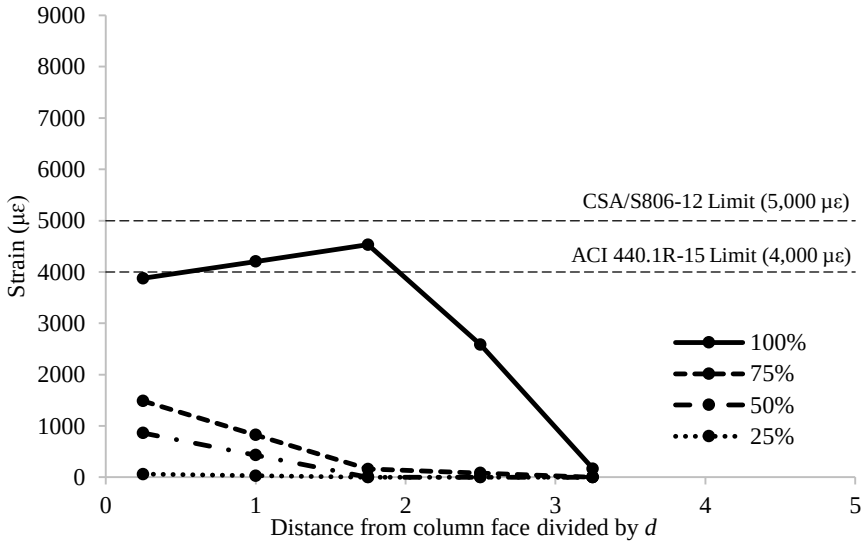

b) N-1.0-C5 (Diagonal)

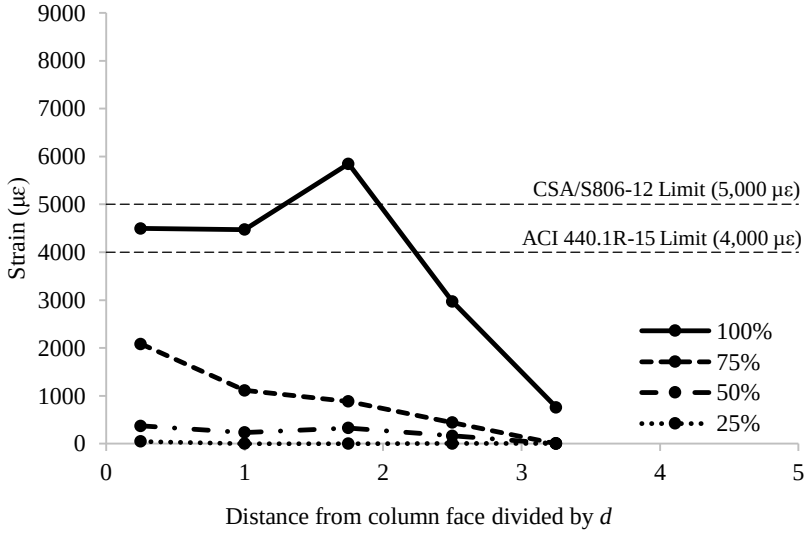

c) N-1.0-C5 (Perpendicular)

Figure 4.17: Shear reinforcement strains versus distance from column face for N-1.0-C5 - continued

4.3.5. Ultimate Strength

The ultimate capacity at failure for Connection N-1.0-XX* was adjusted/normalized for varying concrete strength. The failure load was multiplied by $\sqrt[3]{43/f_c'}$, where 43 MPa is the concrete compressive strength of Series 2 connections, as given in Table 4.5. For Series 2 connections, regardless of the mode of failure and the shear reinforcement ratio, the well-anchored shear reinforcement intercepted the shear cracks and prevented them from widening and extending, which resulted in considerable increase in the ultimate capacity. Connections N-1.0-S5 and N-1.0-S6 (with headed studs) and Connection N-1.0-C5 (with corrugated bars) had 51, 48 and 34% higher capacity than Connection N-1.0-XX* (without shear reinforcement), respectively. It was expected for Connection N-1.0-S6 to fail in flexure at a higher load; however, due to the large stud spacing (0.75 *d*) and the formation of a steep shear crack, it failed at a slightly lower failure load compared to Connection N-1.0-S5, as discussed earlier.

The flexural capacities of the connections were calculated using the yield line theory (Gar et al. 2014; Gouda and El-Salakawy 2016a). Table 4.5 shows a comparison between the actual failure loads, V_{Test}, and the predicted flexural capacities, V_{flex}. For Series 2 connections, Connections N-1.0-S5 and N-1.0-S6 had a V_{Test}/V_{flex} ratios of 0.96 and 0.94, respectively, which might indicate a flexural failure even though they failed in punching failure outside and inside the shear-reinforced zone, respectively. This would happen when both flexural and punching capacities are close to each other. These ratios decreased to 0.85 for Connection N-1.0-C5; which failed, as stated earlier, in punching inside the shear-reinforced zone (Appendix C)

Table 4.5: Failure and normalized load and flexural capacities for Series 2 connections

Connection	Concrete strength, f'_c (MPa)	Failure load, V_{Test} (kN)	Normalized failure load (kN)	Flexural capacity		Failure mode
				V_{flex}[a] (kN)	V_{Test}/V_{flex}	
N-1.0-S5	43	595	595	621	0.96	Flexural/Punching
N-1.0-S6	43	583	583	621	0.94	Flexural/Punching
N-1.0-C5	43	527	527	621	0.85	Punching
N-1.0-XX*	38	378	394	591	0.64	Punching

[a] Calculated using actual f'_c

4.3.6. Proposed Design Equations for Shear-Reinforced Slab-Column Connections

As mentioned in Section 2.4.2, the CSA/S806-12 (CSA 2012) and the ACI 440.1R-15 (ACI Committee 440 2015) provide no provisions for the design of FRP-RC slab-column connections with shear reinforcement. Equations 2.59 to 2.64 proposed by Gouda and El-Salakawy (2016b), were used to calculate the predicted capacities of the slab-column connections with studs shear reinforcement as listed in Table 4.6. Furthermore, in a similar manner, Equations 4.1 and 4.4 were obtained to calculate the punching shear capacity for slabs with stirrup shear reinforcement using the Canadian and American provisions, respectively. Strain limits of 5,000 με and 4,000 με were used for designing shear reinforcement as specified in the CSA/S806-12 (CSA 2012) and the ACI 440.1R-15 (ACI Committee 440 2015), respectively. Moreover, Eqs. 4.2-4.3 and 4.5-4.6 were obtained for the spacing limits for the Canadian and American provisions, respectively. The prediction of the modified code equations (Table 4.6) were calculated at a distance of *d*/2 from the column face or from the outermost peripheral line of shear reinforcement when failure is inside or outside the shear-reinforced zone (Appendix B), respectively.

CSA/S806-12 (Modified). *With shear reinforcement (Proposed)*

$$v_{c,inner(Stirrups)} = 0.028\lambda\phi_c\left(E_f\rho_f f_c^{'}\right)^{1/3} \quad \text{Eq. [4.1]}$$

$$s \le 0.75d \text{ when } v_f \le 0.0825\lambda\phi_c\left(E_f\rho_f f_c^{'}\right)^{1/3} \quad \text{Eq. [4.2]}$$

$$s \le 0.5d \text{ when } v_f > 0.0825\lambda\phi_c\left(E_f\rho_f f_c^{'}\right)^{1/3} \quad \text{Eq. [4.3]}$$

ACI 440.1R-15 (Modified). *With shear reinforcement (Proposed)*

$$v_{c,inner(Stirrups)} = 0.4\sqrt{f_c^{'}}k \quad \text{Eq. [4.4]}$$

$$s \le 0.75d \text{ when } v_f \le 1.2\phi\sqrt{f_c^{'}}k \quad \text{Eq. [4.5]}$$

$$s \le 0.5d \text{ when } v_f > 1.2\phi\sqrt{f_c^{'}}k \quad \text{Eq. [4.6]}$$

4.3.7. Predicted Punching Capacity for Connections with Shear Reinforcement

For Connection N-1.0-S5 (with five peripheral rows of studs), the actual capacity is compared to the predicted outer capacity as it failed outside the shear-reinforced zone. The same trend for Series 1 without shear reinforcement continued with the modified CSA/S806-12 provisions provided accurate prediction with V_{Test}/V_{Pred} equals 1.01, while, the modified ACI 440.1R-15 highly underestimated the capacities with V_{Test}/V_{Pred} equals 1.79. Adding another row of headed studs in Connection N-1.0-S6 (with six peripheral rows of studs) increased the outer capacity and changed the stress distribution inside the shear reinforcement. This is evident in the increased strain readings in the column vicinity for Connection N-1.0-S6 compared to Connection N-1.0-S5, resulting into a failure inside the shear-reinforced zone, as discussed earlier. However, both codes failed to predict the failure mode in which they predicted a failure outside the shear-reinforced zone. Also, the predictions of the modified CSA/S806-12 and the modified ACI 440.1R-15 regarding the upper spacing load limit calculated at the critical section at *d*/2 from the column face

are 528 and 304 kN, respectively. These values are less than the failure load of Connection N-1.0-S6, which suggest that the provided spacing should be reduced to 0.5 *d*, in order to reduce the tendency of shear reinforcement to miss the shear crack, which is believed to be the case for Connection N-1.0-S6. Thus, the predictions of both codes are inaccurate in case of Connection N-1.0-S6 without considering/satisfying the proposed shear reinforcement spacing limits. This resulted into an apparent overestimation of the predicted capacity by the modified CSA/S806-12 with V_{Test}/V_{Pred} of 0.85. However, the modified ACI 440-1R-15 provided V_{Test}/V_{Pred} of 1.51.

On the other hand, for Connection N-1.0-C5 (with five peripheral rows of corrugated bars), the modified CSA/S806-12 provisions provided reasonable predictions and an acceptable safety margin with V_{Test}/V_{Pred} of 1.34. However, the modified ACI 440-1R-15 highly underestimated the capacity with V_{Test}/V_{Pred} of 1.93.

Table 4.6: Predictions for Series 2 connections

Connection	Failure load, V_{Test} (kN)	CSA/S806-12			ACI 440.1R-15		
		Predicted capacity, V_{Pred}		V_{Test}/V_{Pred}[e]	Predicted capacity, V_{Pred}		V_{Test}/V_{Pred}[e]
		Inner[a] (kN)	Outer[b] (kN)		Inner[c] (kN)	Outer[d] (kN)	
N-1.0-S5	595	759	587	1.01	549	332	1.79
N-1.0-S6	583	759	684	0.85	549	387	1.51
N-1.0-C5	527	394	568	1.34	273	321	1.93

[a] Calculated using Eqs. [2.59], [2.61] and [4.1]
[b] Calculated using Eq. [2.60]
[c] Calculated using Eqs. [2.62], [2.64] and [4.4]
[d] Calculated using Eq. [2.63]
[e] Calculated based on the least V_{Pred} value

CHAPTER 5: CONCLUSIONS AND FUTURE WORK

5.1. SUMMARY AND CONCLUSIONS

In this study, the behaviour of FRP-RC slab-column interior connections was investigated. Six full-scale slab-column interior connections were constructed and tested to failure under a combination of shear force and unbalanced moment. All connections had the same dimensions, representing the isolated region of negative moment around an interior column and bounded by the lines of contra-flexure. All connections were reinforced in flexure with a single orthogonal mesh of SC-GFRP bars in the tension side only. The connections were divided into two series; each series consisted of three connections. Series 1 investigated the effect of flexural reinforcement ratio on connections made of HSC, while Series 2 investigated the effect of GFRP shear reinforcement type on connections made of NSC.

Based on the results of the tested connections, the following conclusions can be drawn:

5.1.1. Conclusions from Series 1 Connections (Flexural reinforcement ratio)

1. All tested connections failed in a clear brittle punching failure with no signs of flexural failure. The punching failure was characterized by a sudden drop in the vertical load with punching of the column through the slab.
2. Increasing the flexural reinforcement ratio decreased the failure cone radius, i.e., led to a steeper inclination of the shear crack. Increasing the flexural reinforcement ratio from 1.0% to 1.5 and 2.0% decreased the failure cone radius from 1.72 d to 1.56 d and 1.14 d, respectively. Consequently, it increased the failure cone angle from 30° to 33°, and 41°, respectively.

3. The flexural reinforcement ratio had a significant effect on the punching capacity, post-cracking stiffness and deflection of HSC connections. Increasing the flexural reinforcement ratio by 50 and 100% increased the punching capacity by 15 and 27% and the post-cracking stiffness by 46 and 100%, respectively, and decreased the deflection at service by 52 and 77%, respectively.
4. For all connections, the flexural reinforcement strain profiles were inversely proportional to the distance from the column face, which indicates that no bond slippage occurred during the test, i.e., the sand-coated GFRP bars provided adequate bond performance.
5. The utilization of HSC increased the cracking load and the punching capacity as well as enhanced the pre-cracking behaviour compared to the NSC connection. As the concrete strength increased from 38 to 80 MPa (111% increase), the cracking load and punching capacity increased by 26 and 22%, respectively. In addition, compared to the NSC connection, HSC connection had lower deflection at the same load level.
6. The punching shear provisions of the CSA/S806-12 (CSA 2012) provided reasonable predictions with an acceptable margin of safety and an average V_{Test}/V_{Pred} of 1.18 ± 0.02 (COV = 2.0%). In addition, the predictions of the Japan Society of Civil Engineers code (JSCE 1997) were slightly conservative to the actual capacities with an average V_{Test}/V_{Pred} of 1.34 ± 0.03 (COV = 2.0%). On the other hand, the ACI 440.1R-15 (ACI Committee 440 2015) highly underestimated the capacities with an average V_{Test}/V_{Pred} of 1.80 ± 0.06 (COV = 3.4%). This is attributed to the fact that the punching shear equation of the ACI 440.1R-15 (ACI Committee 440 2015) only accounts for the uncracked concrete contribution to resist the applied shear stresses.

7. For CSA/S806-12 (CSA 2012), the obtained average V_{Test}/V_{Pred} will reduce to 1.05 ± 0.006 (COV = 0.6%) if the limit on the maximum concrete strength is waived and the actual concrete strength is used. However, the margin of safety will be reduced.

5.1.2. Conclusions from Series 2 Connections (Shear reinforcement)

1. Regardless of the mode of failure and the provided shear reinforcement type and ratio, both types of shear reinforcement controlled the widening and propagation of shear cracks, which enhanced the post-cracking stiffness and decreased the deflection at same load level of the shear-reinforced connections. Connections N-1.0-S5, N-1.0-S6 (with headed studs) and N-1.0-C5 (with corrugated bars) had 36, 32 and 14% higher post-cracking stiffness factor than Connection N-1.0-XX* (without shear reinforcement).
2. The use of well-anchored shear reinforcement significantly increased the carrying capacity and deflection at failure. Connections N-1.0-S5, N-1.0-S6 and N-1.0-C5 had 51, 48 and 34% higher punching capacity and 66, 61 and 60% higher deflections at failure than Connection N-1.0-XX*, respectively.
3. Similar to Series 1, no bond slippage occurred during the test as the flexural reinforcement strain profiles were inversely proportional to the distance from the column face.
4. The headed-ends of the shear studs provided adequate anchorage which allowed the studs to develop tensile strains as high as 5,340 με (65.0% of the usable strain provided by the manufacturer) without any signs of slippage. This strain value represents 107% and 134% of the strain limits in the transverse FRP reinforcement of 5,000 and 4,000 με specified in the CSA/S806-12 (CSA 2012) and the ACI 440.1R-15 (ACI Committee 440 2015), respectively.

5. The vertical stems of the corrugated bars managed to develop strains as high as 5,850 με (23.0% of their ultimate tensile strain), which indicates that the GFRP corrugated bars were able to reach their potential capacity. However, further investigation is required to examine the anchorage efficiency of the GFRP corrugated bars with larger bar diameters and/or less stem spacing, if their manufacturing is feasible.
6. For Connection N-1.0-S5 (failed outside the shear-reinforced zone), the modified CSA/S806-12 equations proposed by Gouda and El-Salakawy (2016b) provided accurate prediction with V_{Test}/V_{Pred} equals 1.01, while, the modified ACI 440.1R-15 highly underestimated the capacities with V_{Test}/V_{Pred} equals 1.79. On the other hand, the modified code predictions are not accurate for Connection N-1.0-S6. As both codes predicted a failure outside the shear-reinforced zone, while, in fact, it failed in a mixed flexural-punching mode inside the shear-reinforced zone due to the large stud spacing.
7. For Connection N-1.0-C5, the modified CSA/S806-12 provisions provided reasonable prediction and an acceptable margin of safety with V_{Test}/V_{Pred} of 1.34. However, the modified ACI 440-1R-15 highly underestimated the capacity with V_{Test}/V_{Pred} of 1.93.

5.2. FUTURE WORK

The following are suggestions for further studies on the punching shear behaviour of GFRP-RC slab-column interior connections:

1. Studying the seismic response of FRP-RC slab-column interior connections.
2. Further investigation of the effect of shear reinforcement (e.g., less stud/stem spacing, corrugated bars with larger bar diameters, different arrangements)
3. The size effect (e.g., slab thickness, column size, column aspect ratio).
4. Effect of openings.

REFERENCES

ACI-ASCE Committee 326. (1962). "Shear and Diagonal Tension." *ACI Journal Proceedings*, 59(3), 353–396.

ACI Committee 318. (1971). "Building Code Requirements for Reinforced Concrete." *ACI 318-71*, American Concrete Institute, Farmington Hills, MI, 78 p.

ACI Committee 318. (1995). "Building Code Requirements for Reinforced Concrete." *ACI 318-95*, American Concrete Institute, Farmington Hills, MI, 369 p.

ACI Committee 318. (2005). "Building Code Requirements for Reinforced Concrete." *ACI 318-05*, American Concrete Institute, Farmington Hills, MI, 427 p.

ACI Committee 318. (2014). "Building Code Requirements for Structural Concrete and Commentary." *ACI 318- 14*, American Concrete Institute, Farmington Hills, MI, 524 p.

ACI Committee 363. (2010). "Report on High Strength Concrete." *ACI 363R-10*, American Concrete Institute, Farmington Hills, MI, 65 p.

ACI Committee 421. (2008). "Guide to Shear Reinforcement for Slabs." *ACI 421.1R-08*, American Concrete Institute, Farmington Hills, MI, 27 p.

ACI Committee 440. (2006). "Guide for the Design and Construction of Structural Concrete Reinforced with FRP Bars." *ACI 440.1R-06*, American Concrete Institute, Farmington Hills, MI, 44 p.

ACI Committee 440. (2015). "Guide for the Design and Construction of Structural Concrete Reinforced with Fiber-Reinforced Polymer (FRP) Bars." *ACI 440.1R-15*, American Concrete Institute, Farmington Hills, MI, 88 p.

Alexander, S. D. B. and Simmonds, S. H. (1986). "Shear-Moment Transfer in Slab Column Connections." *Structural Engineering Report No. 141*, University of Alberta, Edmonton.

ASTM. (2016). "Standard Test Method for Tensile Properties of Fiber Reinforced Polymer Matrix." *ASTM D7205/D7205M*, American Society for Testing and Materials, West Conshohocken, PA.

Banthia, N., Al-Asaly, M. and Ma, S. (1995). "Behavior of Concrete Slabs Reinforced with Fiber-Reinforced Plastic Grid." *Journal of Materials in Civil Engineering*, 7(4), 252–257.

Bentur, A., Diamond, S. and Berke, N. (1997). "Steel Corrosion in Concrete: Fundamentals and Civil Engineering Practice." London: E & FN Spon.

Birkle, G. and Dilger, W. (2008). "Influence of Slab Thickness on Punching Shear Strength." *ACI Materials Journal*, 105(2), 180–188.

British Standards Institution. (1997). "Structural Use of Concrete, BS 8110: Part 1: Code of Practice for Design and Construction." London, United Kingdom, 172 p.

Corley, W. G. and Hawkins, N. M. (1968). "Shearhead Reinforcement for Slabs." *ACI Journal Proceedings*, 65(10), 811–824.

Criswell, M. E. and Hawkins, N. M. (1974). "Shear Strength of Slabs: Basic Principle and Their Relation to Current Methods of Analysis." *ACI Special Publication*, SP-42, 641–676.

CSA. (2004). "Design of Concrete Structures." *CAN/CSA-A23.3-04. Canadian Standards Association*, Toronto, Ontario, 240 p.

CSA. (2012). "Design and Construction of Building Structurs with Fibre-Reinforced Polymer." *CAN/CSA S806- 12, Canadian Standards Association,* Toronto, ON, Canada.

CSA. (2014a). "Design of Concrete Structures." *CAN/CSA S23.3- 14, Canadian Standards Association,* Toronto, ON, Canada.

CSA. (2014b). "Concrete materials and methods of concrete construction/Test methods and standard practices for concrete." *CAN/CSA A23.1/A23.2-14, Canadian Standards*

Association, Toronto, ON, Canada.

Dilger, W., Birkle, G. and Mitchell, D. (2005). "Effect of Flexural Reinforcement on Punching Shear Resistance." *ACI Special Publication*, 232, 57–74.

Dilger, W. and Ghali, A. (1981). "Shear Reinforcement for Concrete Slabs." ASCE, *Journal of the Structural Division*, 107, 2403–2420.

Dulude, C., Hassan, M., Ahmed, E. and Benmokrane, B. (2013). "Punching Shear Behavior of Flat Slabs Reinforced with Glass Fiber-Reinforced Polymer Bars." *ACI Structural Journal*, 110(5), 723–734.

El-Gamal, S., El-Salakawy, E. and Benmokrane, B. (2005). "A New Punching Shear Equation for Two-Way Concrete Slabs Reinforced with FRP Bars." *ACI Special Publication*, SP-230, 877–894.

El-Gendy, M. and El-Salakawy, E. (2016a). "Effect of Shear Studs and High Moments on Punching Behavior of GFRP-RC Slab – Column Edge Connections." ASCE, *Journal of Composites for Construction*, 20(4), 4016007.

El-Gendy, M. and El-Salakawy, E. (2016b). "Punching Shear Behavior of GFRP-RC Slab-Column Edge Connections." in "Towards Sustainable Infrastructure with Fiber Reinforced Polymer Composites." *ACI Special Publication*, SP-06, in press, 20 p.

El-Ghandour, A. W., Pilakoutas, K. and Waldron, P. (1999). "New Approach for Punching Shear Capacity Prediction of Fiber Reinforced Polymer Reinforced Concrete Flat Slabs." *ACI Special Publication*, SP-188, 135–144.

El-Ghandour, A. W., Pilakoutas, K. and Waldron, P. (2003). "Punching Shear Behavior of Fiber Reinforced Polymers Reinforced Concrete Flat Slabs : Experimental Study." ASCE, *Journal of Composites for Construction*, 7(3), 258–265.

El-Salakawy, E., Polak, M. A. and Soliman, M. H. (1998). "Slab-column edge connections subjected to high moments." *Canadian Journal of Civil Engineering*, 25(3), 526–538.

El-Salakawy, E., Polak, M. A. and Soliman, M. H. (2000). "Reinforced Concrete Slab – Column Edge Connections With Shear Studs." *Canadian Journal of Civil Engineering*, 27(2), 338–348.

Elgabry, A. A. and Ghali, A. (1987). "Tests on Concrete Slab-Column Connections with Stud-Shear Reinforcement Subjected to Shear-Moment Transfer." *ACI Structural Journal*, 84(5), 433–442.

Elstner, R. C. and Hognestad, E. (1956). "Shearing Strength of Reinforced Concrete Slabs." *ACI Journal Proceedings*, 53(7), 29–58.

European Standard, EN. 1992-1-1. (2004). "Eurocode 2: Design of concrete structures, Part 1, General Rules and Rules for Buildings." *British Standard*, London, United Kingdom, 230 p.

Gar, S. P., Mander, J. B., Head, M. and Hurlebaus, S. (2014). "FRP Slab Capacity Using Yield Line Theory." *Journal of Composites for Construction*, 18(6), 4014021.

Gardner, N. J. (1990). "Relationship of the Punching Shear Capacity of Reinforced Concrete Slabs With Concrete Strength." *ACI Structural Journal*, 87(1), 66–71.

Gardner, N. J. and Shao, X. Y. (1996). "Punching shear of continuous flat reinforced concrete slabs." *ACI Structural Journal*, 93(2), 218–228.

Gayed, R. B. and Ghali, A. (2008). "Unbalanced Moment Resistance in Slab-Column Joints: Analytical Assessment." *Journal of Structural Engineering*, 134(5), 859–864.

Gentry, T. R. and Husain, M. (1999). "Thermal Compatibility of Concrete and Composite Reinforcements." *Journal of Composites for Construction*, 3(2), 82–86.

Ghali, A., Dilger, W. and Ramez, B. (2013). "Punching of Concrete Slabs : Interpretation of Test

Results." *Journal of Structural Engineering*, 139(6), 869–874.

Ghannoum, C. M. (1998). "Effect of High-Strength Concrete on the Performance of Slab-column Specimens." MSc Thesis, McGill University, Montréal, QC, Canada.

Gouda, A. (2015). "Punching Shear Behaviour of FRP-Reinforced Concrete Interior Slab-Column Connections." PhD Thesis, University of Manitoba, 241 p.

Gouda, A. and El-Salakawy, E. (2016a). "Punching Shear Strength of GFRP-RC Interior Slab–Column Connections Subjected to Moment Transfer." ASCE, *Journal of Composites for Construction*, 20(1), 4015037.

Gouda, A. and El-Salakawy, E. (2016b). "Behavior of GFRP-RC Interior Slab-Column Connections with Shear Studs and High-Moment Transfer." ASCE, *Journal of Composites for Construction*, 20(4), 4016005.

Guandalini, S., Burdet, O. L. and Muttoni, A. (2009). "Punching Tests of Slabs with Low Reinforcement Ratios." *ACI Structural Journal*, 106(1), 87–95.

Hallgren, M. and Kinnunen, S. (1996). "Increase of Punching Shear Capacity by Using High Strength Concrete." *4th International Symposium on Utilization of High-Strength/High-Performance Concrete, Paris*, 1037–1046.

Hassan, M., Ahmed, E. and Benmokrane, B. (2013). "Punching-Shear Strength of Normal and High-Strength Two-Way Concrete Slabs Reinforced with GFRP Bars." *Journal of Composites for Construction*, 17(6), 4013003.

Hassan, M., Ahmed, E. and Benmokrane, B. (2014a). "Punching-shear design equation for two-way concrete slabs reinforced with FRP bars and stirrups." *Construction and Building Materials*, 66(15), 522–532.

Hassan, M., Ahmed, E. and Benmokrane, B. (2014b). "Punching Shear Behavior of Two-Way

Slabs Reinforced with FRP Shear Reinforcement." *Journal of Composites for Construction*, 19(1), 4014030.

Hawkins, N. M. (1974). "Shear Stength of Slabs with Moments Transferred to Columns." *ACI Special Publication*, 42, 817–846.

Hawkins, N. M., Criswell, M. E. and Roll, F. (1974). "Shear Strength of Slabs Without Shear Reinforcement." *ACI Special Publication*, 42, 677–720.

Hawkins, N. M. and Mitchell, D. (1979). "Progressive Collapse of Flat Plate Structures." *ACI Journal Proceedings*, 76(7), 775–808.

Heinzmann, D., Etter, S., Villiger, S. and Jaeger, T. (2012). "Punching Tests on Reinforced Concrete Slabs with and without Shear Reinforcement." *ACI Structural Journal*, 109(6), 787–794.

Hsueh, P. K. (1966). "The Yield-Line Theory for Concrete Slabs." A Master's Report, Kansas State University, Manhattan, Kansas.

ISIS canada. (2007). "Reinforcing Concrete Structures with Fibre Reinforced Polymers - Design Manual No. 3." The Canadian Network of Centres of Excellence on Intelligent Sensing for Innovative Structures, *ISIS Canada Research Network*, Winnipeg, Manitoba, 151 p.

JSCE. (1997). "Recommendation for Design and Construction of Concrete Structures Using Continuous Fibre Reinforcing Materials." Japan Society of Civil Engineers, *Concrete Engineering*, Series 23, Tokyo, Japan, 325 p.

JSCE. (2007). "Standard Specification for Concrete Structures." Japan Society of Civil Engineers, Tokyo, Japan, 469 p.

Kodur, V. K. R. and Baingo, D. (1998). "Fire Resistance of FRP Reinforced Concrete Slabs." *IRC Internal Report No. 758. Ottawa: National Research Council of Canada*, 44 p.

Lee, J., Yoon, Y., Cook, W. and Mitchell, D. (2009). "Improving Punching Shear Behavior of Glass Fiber-Reinforced Polymer Reinforced Slabs." *ACI Structural Journal*, 106(4), 427–434.

Luo, Y. H. and Durrani, A. J. (1995). "Equivalent Beam Model for Flat-Slab Buildings:Part I: Interior Connections." *ACI Structural Journal*, 92(1), 115–124.

Marzouk, H., Emam, M. and Hilal, M. S. (1996). "Effect of High-Strength Concrete Columns on the Behavior of Slab-Column Connections." *Structural Journal*, 93(5), 545–554.

Marzouk, H., Emam, M. and Hilal, M. S. (1998). "Effect of High-Strength Concrete Slab on the Behavior of Slab-Column Connections." *ACI Structural Journal*, 95(3), 227–237.

Marzouk, H. and Hussein, A. (1991). "Punching Shear Analysis of Reinforced High-Strength Concrete Slabs." *Canadian Journal of Civil Engineering*, 18(6), 954–963.

Marzouk, H. and Hussein, A. (1992). "Experimental Investigation on the Behavior of High-Strength Concrete Slabs." *ACI Structural Journal*, 88(6), 701–713.

Marzouk, H., Osman, M. and Helmy, S. (2000). "Behavior of High-Strength Lightweight Aggregate Concrete Slabs Under Column Load and Unbalanced Moment." *ACI Structural Journal*, 97(6), 860–866.

Masterson, D. M. and Long, A. E. (1974). "The Punching Strength of Slabs, a Flexural Approach Using Finite Elements." *ACI Special Publication*, 42, 747–768.

Matthys, S. and Taerwe, L. (2000). "Concrete Slabs Reinforced with FRP Grids. II: Punching Resistance." *Journal of Composites for Construction*, 4(3), 154–161.

Megally, S. and Ghali, A. (1994). "Design Considerations for Slab-Column Connections in Seismic Zones." *ACI Structural Journal*, 91(3), 303–314.

Menétrey, P. (1998). "Relationships between Flexural and Punching Failure." *ACI Structural*

Journal, 95(4), 412–419.

Mitchell, D., Cook, W. and Dilger, W. (2005). "Effects of Size, Geometry and Material Properties on Punching Shear Resistance." *ACI Special Publication*, 232, 39–56.

Moe, J. (1961). "Shearing Strength of Reinforced Concrete Slabs and Footings Under Concentrated Loads." Illinois, USA, 139 p.

Mokhtar, A., Ghali, A. and Dilger, W. (1985). "Stud Shear Reinforcement for Flat Concrete Plates." *ACI Journal Proceedings*, 82(5), 676–683.

Mortin, J. D. (1989). "Connection of Concrete Slabs with Edge Cloumns." MSc Thesis, University of Calgary, 202 p.

Mortin, J. D. and Ghali, A. (1991). "Connection of Flat Plates to Edge Columns." *ACI Structural Journal*, 88(2), 191–198.

Nguyen-Minh, L. and Rovňák, M. (2013). "Punching Shear Resistance of Interior GFRP Reinforced Slab-Column Connections." *Journal of Composites for Construction*, 17(1), 2–13.

NRCC. (2015). "National Building Code of Canada." National Research Council of Canada, Ottawa, Ontario, 1404 p.

Osman, M., Marzouk, H. and Helmy, S. (2000). "Behavior of High-Strength Lightweight Concrete Slabs under Punching Loads." *ACI Structural Journal*, 97(3), 492–498.

Ospina, C. E. (2005). "Alternative Model for Concentric Punching Capacity Evaluation of Reinforced Concrete Two-Way Slabs." *ACI Concrete International*, 27(9), 53–57.

Ospina, C. E., Alexander, S. D. B. and Cheng, L. J. R. (2003). "Punching of Two-Way Concrete Slabs with Fiber-Reinforced Polymer Reinforcing Bars or Grids." *ACI Structural Journal*, 100(5), 589–598.

Ozden, S., Ersoy, U. and Ozturan, T. (2006). "Punching Shear Tests of Normal- and High-Strength Concrete Flat Plates." *Canadian Journal of Civil Engineering*, 33(11), 1389–1400.

Polak, M. A., El-Salakawy, E. and Hammill, N. L. (2005). "Shear Reinforcement for Concrete Flat Slabs." *ACI Special Publication*, 232, 75–96.

Pultrall Inc. (2015). "Private communication." ADS Composites Group, Thetford Mines, QC, Canada.

Ramdane, K. E. (1996). "Punching Shear of High Performance Concrete Slabs." *4th International Symposium on Utilization of High-Strength/High-Performance Concrete*, Paris, 1015-1026.

Richart, F. E. (1948). "Reinforced Concrete Wall and Column Footings." *ACI Journal Proceedings*, 45(10), 97–127.

Ritchie, M., Ghali, A., Dilger, W. and Gayed, R. B. (2006). "Unbalanced Moment Resistance by Shear in Slab-Column Connections : Experimental Assessment." *ACI Structural Journal*, 103(1), 74–82.

Rizk, E., Marzouk, H. and Hussein, A. (2011a). "Punching Shear of Thick Plates with and without Shear Reinforcement." *ACI Structural Journal*, 108(5), 581–591.

Rizk, E., Marzouk, H., Hussein, A. and Hossin, M. (2011b). "Effect of reinforcement ratio on punching capacity of RC plates." *Canadian Journal of Civil Engineering*, 38(7), 729–740.

Robertson, I. N., Kawai, T., Lee, J. and Enomoto, B. (2002). "Cyclic Testing of Slab-Column Connections with Shear Reinforcement." *ACI Structural Journal*, 99(5), 605–613.

Scordelis, A. C., Lin, T. Y. and May, H. R. (1958). "Shearing Strength of Prestressed Lift Slabs." *ACI Journal Proceedings*, 55(10), 485–506.

Seible, F., Ghali, A. and Dilger, W. (1980). "Preassembled Shear Reinforcing Units for Flat Plates." *ACI Journal Proceedings*, 77(1), 28–35.

Sherif, A. G. and Dilger, W. (1996). "Critical review of the CSA A23.3-94 punching shear strength provisions for interior columns." *Canadian Journal of Civil Engineering*, 23(5), 998–1011.

Stein, T. (2006). "Punching and Flexural Strength of Flat Plates." *University of Calgary*, 136 p.

Stein, T., Ghali, A. and Dilger, W. (2007). "Distinction between Punching and Flexural Failure Modes of Flat Plates." *ACI Structural Journal*, 104(3), 357–365.

Tureyen, A. K. and Frosch, R. J. (2003). "Concrete Shear Strength : Another Perspective." *ACI Structural Journal*, 100(5), 609–615.

Wheeler, W. H. (1936). "This Flat-Slab Floors Prove Rigid Under Test." *Engineering News Record*, 116(2), 49–50.

Whitney, C. S. (1957). "Ultimate Shear Strength of Reinforced Concrete Flat Slabs , Footings , Beams , and Frame Members Without Shear Reinforcement." *ACI Journal Proceedings*, 54(10), 265–298.

Zaghlool, E. R. F. and De Pavia, H. A. R. (1973). "Tests of Flat-Plate Corner Column-Slab Connections." *Journal of the Structural Division*, 99(3), 551–572.

Zaghloul, A. (2002). "Behaviour and Strength of CFRP Reinforced Flat Plate Interior Column Connections Subjected to Shear and Unbalanced Moment." Master of Applied Science, Carleton University, Ottawa, Ontario, Canada.

Zaghloul, A. (2007). "Punching Shear Strength of Interior and Edge Column-Slab Connections in CFRP Reinforced Flat Plate Structures Transferring Shear and Moment." Carleton University, Ottawa, Ontario, Canada .

Zaghloul, A. and Razaqpur, A. G. (2004). "Punching Shear Strength of Concrete Flat Plates Reinforced With CFRP Grids." *Proceedings of the 4th Conference on Advanced Composite Materials in Bridges and Structures*, Calgary, Alberta, 1-8.

Zaidi, A. and Masmoudi, R. (2008). "Thermal effect on fiber reinforced polymer reinforced concrete slabs." *Canadian Journal of Civil Engineering*, 35(3), 312–320.

Zhang, Q., Marzouk, H. and Hussein, A. (2005). "A Preliminary Study of High Strength Concrete Two-Way Slabs Reinforced with GFRP Bras." *Proceedings of the 33rd CSCE Annual Conference: General Conference and International History Symposium*, GC-318-1 to GC-318-10.

APPENDIX A

Analysis of a Parking Garage Flat Plate

A.1. Layout of the Flat Plate System

Figure A-1 shows a plan view of a portion of a typical floor in a parking garage structure consisting of 6.5-m long square bays, all columns measure 300 × 300 mm. Two orthogonal strips are designed: vertical and horizontal strips as presented.

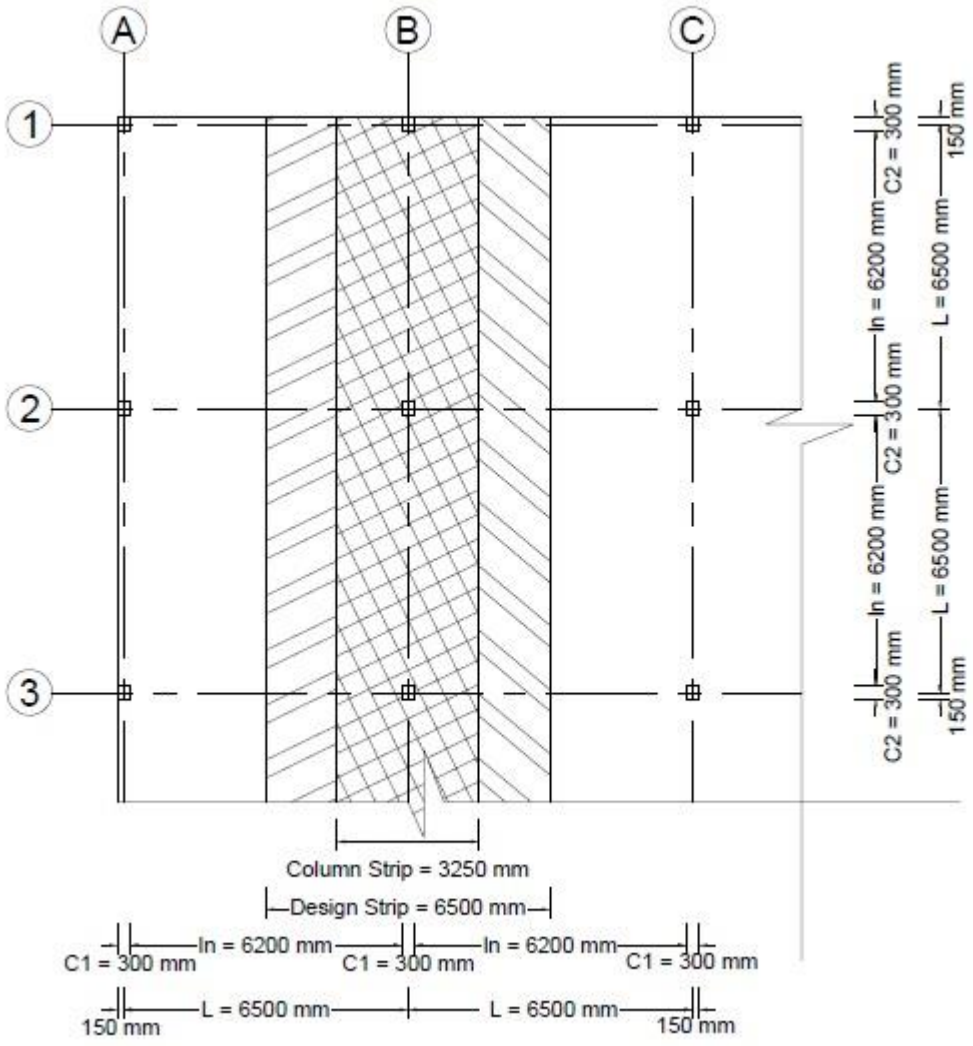

a) Vertical strip

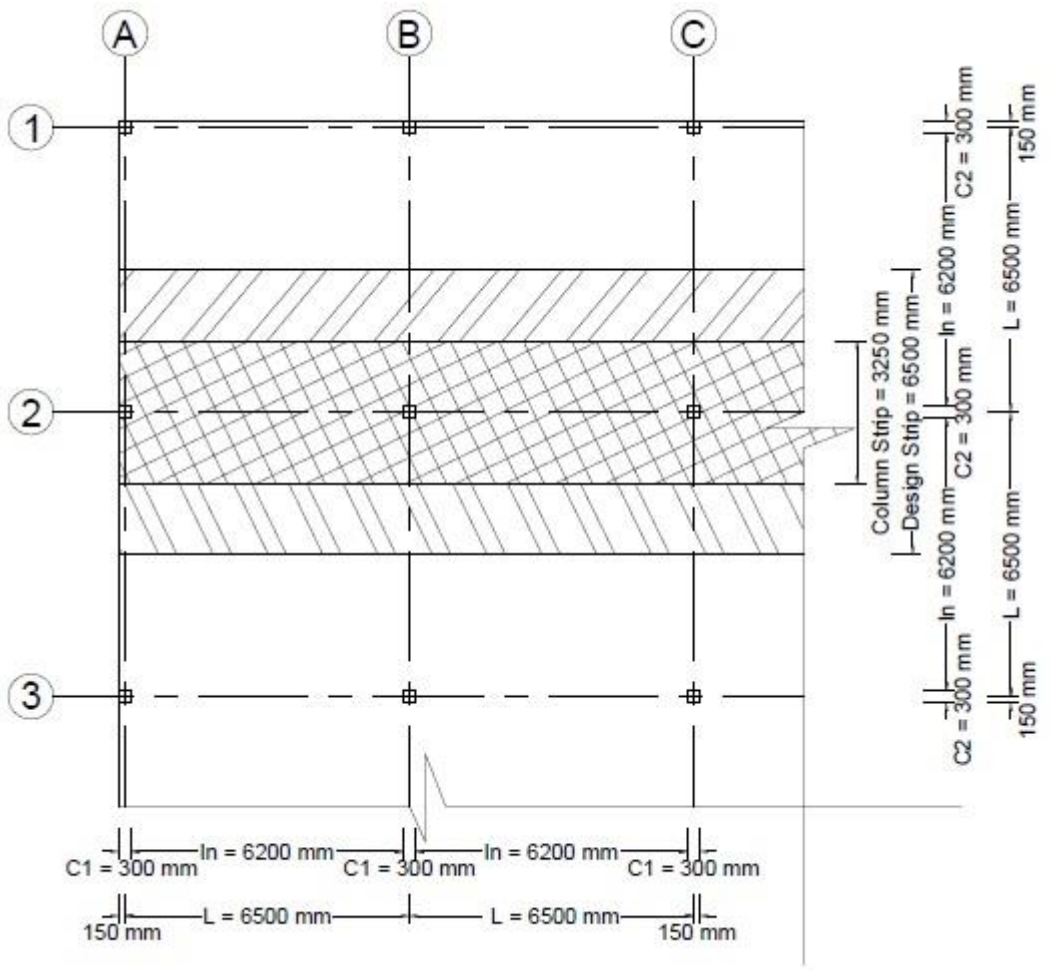

b) Horizontal Strip

Figure A-1: Design strips

A.2. Properties of Concrete

Compressive strength of concrete f_c' = 40 *MPa*

Material resistance factor $\emptyset_c$ = 1.0

Ultimate compressive strain of concrete ε_{cu} = 0.0035 **Clause 10.1.3 (CSA 2014a)**

α_1 = 0.85 – 0.0015 f_c' = 0.79 **Clause 10.1.7 (CSA 2014a)**

β_1 = 0.97 – 0.0025 f_c' = 0.87 **Clause 10.1.7 (CSA 2014a)**

A.3. Loads

L.L. = 2.4 kN / m^2 **(NRCC 2015)**

D.L. = *self-weight + partition allowance* = 24 * 0.2 + 1 = 5.8 kN / m^2 **(NRCC 2015)**

Factored load = 1.4 D.L. = 8.12 kN / m^2 **(NRCC 2015)**

Or = 1.25 D.L. + 1.5 L.L. = 10.85 kN / m^2 (Governs)

A.4. Slab Thickness "h_s"

Minimum slab thickness $h_s = \frac{l_n(0.6+\frac{f_y}{1{,}000})}{30}$ **Clause 13.2.3 (CSA 2014a)**

$$= \frac{6200\left(0.6+\frac{415}{1{,}000}\right)}{30} = 209.77\ mm$$

Take $h_s = 200\ mm$

A.5. Analysis of a sand-coated GFRP-RC Parking Garage Flat Plate (According to CSA/A23.3-14 and CSA/S806-12)

A.5.1. Properties of reinforcement

Use No. 16 bars $d_b = 15.9\ mm$ $A_b = 198\ mm^2$

Ultimate tensile strength of GFRP $f_{frp_u} = 1{,}684.8\ MPa$

Ultimate tensile strain for GFRP $\varepsilon_{frp_u} = 0.026$

Modulus of elasticity for GFRP $E_{frp} = 64{,}957\ MPa$

Material resistance factor $\emptyset_f = 1.0$

A.5.2. Vertical Strip (Upper Layer)

A.5.2.1. Effective depth "d"

Take concrete clear cover = 24 *mm*

Effective depth d = $h_s - clear\ cover - \frac{d_b}{2} = 168\ mm$

A.5.2.2. Design Moments

$M_o = \frac{w_f * l_{2a} * {l_n}^2}{8} = 338.87\ kN.m$ **Clause 13.9.2.2 (A23.3-2014a)**

Table A-1: Moment distribution in a design strip (vertical strip)

Axis	1		2			3	Units	Clause
l_n	6200			6200				
M_{Design}	26	52	70	65	35	65	%	13.9.3
	88.1	176.2	237.2	220.3	118.6	220.3	kN.m	
$M_{Col.\ Str}$	100	55 – 65	70 – 90	70 – 90	55 – 65	70 – 90	%	13.11.2
	88.1	96.9 – 114.5	**166 – 213.5**	154.2 – 198.3	65.2 – 77.1	154.2 – 198.3	kN.m	
$M_{Fld.\ Str}$	0	35 – 45	10 – 30	10 – 30	35 – 45	10 – 30	%	13.11.2
	0	61.7 – 79.3	23.7 – 71.2	22 – 66.1	41.5 – 53.4	22 – 66.1	kN.m	

A.5.2.3. Reinforcement

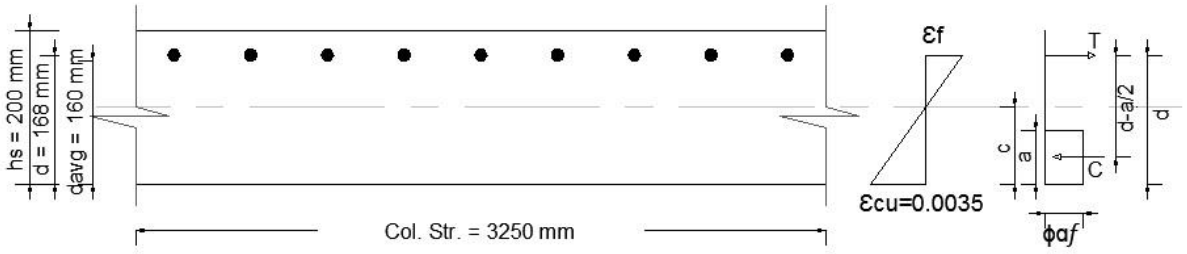

Figure A-2: Strain distribution and equivalent stress block (top layer)

$M_r = \alpha_1 \emptyset_c f_c' b \beta_1 c * \left(d - \frac{\beta_1 c}{2}\right)$

$c = 14.8\ mm$

From strain compatibility:

$\varepsilon_f = \varepsilon_{cu}\left(\frac{d}{c} - 1\right) = 0.036 > \varepsilon_{frp_u} = 0.026$

Try $A_{f_{min}} = \frac{400}{E_{frp}} A_g = 4{,}002.64\ mm^2$ **Clause 8.4.2.3 (CSA 2012)**

$c = 36.58\ mm \qquad \varepsilon_f = 0.0126$

$f_{frp} = 64{,}957 * 0.0126 = 818.46\ MPa < f_{frp_u} = 1{,}684.8\ MPa$

$M_r = 497.08\ kN.m > 213.5\ kN.m$

$A_f = \frac{b}{s} * A_b \Rightarrow s = 160.77\ mm$ Use #16 @ 160 mm c/c

$A_{f_{act}} = \frac{3{,}250}{160} * 198 = 4{,}021.88\ mm^2$

Check for the Balanced Reinforcement Ratio "ρ_b "

$\rho = \frac{A_{f_{act}}}{d * b_b} = 0.737\%$

$\rho_b = \frac{\alpha_1 \emptyset_c f_c' \beta_1}{\emptyset_f f_{frp_u}} \left[\frac{\varepsilon_{cu}}{\varepsilon_{cu} + \varepsilon_{frp_u}}\right] = 0.194\%$

$\rho > \rho_b$ (Over-reinforced) Ok

Check for Unbalanced Moment **Clause 13.9.4 (CSA 2014a)**

$M_{Unb} = 0.07\left(\left(w_{df} + 0.5 w_{lf}\right) l_{2a} {l_n}^2 - {w'}_{df} {l'}_{2a} (l'_n)^2\right)$

$M_{Unb} = 0.07\left((7.25 + 0.5 * 3.6) 6.5 * 6.2^2 - 7.25 * 6.5 * 6.2^2\right) = 31.48\ kN.m$

$\gamma_f = \frac{1}{1 + \frac{2}{3}\sqrt{\frac{b_1}{b_2}}} = \frac{1}{1 + \frac{2}{3}\sqrt{\frac{460}{460}}} = 0.6$ **Clause 13.10.2 (CSA 2014a)**

$\gamma_f * M_{Unb} = 0.6 * 31.48 = 18.9\ KN.m < (M_r = 497.08\ kN.m)$ Ok

A.5.2.4. Development Length **Clause 9.3.2 (CSA 2012)**

$l_d = 1.15\ \frac{k_1 k_2 k_3 k_4 k_5}{d_{cs}} \frac{f_{frp}}{\sqrt{f_c'}} A_b$

$k_1 =$ 1.0 *for horizontal reinforcement placed in such a way that less than* 300 *mm of fresh concrete is cast in the member below the development length*

$k_2 = 1.0\ for\ normal\ density\ concrete$

$k_3 = 0.8\ for\ A_b \leq 300\ mm^2$

$k_4 = 1.0\ for\ for\ GFRP$

$k_5 = 1.0\ for\ sand - coated\ bars$

d_{cs} is the smaller of the distance from the closest concrete surface to the centre of the bar being developed; or two-thirds of the centre-to-centre spacing of the bars being developed

$d_{cs} = 200 - 168 = 32\ mm$ (Governs)

Or $= \frac{2}{3} * 168 = 112\ mm$

$d_{cs} = 32\ mm < 2.5\ d_b = 40\ mm$ Ok

$\sqrt{f_c'} = \sqrt{40} = 6.3 > 5\ MPa \Rightarrow \quad take\ \sqrt{f_c'} = 5\ MPa$ **Clause 9.3.2 (CSA 2012)**

$l_d = 1.15\ \frac{1*1*0.8*1*1}{32} * \frac{818.46}{5}\ 198 = 810.3\ mm$

A.5.2.5 Serviceability Check

A.5.2.5.1. Service Stress Calculations

Specified loads $w_s = D.L. + L.L. = 8.2\ kN/m^2$ **(NRCC 2015)**

Service moment $M_s = \frac{w_s * l_{2a} * {l_n}^2}{8} = 256.1\ kN.m$

Service moment at the interior connection $= 0.7 * 0.9 * 256.1 = 161.3\ kN.m$

$E_c = \left(3{,}300\sqrt{f_c'} + 6{,}900\right)\left(\frac{\gamma_c}{2{,}300}\right)^{1.5} = 30{,}466\ MPa$ **Clause 8.6.2.2 (A23.3-2014a)**

$n = \frac{E_f}{E_c} = 2.13$

$k = \sqrt{2\rho n + (\rho n)^2} - \rho n = 0.158$

$j = 1 - \frac{k}{3} = 0.947$

Service stress $f_s = \frac{M_s}{A_f j d} = 252\ MPa\ < 0.25\ f_{frp_u} = 421.2\ MPa$ Ok

A.5.2.5.2. Crack Control Parameter

$d_c = h_s - d = 32\ mm$

$A = 2 * S * d_c = 10{,}240\ mm^2$

$z = f_s k_b \frac{E_s}{E_f} \sqrt[3]{d_c A} = 42{,}151\ N/mm > 38{,}000\ N/mm$ **Clause 8.3.1 (CSA 2012)**

Try # 16 @ 145 mm c/c for the whole specimen

$A_{f_{act}} = 4{,}437.93\ mm^2 \qquad \rho = \frac{A_{f_{act}}}{d * b_b} = 0.813\%$

Service stress $f_s = 229.2\ MPa$

$A = 2 * S * d_c = 9{,}280 mm^2$

$z = f_s k_b \frac{E_s}{E_f} \sqrt[3]{d_c A} = 37{,}100\ N/mm \cong 38{,}000\ N/m$ Ok

Summary:

- **Place # 16 @ 145 mm c/c for the upper layer.**

A.5.3. Horizontal Strip (Lower Layer)

A.5.3.1. Reinforcement

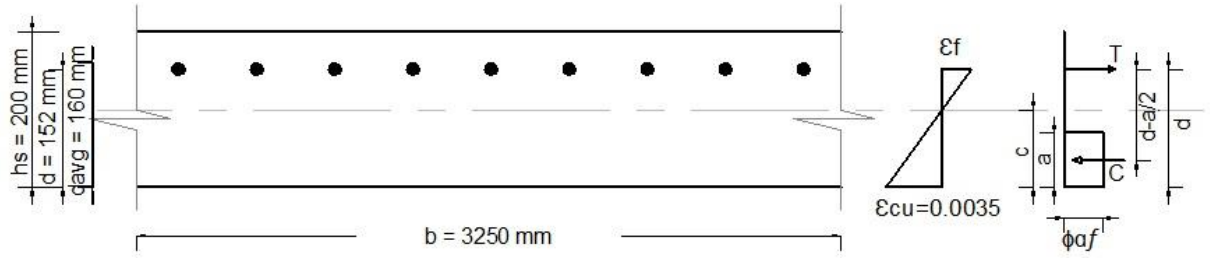

Figure A-2: Strain distribution and equivalent stress block (lower layer)

Try $A_{f_{min}} = \frac{400}{E_{frp}} A_g = 4{,}002.64\ mm^2$ **Clause 8.4.2.3 (CSA 2012)**

$c = 34.58\ mm \qquad \varepsilon_f = 0.0119$

$f_{frp} = 64{,}957 * 0.0119 = 773\ MPa < f_{frp_u} = 1{,}684.8\ MPa$

$M_r = 423.16\ KN.m > 213.5\ KN.m$

$A_f = \frac{b}{s} *\ A_b \ \Rightarrow \quad s = 160.77\ mm$ Use #16 @ 160 mm c/c

$A_{f_{act}} = \frac{3{,}250}{160} * 198 = 4{,}021.88\ mm^2$

A.5.3.2. Serviceability Check

A.5.3.2.1. Service Stress Calculations

$k = \sqrt{2\rho n + (\rho n)^2} - \rho n \ = 0.168$

$j = 1 - \frac{k}{3} = 0.944$

Service stress $f_s = \frac{M_s}{A_f j d} = 279.51\ MPa$

A.5.3.2.2. Crack Control Parameter

$d_c = h_s - d = 48\ mm$

$A = 2 * S * d_c = 15360\ mm^2$

$z = f_s k_b \frac{E_s}{E_f} \sqrt[3]{d_c A} = 61{,}264\ N/mm > 38{,}000\ N/mm$ **Clause 8.3.1 (CSA 2012)**

Try # 16 @ 110 mm c/c for the whole specimen

$A_{f_{act}} = 5{,}850\ mm^2$

$\rho = \frac{A_{f_{act}}}{d * b_b} = 1.184\%$

$k = \sqrt{2\rho n + (\rho n)^2} - \rho n = 0.202$

$j = 1 - \frac{k}{3} = 0.933$

Service stress $f_s = \frac{M_s}{A_f j d} = 194.43\ MPa$

$A = 2 * S * d_c = 10{,}560 mm^2$

$z = f_s k_b \frac{E_s}{E_f} \sqrt[3]{d_c A} = 37{,}612\ N/mm \cong 38{,}000\ N/m$ Ok

Summary:

- **Place # 16 @ 110 mm c/c for the lower layer.**

APPENDIX B

Shear Capacity of Connections

B.1. Shear Capacity of Connections without Shear Reinforcement

B.1.1. Properties of the Critical Section

$d_v = 160\ mm$

$b_1 = c_1 + 2 * \frac{d_v}{2} = 300 + 2 * \frac{160}{2} = 460\ mm$

$b_2 = c_2 + 2 * \frac{d_v}{2} = 300 + 2 * \frac{160}{2} = 460\ mm$

$b_\circ = 2 * (b_1 + b_2) = 2(460 + 460) = 1{,}840\ mm$

$e = \frac{b_1}{2} = \frac{460}{2} = 230\ mm$

$\beta_c = \frac{long\ side}{short\ side} = \frac{300}{300} = 1$

$J = \frac{d_v * {b_1}^3}{6} + \frac{{d_v}^3 * b_1}{6} + \frac{d_v * b_2 * {b_1}^2}{2} = 1.069653333 * 10^{10}\ mm^4$

$A_c = d_v * b_\circ = 160 * 1{,}840 = 294{,}400\ mm^2$

Where *e* is the distance between the centroid and the inner side of the critical section, *J* is a property of the critical shear section analogous to the polar moment of inertia and A_c is the area of concrete of assumed critical section

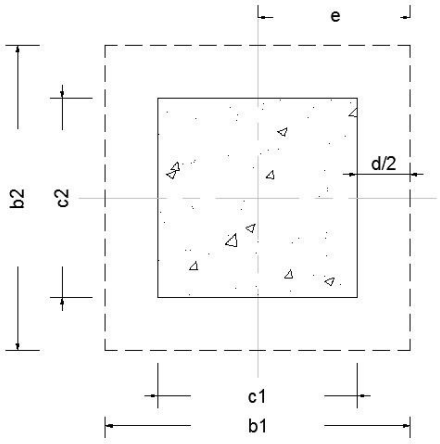

Figure B.1: Critical section at *d*/2 from the column face

Unbalanced Moment

$M/V = 0.15\ m$

Fraction to be transferred by eccentricity of shear **Clause 13.3.5.3 (A23.3-2014a)**

$$\gamma_v = 1 - \frac{1}{1+\frac{2}{3}\sqrt{\frac{b_1}{b_2}}} = 0.4$$

B.1.2. Connection H-1.0-XX

B.1.2.1. Material Properties

B.1.2.1.1. Concrete

Actual compressive strength of concrete $f_c' = 80\ MPa$

Material resistance factor $\varphi_c = 1.0$

Concrete density factor $\lambda = 1.0$

Modulus of elasticity $E_c = \left(3{,}300\sqrt{f_c'} + 6{,}900\right)\left(\frac{\gamma_c}{2{,}300}\right)^{1.5} = 39{,}950\ MPa$

Clause 8.6.2.2 (A23.3-2014a)

B.1.2.1.2. Flexural Reinforcement

Average reinforcement ratio, $\rho = 0.98\%$

Modulus of elasticity $E_f = 64{,}957\ MPa$

Modular ratio, $n = \frac{E_f}{E_c} = 1.63$

B.1.2.2. Shear Capacity According to CSA/S806-12 **Clause 8.7.2**

Compressive strength of concrete, f_c', shall not exceed 60 MPa **Clause 8.7.3**

$$v_r = v_c = \left(1 + \frac{2}{\beta_c}\right)\left[0.028\lambda\varphi_c(E_F\rho_F f_c')^{\frac{1}{3}}\right] = 2.82\ MPa$$

$$v_r = v_c = \left[\left(\frac{\alpha_s d}{b_o}\right) + 0.19\right] 0.147\lambda\varphi_c(E_F\rho_F f_c')^{\frac{1}{3}} = 2.65\ MPa$$

$$v_r = v_c = 0.056\lambda\varphi_c(E_F\rho_F f_c')^{\frac{1}{3}} = \mathbf{1.88}\ MPa$$ **(Governs)**

$$V = \mathbf{401}\ kN$$

B.1.2.3. Shear Capacity According to ACI 440.1R-15 **Clause 8.4**

$k = \sqrt{2\rho n + (\rho n)^2} - \rho n = 0.162$

$v_r = v_c = \frac{4}{5} k \sqrt{f'_c} = \mathbf{1.16}\ MPa$

$$V = \mathbf{248}\ kN$$

B.1.2.4. Shear Capacity According to JSCE 1997 **Clause 6.3.4**

$\beta_d = \sqrt[4]{1{,}000/d} = 1.58;\ if\ \beta_d > 1.5\ then\ \beta_d = 1.5$

$\beta_p = \sqrt[3]{100\rho E_{fu}/E_\circ} = 0.68$

$\beta_r = 1 + \dfrac{1}{1 + 0.25\dfrac{u}{d}} = 1.35$

$f_{pcd} = 0.2\sqrt{f'_{cd}} = 1.79;\ f_{pcd}\ shall\ be\ \leq 1.2$

$v_r = v_c = \frac{\beta_d * \beta_p * \beta_r * f_{pcd}}{\gamma_b} = \mathbf{1.64}\ MPa$

$$V = \mathbf{352}\ kN$$

B.2. Shear Capacity of Connections with Shear Reinforcement

B.2.1. General

There are no provisions in North American codes regarding the design of FRP-RC slab-column connections with shear reinforcement. A modified equations proposed by Gouda and El-Salakawy (2016b), which are based on the relationship between steel slab-column connections with and without stud shear reinforcement in both the CSA/A23.3-14 (CSA 2014a) and the ACI 318-14 (ACI Committee 318 2014), were used to calculate the predicted capacities of the connections. With a similar manner, the equations for slabs reinforced with stirrups were obtained. The critical section outside the shear-reinforced zone was located at 624 mm (3.90 *d*), 744 mm (4.65 *d*) and

600 mm (3.75 *d*) from the column face for connections N-1.0-S5, N-1.0-S6 and N-1.0-C5, respectively. Moreover, the spacing between shear reinforcement was taken as 120 mm (0.75 *d*) for all connections.

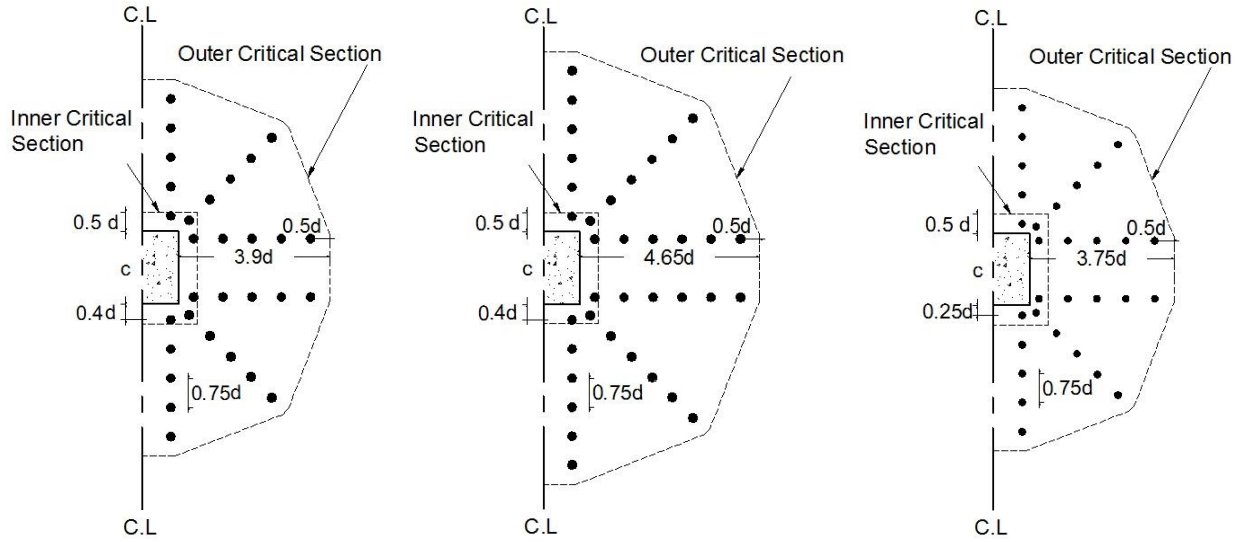

a) N-1.0-S5 b) N-1.0-S6 c) N-1.0-C5

Figure B.2: Arrangement of shear reinforcement and critical sections

B.2.2. Material Properties

B.2.2.1. Concrete Properties

Actual compressive strength of concrete $f_c' = 43\ MPa$

Material resistance factor $\varphi_c = 1.0$

Concrete density factor $\lambda = 1.0$

Modulus of elasticity $E_c = \left(3{,}300\sqrt{f_c'} + 6{,}900\right)\left(\frac{\gamma_c}{2{,}300}\right)^{1.5} = 31{,}300\ MPa$

Clause 8.6.2.2 (A23.3-2014a)

B.2.2.2. Flexural Reinforcement (SC-GFRP No. 16)

Average reinforcement ratio, $\rho = 0.98\%$

Modulus of elasticity $E_f = 64{,}957\ MPa$

Properties of Cracked Transformed Section

Modular ratio, $n = \frac{E_f}{E_c} = 2.07$

$k = \sqrt{2\rho n + (\rho n)^2} - \rho n = 0.181$ **Clause 7.3 (440.1R-15)**

$c = kd = 29.0\ mm$

B.2.2.3. Shear Reinforcement

Headed studs (GFRP No. 13)

Modulus of elasticity $E_{fs} = 67{,}547\ MPa$

Area $= 126.71\ mm^2$

Head pull-out load capacity $= 70\ kN$

Usable design strain provided by the manufacturer $= 0.818\%$

$S = 0.75d = 120\ mm$

$S_\circ = 0.4d = 64\ mm$

Corrugated bars (SC-GFRP No. 10)

Modulus of elasticity $E_{fs} = 52{,}003\ MPa$ (for the straight portion)

Area $= 71.29\ mm^2$

Ultimate strain $= 2.5\%$

$S = 0.75d = 120\ mm$

$S_\circ = 0.25d = 40\ mm$

B.2.3. Connection N-1.0-C5

B.2.3.1. Properties of Critical Section (at a distance 3.75*d* from the column face)

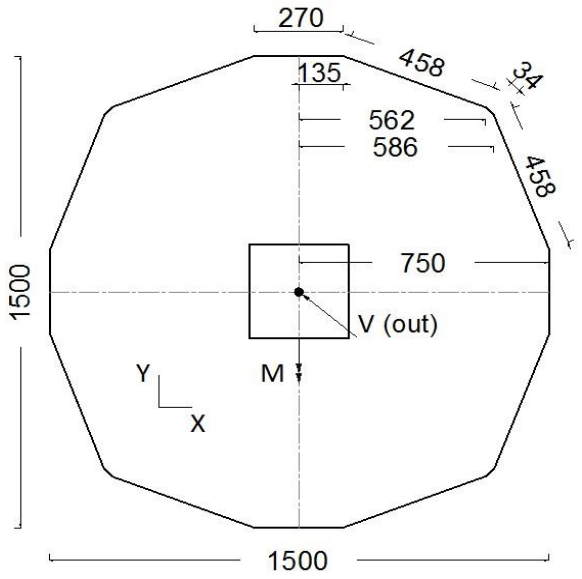

Figure B.3: Critical section outside shear-reinforced zone (N-1.0-C5)

$$J = d\Sigma \frac{length}{3}\left(x^2{}_i + x_i x_j + x^2{}_j\right) = 2.278 \times 10^{11}\ mm^4$$

$$b_\circ = \sum Segment = 4{,}876.2\ mm$$

Fraction to be transferred by eccentricity of shear **Clause 13.3.5.3 (A23.3-2014a)**

$$\gamma_v = 1 - \frac{1}{1+\frac{2}{3}\sqrt{\frac{b_1}{b_2}}} = 1 - \frac{1}{1+\frac{2}{3}\sqrt{\frac{1{,}500}{1{,}500}}} = 0.4$$

B.2.3.2. Capacity According to the Modified CSA/A23.3-14

B.2.3.2.1. Shear Strength at the Inner Shear Perimeter (at a distance *d*/2 from the column face)

Concrete Contribution

$$v_{c,inner} = 0.028\lambda\phi_c\left(E_f \rho_f f_c^{'}\right)^{1/3} = 0.84MPa$$ **Clause 13.3.9.3 (CSA 2014a) Modified**

Corrugated bars Contribution

$$v_s = \frac{\phi_s A_{vs} f_y}{b_o s} = \frac{\phi_s A_{vs} f_{fu}}{b_o s}$$ **Clause 13.3.9.4 (CSA 2014a) Modified**

$$f_{fu} = 0.005 E_f = 0.005 \times 52,003 = 260.0 MPa$$ **Clause 8.4.4.9 (CSA 2012)**

$$v_s = 1.01 MPa$$

Punching Shear Capacity

$$v_r = v_c + v_s = 1.85 MPa$$

$$V_{inner} = \mathbf{394}\ kN$$

B.2.3.2.2. Shear Strength at the Outer Shear Perimeter (at a distance 3.75*d* from the column face)

$$v_c = 0.028 \lambda \phi_c \left(E_f \rho_f f_c^{'} \right)^{1/3} = 0.84 MPa$$ **Clause 13.3.7.4 (A23.3-2014a) Modified**

$$V_{outer} = \mathbf{568}\ kN$$

Failure is expected to be **inside** the shear-reinforced zone

B.2.3.3. Capacity According to the Modified ACI 318-14

B.2.3.3.1. Shear Strength at the Inner Shear Perimeter (at a distance *d*/2 from the column face)

Concrete Contribution

$$V_c = \frac{2}{5} \sqrt{f_c^{'}} b_o k d = 139.77 kN$$ **Clause 22.6.6.1 (318-14) Modified**

$$v_c = \frac{V_c}{b_o d} = 0.475 MPa$$

Corrugated bars Contribution

$$f_{fu} = 0.004 E_f = 208.0 MPa$$ **Clause 8.2 (440.1R-15)**

$$v_s = \frac{A_{vs} f_y}{b_o s} = \frac{A_{vs} f_{fu}}{b_o s} = 0.805 MPa$$ **Clause 22.6.7.2 (318-14) Modified**

Punching Shear Capacity

$$v_n = v_c + v_s = 1.28\ MPa$$

$$V_{inner} = \mathbf{273}\ kN$$

B.2.3.3.2. Shear Strength at the Outer Shear Perimeter (at a distance 3.75*d* from the column face)

$$V_n = V_c = \frac{2}{5}\sqrt{f_c'} b_o k d$$ **Clause 22.6.6.1 (318-14) Modified**

$$v_n = v_c = \frac{2}{5}\sqrt{f_c'} k = 0.475 MPa$$

$$V_{outer} = \mathbf{321}\ kN$$

Failure is expected to be **inside** the shear-reinforced zone

APPENDIX C

Flexural Capacity of Connections

C.1. Yield Line Pattern

Figures C.1 and C.2 show the yield line pattern and the moments and rotations about slab parts, respectively, used to calculate the flexural capacities of the connections (Gouda and El-Salakawy 2016), the pattern is defined by four parameters *a*, *b*, *c* and *d*. Deflection equal to δ was assumed to occur at points E and F and the deflections at points G and H was assumed to equal to δ^1. The principal of virtual work is being used to analyze the pattern.

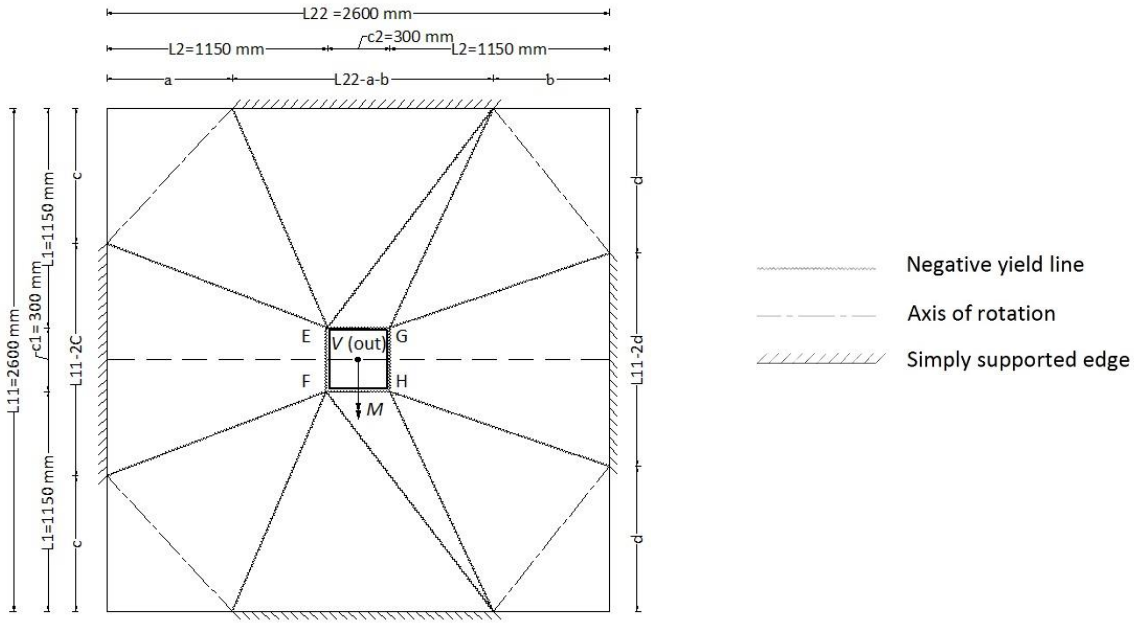

Figure C.1: Yield line pattern

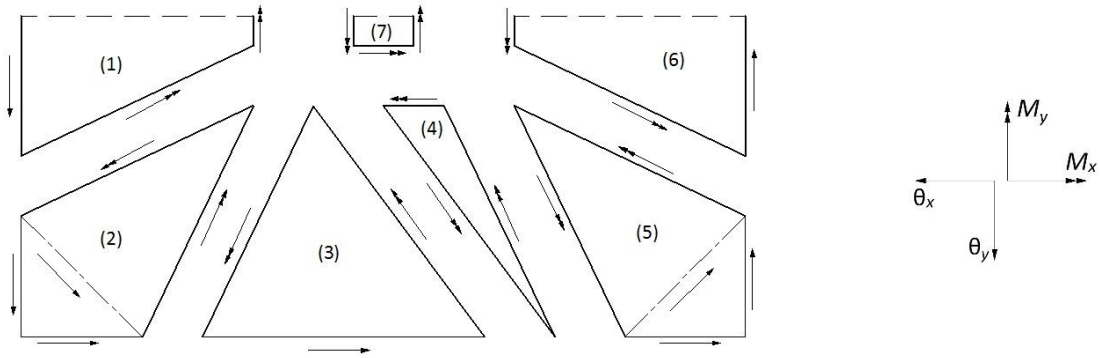

Figure C.2: Moments and rotations about slab parts

C.2. Equivalent Plastic Moment Calculations, M_p

C.2.1. Connection N-1.0-S5

C.2.1.1. Direction parallel to the Direction of the Applied Moment, M_{py}

$$I_g = \frac{b \times h^3}{12} = \frac{1{,}000 \times 200^3}{12} = 666.67 \times 10^6\ mm^4$$

$$A_f = 1{,}546.88\ mm^2 \qquad \rho_f = 0.0092 \qquad n = 2.07 \qquad k = 0.18$$

$$I_{cr} = \frac{b \times (kd)^3}{3} + n \times A_f \times (d - kd)^2 = 70 \times 10^6\ mm^4$$

$$M_{cr} = f_r \times \frac{I_g}{y_t} = 26.23\ kN.m$$

$$f_f = 0.5 E_f \varepsilon_{cu} \left[\left(1 + \frac{4\alpha_1 \beta_1 \phi_c f'_c}{\rho_f \phi_f E_f \varepsilon_{cu}} \right)^{1/2} - 1 \right] = 742.4\ MPa$$

$$c = \frac{\phi_f A_f f_f}{\alpha_1 \beta_1 \phi_c f'_c b} = 39.4\ mm$$

$$M_n = \phi_f A_f f_f \times \left(d - \frac{\beta_1 c}{2} \right) = 173.4\ kN.m$$

$$M_{py} = 0.5 M_n + 0.5 \left(1 - \frac{I_{cr}}{2 I_g} \right) \left(\frac{M_{cr}}{M_n} \right) M_{cr} = 88.6\ kN.m$$

C.2.1.2. Direction Perpendicular to the Direction of the Applied Moment, M_{px}

$$A_f = 1{,}546.88\ mm^2 \qquad \rho_f = 0.0101 \qquad n = 2.07 \qquad k = 0.185$$

$$I_{cr} = \frac{b \times (kd)^3}{3} + n \times A_f \times (d - kd)^2 = 56.6 \times 10^6\ mm^4$$

$$M_{cr} = f_r \times \frac{I_g}{y_t} = 26.23\ kN.m$$

$$f_f = 0.5 E_f \varepsilon_{cu} \left[\left(1 + \frac{4\alpha_1 \beta_1 \phi_c f'_c}{\rho_f \phi_f E_f \varepsilon_{cu}} \right)^{1/2} - 1 \right] = 704.0\ MPa$$

$$c = \frac{\phi_f A_f f_f}{\alpha_1 \beta_1 \phi_c f'_c b} = 37.4\ mm$$

$$M_n = \phi_f A_f f_f \times \left(d - \frac{\beta_1 c}{2}\right) = 148.0\ kN.m$$

$$M_{px} = 0.5M_n + 0.5\left(1 - \frac{I_{cr}}{2I_g}\right)\left(\frac{M_{cr}}{M_n}\right)M_{cr} = \ 76.0\ kN.m$$

C.3. Virtual Work Calculations

C.3.1. Internal Work, *U*

The internal virtual work done by the slab parts is calculated from Equation C.1.

$$U = M\theta l \qquad \text{Eq. [C.1]}$$

Where *U* is the internal work done along the yield line, *M* is the moment of resistance per unit width of the slab, θ is the produced rotations of the slab parts and *l* is the length of the yield line.

Accordingly the total internal work done is:

$$U = 2 \times \left[M_{py}\delta\frac{L11 - 2c}{2 \times L2} + \frac{M_{px}\delta a^2}{L2 \times c + a(L1 - c)} + \frac{M_{py}\delta c^2}{L1 \times a + c(L2 - a)} + M_{px}\delta\frac{L22 - a - b}{L1}\right.$$
$$\left. + \frac{M_{px}\delta^1 b^2}{L2 \times d + b(L1 - d)} + \frac{M_{py}\delta^1 d^2}{L1 \times b + d(L2 - b)} + M_{py}\delta^1\frac{L11 - 2d}{2 \times L2}\right]$$

$$k = \frac{M_{py}}{M_{px}} \qquad z = \frac{\delta^1}{\delta} > 1.0$$

$$U = 2 \times M_{px}\delta\left[k\frac{L11 - 2c}{2 \times L2} + \frac{a^2}{L2 \times c + a(L1 - c)} + \frac{kc^2}{L1 \times a + c(L2 - a)} + \frac{L22 - a - b}{L1}\right.$$
$$\left. + \frac{zb^2}{L2 \times d + b(L1 - d)} + \frac{kzd^2}{L1 \times b + d(L2 - b)} + kz\frac{L11 - 2d}{2 \times L2}\right]$$

C.3.2. External Work, *E*

$$E = V\frac{\delta^1 + \delta}{2} + M\frac{\delta^1 - \delta}{c2} = V\left[\frac{\delta^1 + \delta}{2} + \gamma\frac{\delta^1 - \delta}{c2}\right]$$

Where $\gamma = \frac{M}{V}$

$$E = V\left[\frac{\delta^1 c2+\delta c2+2\gamma\delta^1-2\gamma\delta}{2c2}\right] = V\delta\left[\frac{zc2+c2+2\gamma z-2\gamma}{2c2}\right] = V\delta\left[\frac{(c2-2\gamma)+z(c2+2\gamma)}{2c2}\right]$$

External work = Internal work

$$V\delta\left[\frac{(c2-2\gamma)+z(c2+2\gamma)}{2c2}\right] = 2\times M_{px}\delta[k\frac{L11-2c}{2\times L2}+\frac{a^2}{L2\times c+a(L1-c)}$$

$$+\frac{kc^2}{L1\times a+c(L2-a)}+\frac{L22-a-b}{L1}+\frac{zb^2}{L2\times d+b(L1-d)}+\frac{kzd^2}{L1\times b+d(L2-b)}$$

$$+kz\frac{L11-2d}{2\times L2}]$$

$$\rightarrow V = \frac{4\times M_{px}c2}{(c2-2\gamma)+z(c2+2\gamma)}\left[k\frac{L11-2c}{2\times L2}+\frac{a^2}{L2\times c+a(L1-c)}+\frac{kc^2}{L1\times a+c(L2-a)}+\frac{L22-a-b}{L1}+\frac{zb^2}{L2\times d+b(L1-d)}+\right.$$

$$\left.\frac{kzd^2}{L1\times b+d(L2-b)}+kz\frac{L11-2d}{2\times L2}\right]$$

This equation gives the vertical load applied to the connection as a function of a, b, c and d (Table C.1)

Table C.1: Flexural capacities of the connections

Connection	Flexural capacity, V_{flex} (kN)
H-1.0-XX	816
H-1.5-XX	972
H-2.0-XX	1,094
N-1.0-S5	621
N-1.0-S6	621
N-1.0-C5	621